

IPPT Reports on Fundamental Technological Research

2/2014

Łukasz J. Nowak

Adaptive feedback control system for reduction of vibroacoustic emission

PhD Dissertation

Supervisor: dr hab. inż. Mirosław Meissner

Auxiliary supervisor: dr inż. Tomasz G. Zieliński

Institute of Fundamental Technological Research

Polish Academy of Sciences

Warsaw 2014

IPPT Reports on Fundamental Technological Research

ISSN 2299-3657

ISBN 978-83-89687-90-6

Editorial Board/Kolegium Redakcyjne:

Wojciech Nasalski (Editor-in-Chief/Redaktor Naczelny),
Paweł Dłużewski, Zbigniew Kotulski, Wiera Oliferuk,
Jerzy Rojek, Zygmunt Szymański, Yuriy Tasinkevych

Reviewers/Recenzenci:

prof. dr hab. inż. Andrzej Dobrucki
dr hab. inż. Jerzy Wiciak, prof. AGH

Received on 14.11.2014

Copyright © 2014 by IPPT PAN

Instytut Podstawowych Problemów Techniki Polskiej Akademii Nauk (IPPT PAN)
(Institute of Fundamental Technological Research Polish Academy of Sciences)
Pawińskiego 5B, PL 02-106 Warsaw, Poland

Printed by/Druk:

EXPOL, P. Rybiński J. Dąbek Sp. J., Brzeska 4, 87-800 Włocławek, Poland

Acknowledgements

I would like to express my deepest gratitude to the supervisors of my thesis: Mirostaw Meissner, D.Sc. and Tomasz G. Zieliński, PhD, for their invaluable contribution and excellent guidance. This study owes much to their kind support. I am also particularly indebted to my wife and daughter, Karolina and Maja, who have always supported me in my work and have been the sources of inspiration and motivation for undertaking new challenges. It is also my duty to gratefully acknowledge the financial support of National Science Centre – Project "Adaptive Composite Noise Absorbers" (No. UMO-2011/01/N/ST8/07755) and the financial support of Structural Funds in the Operational Programme Innovative Economy, financed from the European Regional Development Fund – Project „Smart technologies for safety engineering SMART and SAFE” (No. TEAM/2008-1/4, operated within the Foundation for Polish Science Team Programme), thanks to which the realization of research described in the present study was possible.

Adaptive feedback control system for reduction of vibroacoustic emission

Łukasz Nowak

Institute of Fundamental Technological Research, Polish Academy of Sciences

Abstract

The aim of the present study is to introduce the possibilities of modifying vibrations of a thin plate structure with arbitrary boundary conditions using the developed, original active feedback control system in such manner that the amplitude of the acoustic pressure field generated by the plate is minimized in a selected point of the ambient space.

Theoretical investigations on the phenomena underlying the processes of detection and excitation of vibrations of thin plate structures using piezoelectric transducers are presented. An original algorithm for computation of the free-field acoustic radiation characteristics of vibrating plate structures with arbitrary boundary conditions has been developed and implemented. The algorithm provides a significant reduction of the required computational time and cost. Novel optimal control and adaptation algorithms for determining optimal feedback gain values, for which the amplitude of acoustic pressure is minimized in a given point of the ambient space surrounding the controlled structure, have also been developed.

The active vibroacoustic control system used in experimental investigations has been designed and constructed in accordance with an original concept, with separated, independent analogue feedback paths. The results of experiments carried out in an anechoic chamber showed that under the assumed conditions it is possible to obtain significant levels of reduction of noise emitted by the controlled plate structure, excited to vibrate by an external force.

Adaptacyjny system sterowania ze sprzężeniem zwrotnym dla redukcji transmisji wibroakustycznej

Łukasz Nowak

Instytut Podstawowych Problemów Techniki, Polska Akademia Nauk

Abstrakt

Podstawowym celem niniejszej pracy jest przedstawienie możliwości detekcji i kontroli drgań cienkich konstrukcji płytowych o dowolnych warunkach mocowania za pomocą zaprojektowanego, oryginalnego aktywnego układu sterowania bazującego na sensorach i aktuatorach piezoelektrycznych, w celu minimalizacji amplitudy ciśnienia akustycznego w wybranym punkcie przestrzeni otaczającej strukturę.

Przedstawiony został opis teoretyczny rozpatrywanych zjawisk leżących u podstaw procesów detekcji i wzbudzania drgań struktur płytowych za pomocą przetworników piezoelektrycznych. Opracowano i zaimplementowano oryginalny algorytm wyznaczania rozkładu pola ciśnienia akustycznego w otoczeniu płyty drgającej w wolnej przestrzeni, umożliwiający minimalizację czasu i kosztu niezbędnych obliczeń numerycznych. Opracowane zostały także oryginalne algorytmy sterowania optymalnego i adaptacji, umożliwiające szybkie i efektywne wyznaczenie optymalnych wartości wzmocnień pętli sprzężeń zwrotnych układu sterowania, dla których następuje minimalizacja amplitudy ciśnienia akustycznego w wybranym punkcie przestrzeni otaczającej kontrolowaną strukturę płytową.

System sterowania aktywnego wykorzystany do badań doświadczalnych został zaprojektowany i skonstruowany według oryginalnej koncepcji z wydzieleniem niezależnych, analogowych torów sprzężeń zwrotnych. Wyniki eksperymentów przeprowadzonych w komorze bezdechowej wykazały, iż w badanym układzie możliwe jest znaczne zredukowanie poziomu hałasu emitowanego przez kontrolowaną konstrukcję płytową pobudzoną do drgań przez siłę zewnętrzną.

Symbols and abbreviations

The short list of most frequently used symbols and abbreviations is provided below:

a	– length of a plate
a_p	– length of a piezoelectric transducer
\mathbf{a}	– vector of modal selectivity values of the actuator
A_m	– modal decomposition coefficients of the excitation introduced by an actuator
b	– width of a plate
b_p	– width of a piezoelectric transducer
c_s	– wave propagation velocity in a plate
c_{ijkl}	– fourth-order elasticity tensor
C_{CAB}	– capacity of the wires connecting sensor with the amplifier
C_p	– capacity of a piezoelectric sensor
δ	– Dirac delta function
δ'	– derivative of the Dirac delta function
d_3	– piezoelectric material constant
D	– flexural rigidity
D_k	– electric displacement vector
ϵ_{ki}	– second-order tensor of dielectric constants
e_{kij}	– third-order tensor of piezoelectric coefficients
E	– Young modulus
E_k	– electric field vector
f	– temporal frequency
f_L^V	– lower cutoff frequency of voltage amplifier
f_H^V	– higher cutoff frequency of voltage amplifier

f_L^C	– lower cutoff frequency of charge amplifier
f_H^C	– higher cutoff frequency of charge amplifier
f_c	– cost function
f_{re}	– cost function, real component
f_{im}	– cost function, imaginary component
f_c^{min}	– global minimum of the cost function
F_{Be}	– external load applied per length of a beam
F_{ext}	– external load applied per surface area of a plate
\tilde{F}_{ext}	– spatial distribution of amplitude of pressure applied on the surface of a plate
\mathfrak{F}_n	– amplitude of vibrational mode number n , excited by the external disturbance in the absence of the forces introduced by the control system
\mathbf{F}	– vector of modal amplitudes \mathfrak{F}_n
\mathbf{F}^*	– estimated vector of modal parameters of the external excitation
γ	– regularization parameter
G	– Green's function
G_m	– gain of feedback loop number m
G_m^{max}	– maximum available gain value for feedback loop number m
\mathbf{G}	– vector of feedback gain values
h_s	– thickness of a plate
h_p	– thickness of a piezoelectric transducer
H	– Heaviside step function
I	– cross-sectional moment of inertia
$\underline{\underline{I}}$	– identity matrix
k_a	– wave number of an acoustic wave
k_s	– structural wave number
k_n	– wave number of structural mode no. n
K^f	– material-geometric constant
L	– length of a beam
μ	– double layer potential
M	– number of feedback loops in the control system
$\underline{\underline{M}}$	– control system matrix
ν	– Poisson's ratio
\mathbf{n}	– unit vector normal to the plate's surface
N	– total number of considered modes of vibrations
N_i	– global shape function no. i

N_i^e	– local shape function no. i of element e
ω	– angular frequency
ω_m	– angular eigenfrequency of a structural mode no. m
Φ_n	– shape function of mode no. n
p	– acoustic pressure
P_n^{re}	– modal radiation coefficient (real) of structural mode no. n
P_n^{im}	– modal radiation coefficient (imaginary) of structural mode no. n
\mathbf{P}	– vector of modal radiation coefficients
Q	– electric charge
\tilde{Q}	– amplitude of the harmonically varied sensor charge
ρ_a	– air density
ρ	– density of the material of a plate
\mathbf{r}	– observation point
\mathbf{r}_a	– source point
\mathbf{R}	– vector pointing from a source point to an observation point
\tilde{R}	– gain of the signal conditioning circuit attached to the piezoelectric transducer
σ	– single layer potential
$\underline{\underline{\sigma}}$	– stress tensor
\mathbf{s}	– vector of modal sensitivity values of the piezoelectric sensor
S	– constant cross-section area of a beam
S_{ij}	– second-order strain tensor
\tilde{S}_m	– sensitivity function of a piezoelectric sensor to structural mode no. m
\tilde{S}_{mn}	– sensitivity function of sensor m to structural mode n
$\underline{\underline{\mathcal{S}}}$	– system sensitivity matrix
$\underline{\underline{T}}_{ij}$	– second-order stress tensor
U	– vector of voltage amplitudes of signals induced on the piezoelectric sensors
\tilde{U}_m	– voltage amplitude of signal induced on a piezoelectric sensor no. m
V_n	– amplitude of the normal velocity of the surface of a plate
V	– amplitude of a harmonic voltage driving actuator
w	– displacement, z -direction
\tilde{w}	– frequency-dependent amplitude function of harmonic vibrations
W_n	– amplitude of mode no. n

W – vector of modal amplitudes of vibrations

ADC – analog-to-digital converter

ANC – active noise control

ASAC – active structural acoustic control

AVC – active vibration control

BEM – boundary element method

DAC – digital-to-analog converter

FEM – finite element method

FET – field-effect transistor

IVBEM – indirect variational boundary element method

LQG – linear-quadratic-Gaussian control

LQR – linear-quadratic regulator

VCA – voltage controlled amplifier

Contents

1. Introduction	19
1.1 Problem statement	19
1.2 Motivation	22
1.3 State of the art	23
2. Vibrations of thin beam and plate structures	27
2.1 Theoretical considerations	27
2.2 Numerical simulations	33
2.3 Orthogonality of the eigenfunctions	37
3. Acoustic radiation of vibrating plate structures	41
3.1 Introduction	41
3.2 Structural-acoustic coupling	44
3.2.1 Outline	44
3.2.2 Numerical model	44
3.2.3 Results and discussion	46
3.3 Far-field acoustic radiation of a baffled plate	48
3.4 Free-field acoustic radiation – BEM model	52
3.4.1 Theoretical background	52
3.4.2 Implementation – the algorithm	57
3.5 Experimental investigations, results, and discussion	62
3.6 Conclusions	65
4. Piezoelectric sensors and actuators	71
4.1 State of the art, assumptions, and general description	71
4.2 Piezoelectric sensors	73
4.3 Piezoelectric actuators	75
4.4 Signal conditioning	77
4.5 Some technical aspects on the preparation of the composite structures for active control systems	81
4.6 Numerical and experimental investigations	83
4.6.1 Beam structures	84
4.6.2 Plate and panelled structures	87
4.7 Excitation of resonant vibrations	93
4.8 Conclusions	95

5. Active vibroacoustic control system	97
5.1 Aim and methods	97
5.2 Single feedback loop	101
5.3 Multiple independent feedback loops	106
5.4 Identification of the external disturbance	111
5.5 Implementation of the active control system	116
5.6 Experimental investigations	119
5.7 Conclusions	138
6. Concluding remarks	141
6.1 Summary	141
6.2 Scope of contribution	143
6.3 Recommendations for future work	144
Bibliography	147

List of Figures

2.1	Geometry of the considered problem	28
2.2	Mode shapes and eigenfrequencies of aluminum plate structure with dimensions 20 cm x 30 cm x 2 mm determined numerically using a 2-D plate model for two different types of mountings. Mounting „A”: cantilevered plate; Mounting „B”: plate clamped by a part of one of its shorter edges.	35
3.1	Baffled plate in contact with water on its one side: geometry and discretization.	46
3.2	Mode shapes of the first eight forms of vibrations of the plate with all edges free (without rigid body motion solution at frequency $f = 0$).	47
3.3	Distribution of the amplitude of acoustic pressure in the near-field zone of the vibrating plate structure submerged in water.	49
3.4	Acoustic radiation of a baffled plate – geometry of the problem.	50
3.5	Three-dimensional acoustic radiation beam patterns of two exemplary structural modes of the thin plate structure vibrating at frequency 400 Hz.	52
3.6	The geometry of the considered problem: plate domain.	53
3.7	Aluminium plate structure used in the experimental investigations in an anechoic chamber.	63
3.8	Sound pressure level as a function of the distance in the z -axis from the center of the investigated plate structure vibrating in the 5 th mode: (a) numerical simulation, (b) measurements.	64
3.9	Sound pressure level as a function of the distance in the z -axis from the center of the investigated plate structure vibrating in the 6 th mode: (a) numerical simulation, (b) measurements.	65

3.10 Sound pressure level as a function of the distance in the z -axis from the center of the investigated plate structure vibrating in the 9th mode: (a) numerical simulation, (b) measurements. 66

3.11 Sound pressure level as a function of the distance in the z -axis from the center of the investigated plate structure vibrating in the 13th mode: (a) numerical simulation, (b) measurements. 67

3.12 The distribution of sound pressure levels [dB] in the plane $z = 2$ cm for vibrational mode no. 5 with frequency $f = 120$ Hz. The color graph illustrates the results of the numerical simulations, while the blue circles show the values measured experimentally in corresponding points of space. 68

3.13 The distribution of sound pressure levels [dB] in the plane $z = 2$ cm for vibrational mode no. 9 with frequency $f = 269$ Hz. The color graph illustrates the results of the numerical simulations, while the blue circles show the values measured experimentally in corresponding points of space. 69

3.14 The distribution of sound pressure levels [dB] in the plane $z = 2$ cm for vibrational mode no. 11 with frequency $f = 320$ Hz. The color graph illustrates the results of the numerical simulations, while the blue circles show the values measured experimentally in corresponding points of space. 70

4.1 Piezoelectric sensor: a) schematic symbol, b) charge model, c) voltage model. 78

4.2 Typical signal conditioning circuits for piezoelectric sensors: charge mode amplifier (left) and voltage mode amplifier (right). 78

4.3 Electric scheme of designed and constructed charge amplifier with adjustable gain and cutoff frequency, based on AD745 low noise, FET input operational amplifier. 81

4.4 Developed and constructed charge amplifier with adjustable gain and cutoff frequency: printed circuit board assembly scheme (left) and a picture of an exemplary built device (right) 82

4.5 Technique of attaching a piezoelectric element to a structure made of conductive material, ensuring the electric contact between these elements and avoiding short-circuiting the electrodes. 83

4.6 Normalized sensitivity functions for the rectangle-shaped piezoelectric sensor attached to a cantilevered beam of length 58 cm as a function of the structural mode number and the distance of the sensor from the clamped end of the beam. 85

4.7 Three thin aluminium beams fixed to an experimental stand (left); a glass-fiber composite beam and a sandwich panel made up from the carbon-fiber composite liners with the *Nomex*-honeycomb core (right) used in the experimental investigations. 86

4.8 Results of the numerical simulations: the shape of an exemplary vibrational mode of the considered plate structure made of aluminium (left) and the corresponding distribution of the induced electric charge induced on the theoretical point-sensors made of the considered piezoceramics (right). 88

4.9 Thin aluminium plate with attached piezoelectric transducers in the laboratory stands used in the experimental investigations. . . 89

5.1 General schematic diagram of the developed active vibroacoustic control system (single feedback loop). 116

5.2 Circuit diagram of the final version of the feedback controller used for experimental investigations - analogue part, one single channel (out of four in total). 118

5.3 Final version of four-channel feedback controller used for experimental investigations - analogue part. 119

5.4 Software control panel of the developed active control system. . . 120

5.5 Plate structure used for the experimental investigations. 121

5.6 Laboratory stand used for the experimental investigations on the active vibroacoustic control. 122

5.7 Sound pressure level as a function of gain value of feedback loop no. 1 for the plate vibrating in the 11th structural mode, at frequency 320 Hz. Position of the microphone: x = 2 cm, y = 25 cm, z = 3 cm. 125

5.8 Sound pressure level as a function of gain value of feedback loop no. 2 for the plate vibrating in the 11th structural mode, at frequency 320 Hz. Position of the microphone: x = 2 cm, y = 25 cm, z = 3 cm. 125

5.9 Sound pressure level as a function of gain values of feedback loops no. 1 and 2, for the plate vibrating in the 11th structural mode, at frequency 320 Hz. Position of the microphone: x = 2 cm, y = 25 cm, z = 3 cm. 126

5.10 Sound pressure level as a function of gain value of feedback loop no. 1 for the plate vibrating in the 13th structural mode, at frequency 380 Hz. Position of the microphone: x = 2 cm, y = 25 cm, z = 3 cm. 127

5.11 Sound pressure level as a function of gain value of feedback loop no. 2 for the plate vibrating in the 13th structural mode, at frequency 380 Hz. Position of the microphone: x = 2 cm, y = 25 cm, z = 3 cm. 127

5.12 Sound pressure level as a function of gain values of feedback loops no. 1 and 2, for the plate vibrating in the 13th structural mode, at frequency 380 Hz. Position of the microphone: x = 2 cm, y = 25 cm, z = 3 cm. 128

5.13 Sound pressure level as a function of gain value of feedback loop no. 4 for the plate vibrating in the 14th structural mode, at frequency 411 Hz. Position of the microphone: x = 2 cm, y = 25 cm, z = 3 cm. 129

5.14 Sound pressure level as a function of gain values of feedback loops no. 1 and 2, for plate vibrating in the 14th structural mode, at frequency 411 Hz. Position of the microphone: x = 2 cm, y = 25 cm, z = 3 cm. 129

5.15 Sound pressure level as a function of gain value of feedback loop no. 2 for the plate vibrating in the 9th structural mode, at frequency 269 Hz. Position of the microphone: x = 10 cm, y = 15 cm, z = 5 cm. 130

5.16 Sound pressure level as a function of gain value of feedback loop no. 3 for the plate vibrating in the 9th structural mode, at frequency 269 Hz. Position of the microphone: x = 10 cm, y = 15 cm, z = 5 cm. 131

5.17 Sound pressure level as a function of gain value of feedback loop no. 4 for the plate vibrating in the 9th structural mode, at frequency 269 Hz. Position of the microphone: x = 10 cm, y = 15 cm, z = 5 cm. 132

5.18 Sound pressure level as a function of gain value of feedback loop no. 1 for the plate vibrating in the 13th structural mode, at frequency 380 Hz. Position of the microphone: x = 10 cm, y = 15 cm, z = 5 cm. 132

5.19 Sound pressure level as a function of gain value of feedback loop no. 2 for the plate vibrating in the 13th structural mode, at frequency 380 Hz. Position of the microphone: x = 10 cm, y = 15 cm, z = 5 cm. 133

5.20 Sound pressure level as a function of gain value of feedback loop no. 3 for the plate vibrating in the 13th structural mode, at frequency 380 Hz. Position of the microphone: x = 10 cm, y = 15 cm, z = 5 cm. 133

5.21 Sound pressure level as a function of gain value of feedback loop no. 4 for the plate vibrating in the 13th structural mode, at frequency 380 Hz. Position of the microphone: x = 10 cm, y = 15 cm, z = 5 cm. 134

5.22 Sound pressure level as a function of gain values of feedback loops no. 1 and 2, for the plate vibrating in the 13th structural mode, at frequency 380 Hz. Position of the microphone: x = 10 cm, y = 15 cm, z = 5 cm. 134

5.23 Sound pressure level as a function of gain value of feedback loop no. 1 for the plate vibrating in the 11th structural mode, at frequency 320 Hz. Position of the microphone: x = 10 cm, y = 20 cm, z = 20 cm. 136

5.24 Sound pressure level as a function of gain value of feedback loop no. 2 for the plate vibrating in the 11th structural mode, at frequency 320 Hz. Position of the microphone: x = 10 cm, y = 20 cm, z = 20 cm. 136

5.25 Sound pressure level as a function of gain value of feedback loop no. 4 for the plate vibrating in the 11th structural mode, at frequency 320 Hz. Position of the microphone: x = 10 cm, y = 20 cm, z = 20 cm. 137

5.26 Sound pressure level as a function of gain values of feedback loops no. 1 and 2, for the plate vibrating in the 11th structural mode, at frequency 320 Hz. Position of the microphone: x = 10 cm, y = 20 cm, z = 20 cm. 137

Introduction

1.1 Problem statement

The aim of the present study is to develop and evaluate a novel active vibroacoustic control system, methods, and algorithms enabling for reduction of sound pressure level generated by a vibrating plate structure in a given point of the ambient space. The investigations are limited to low frequency vibrations only (up to about 500 Hz), as in the higher range the acoustic energy can be efficiently dissipated passively using, for example, various porous materials. Thin, rectangle shaped plates with arbitrary (but known in advance) boundary conditions and dimensions much smaller than the radiated acoustic wavelengths are considered. It is assumed, that the structures are excited to vibrate by an external harmonic force with arbitrary spatial distribution, which parameters are unknown and have to be determined. The control system uses a number of small, rectangle shaped piezoelectric transducers attached to the surface of the controlled structure, some of them serving as sensors and providing information about the current state of the plate, while others are used as actuators to introduce the control loads and modify the vibration pattern in such a manner that the noise level in a given point of the ambient space is as low as possible. Steady state harmonic vibrations are considered but it is also assumed that the parameters of the external excitation may change over time and the control system must have the ability to adapt to those changes – specifically, be able to detect transitions between different states and to recalculate the optimal control parameters.

The thesis of the study can be formulated as follows: **vibrations of a thin plate structure with arbitrary boundary conditions excited by an external harmonic force can be modified using an active feedback control system based on a finite number of pairs of piezoelectric sensors and actuators in such a manner that the amplitude of acoustic pressure field generated by the plate will be minimized in a selected point of**

the ambient space.

Theoretical investigations on mechanisms and phenomena underlying the sound generation by the considered structures and the interaction between control system and the plates are presented in the study. Due to the high level of generality most of the considered issues cannot be described using analytical formulas. For that reason the relevant numerical models have been developed and implemented in order to predict the behavior of the considered systems under the assumed conditions. The results of the computations are compared to the results of experimental investigations. The experiments have been carried out using various developed and constructed smart composite structures, electronic measurement and control systems, and laboratory stands. The comparison between the numerical predictions and results of measurements allows to evaluate the correctness of the adopted assumptions. The study provides a detailed analysis of many aspects regarding active vibroacoustic control of plate structures, from the theoretical description of the involved phenomena up to physical implementation and practical validation of the chosen control methods.

The investigated issues have been divided into groups thematically related with various involved mechanisms and phenomena and described in separate chapters. Each of the chapters includes a theoretical description of the problem and the current state of the art in the related field. Adopted assumptions, notations, and the relevant physical and mathematical models are introduced, as well as the descriptions and results of the corresponding numerical and experimental investigations.

The first chapter of the study provides the necessary information on aims and scope of the work, underlying motivation, and general assumptions. The state of the art in the field of active noise and vibration control systems is presented.

The second chapter is devoted to the problem of free and forced vibrations of thin beam and plate structures. Analytical, numerical, and experimental methods of determining modal parameters of the considered structures are introduced. Influence of various factors and assumptions on the consistency between results of analytical and numerical predictions and the results of measurements is investigated.

Vibrations of plates submerged in an acoustic medium are the source of sound radiation to the ambient space. As the main goal of the presented investigations is to minimize the sound pressure level in a given point of the space, the knowledge on the radiation characteristics of the considered structure is required. However, due to the fact that the assumed active control system does

not obtain any information from acoustic pressure sensors – such as microphones – the radiation parameters have to be determined based on the modal amplitudes of vibrations. The solution of this problem is described in Chapter 3. The developed and implemented numerical model using dedicated computational algorithm is presented. Results of the simulations are compared to the results of experimental investigations carried out in an anechoic chamber. The influence of the inertial loading introduced by various acoustic media is investigated.

Chapter 4 describes various issues regarding application of piezoelectric transducers as sensors and actuators in active control of vibrations of thin beam and plate structures. A new form of theoretical description is introduced in order to better describe the ability of sensing and exciting specific structural modes by the transducers. Different theoretical and technical aspects of developing and constructing smart composite structures and the necessary signal conditioning circuits are presented. The results of numerical simulations and experimental investigations carried out using various beam and plate structures made of aluminum and composite materials – including actual materials used in aviation – are introduced.

The results and conclusions obtained during the investigations described in Chapters 2 – 4 form the basis for the development and construction of an active vibroacoustic control system of plate structures, which is the topic of Chapter 5. Detailed assumptions concerning the aim and the methods of control are introduced. The developed algorithms for determining optimal control parameters and modal characteristics of the external excitation force based on the electric signals from sensors are presented and the details concerning the implementation of the system are described. The control performance has been evaluated in experimental investigations carried out in an anechoic chamber.

The obtained conclusions regarding the possibilities and efficiency of active vibroacoustic control of plate structures with the developed system and methods are summarized in Chapter 6. The main completed tasks of the study are listed. The results of the conducted research form the basis for further investigations aimed at improvement of the parameters and extending the scope of the potential applicability of the proposed system or its components. The last section of the present study provides recommendations for the future work in this field.

1.2 Motivation

The subject of the present study falls within the scope of a relatively young and dynamically evolving research field, which is active vibroacoustic control. Over the past several decades a lot of scientific attention has been given to the problem of reduction machinery noise in various industry branches, such as aviation, maritime, rail transport, road transport, and mechanical engineering. Engines, propellers, fans, and other machines are sources of noise and vibrations, which propagate through the connected structural elements making them secondary sources of acoustic radiation. The radiated and induced sound is a persistent problem, which is often very poorly alleviated by passive means, particularly at low frequencies. The exposure of people to noise can cause – depending on the considered sound pressure levels – serious health problems or, at best, significant discomfort. The influence of industrial noise on the natural environment, namely on the behavior of various animal species is another serious problem to which a lot of attention has been recently given. The excessive structural acoustic radiation is also highly undesirable in all fields where the secrecy of operation is crucial. This especially concerns military applications. In the light of the described issues the problem undertaken in the present study appears as very up-to-date and important.

Although the fact that the first attempts of applying active control methods for reduction of machinery noise were reported as far back as in 1930's [1], it was not until the end of the 20th century when the development of technology allowed for practical implementations of such systems. This was especially boosted by the rapid increase of available computational power, which allowed to perform the time-critical, complex control algorithms. Nowadays, the necessary electronic hardware can be built based on small, cheap, and widely available microprocessors, programmable logic devices, or complete modules integrating all the required components. For that reason the conducted investigations can be focused more on developing new, effective methods and algorithms of active vibroacoustic control and less on overcoming technical limitations. Apart from the feasibility of the assumed tasks, an important issue is also the fact that although many scientific investigations have been recently devoted to the considered topic, a lot of new and unsolved problems still remain. This especially concerns real-life complex structures or structures with non-uniform boundary conditions, as most of the research described in literature is focused on vibrations of beams and plates with specific mounting conditions, for which analytical equations of motion can be given. The current state of the art on the considered topic is presented in Section 1.3, while the main original elements contributed

by the present study are listed in Section 6.2. The possibility of dealing with interesting and open interdisciplinary scientific problems is an important motivating factor that justifies taking the challenge of developing the described active vibroacoustic control system.

1.3 State of the art

The problem of minimizing the levels of vibration and acoustic radiation in various mechanical systems has a long history and has been the topic of numerous scientific investigations over the past several decades. As it has been described in Section 1.2, the considered phenomena often have a significant negative impact on human health, natural environment, and operational efficiency and service life of relevant devices and systems. The presented solutions to the problem can be in general divided into three main groups: passive, active, and semi-active methods. The division criterion in this case is the use of energy from external sources.

The passive approach involves using various kinds of dampers which do not require any external power supply for proper operation. Passive methods are widely used in many practical applications, as they are relatively cheap, simple, and maintenance-free. On the other hand, they are also often very inefficient, especially in low frequencies. The porous materials are commonly used for suppressing sound and vibrations due to very good absorption, especially in high frequency regions. The general theory on properties and modeling of such materials can be found, for example, in [2, 3]. Some practical considerations on using porous sound absorbers in audio engineering are presented in [4]. Narrowband acoustic signals can also be effectively suppressed by using reactive devices, such as Helmholtz resonators which are tuned to a single, specified frequency. Vibration dampers can also be based on piezoelectric transducers with passive resonant shunt circuits. The resonant frequency in such a case is determined by the value of capacitance of the transducer and the value of connected inductance. The energy of vibrations is converted to electric energy due to the piezoelectric effect and then dissipated on resistors as heat. Design of such systems and problem of selecting optimal inductance and resistance values is introduced in [5]. However, the efficiency of sound and vibration damping using shunted piezoelectric materials is very poor compared to the active control systems based on piezotransducers.

In the semi-active approach the energy from an external power supply is used only to modify the properties of the selected elements of the damping system

and is not applied directly to the controlled structure. Such a solution ensures lower energy requirements and better stability than the active systems while providing higher damping levels than the passive methods. The semi-active systems can also have the ability to adapt to changes in operating conditions. One of the examples of such devices are dampers with magneto-rheological fluid. The viscosity of such fluid increases in the magnetic field whose intensity can be modified with electric control signals. Consequently, the parameters of the damper can be dynamically altered. Some theoretical background and descriptions of numerical and experimental investigations on such systems can be found in [6–8]. The magneto-rheological dampers are used for example to suppress the vibrations in car industry, or in attenuation of seismic vibrations [9].

The system developed and constructed within the framework of the present study falls within the scope of the last of the described groups of methods, which are the active control techniques. In the active approach the energy from an external power source is converted into the energy of interaction between the actuators and the controlled object. Depending on the aim of the control, three different kinds of active control methods for reduction of noise and vibrations are distinguished: Active Vibration Control (AVC), Active Noise Control (ANC), and Active Structural Acoustic Control (ASAC). The active approach is particularly suitable in the low frequency range, possibly as a complement to the passive means.

In AVC approach the control is focused at minimization of the selected quantities describing vibrations of the structure, such as velocities or accelerations. The information about the state of the structure is obtained from sensors such as accelerometers, piezoelectric transducers, or strain gauges, while the control forces are typically applied using electromagnetic exciters or piezoelectric actuators. Although it is a fact, that in many cases the generated acoustic pressure field will also be suppressed, it does not have to be that way in general. Moreover, as it has been shown by Knyazev and Tartakovskii [10], in some cases reduction of the level of vibrations may actually result in an increased acoustic radiation to the ambient space. This is due to the fact that various forms of vibrations are characterized with different radiation efficiency and that the amplitude of the acoustic pressure cannot be expressed as a simple linear combination of the modal amplitudes. The theoretical background of the AVC methods can be found, for example, in [11–13].

The idea of using the phenomenon of destructive interference to intentionally suppress the undesirable noise was documented and patented in 1930 by a French engineer Henry Coanda and soon after that, in 1933, by a German inventor Paul Lueg [1, 14]. Their concepts assumed the use of microphones, am-

plifiers, and loudspeakers to generate an acoustic signal with the opposite phase to the primary acoustic disturbance. However, neither of them had managed to construct a working prototype, due to the technical limitations at the time. Two decades later other attempts of practical implementations of similar systems for an active reduction of sound were made by Olson and May [15, 16] – once again, with no success. Their devices turned out to work only in a narrow frequency band, with very poor efficiency. Moreover, the control parameters had to be set manually. It took about next forty years for the development and dissemination of electronic systems – especially digital signal processors, microcontrollers, programmable logic devices, and other, similar units – to allow such ideas to come true. The described approach with loudspeakers as secondary acoustic sources used to suppress the unwanted components of the primary acoustic field is now known as the Active Noise Control (ANC). A number of review publications in this field are available, presenting different control algorithms, methods and systems – see, for example, [14, 17–19]. The ANC technologies are now mature enough for widespread use in many practical applications including reduction of helicopter and aircraft cabin noise, car interior silencing systems, headphones, mobile phones, and many others.

The ASAC systems, similar to the case of the AVC methods, act directly on the controlled structure. They also use analogous means for sensing and exciting vibrations. The main difference between the two presented approaches is in the assumed cost function. The ASAC methods are aimed at modification of the vibration pattern of the structures which are the primary noise sources in such a way that the selected parameters characterizing the acoustic pressure field distribution in the ambient space will be minimized. The research on ASAC was initiated by Fuller and his co-workers [20–22] and continued by Hansen and Snyder [23], Thi [24], Thomas [25], Baumann [26], Zieliński [27], and other researchers. Most of the scientific investigations devoted to the ASAC systems are focused on structures with specific mechanical and acoustic boundary conditions which can be described using analytical formulas. A typical example of such structures is simply supported rectangular plates placed in an infinite, rigid baffle, investigated by researchers such as Fuller [11], Pan [28], Elliott [29], and Meirovitch [30]. Baffled plates with arbitrary but uniform boundary conditions were investigated by Berry [31]. Theoretical and experimental studies concerning applications of the ASAC methods on circular plates can be found, for example, in [32–34].

Depending on a type of the coupling between the input and the output of the active control system, there are three different control approaches which are used for active reduction of noise and vibrations:

- feedforward control,
- feedback control,
- hybrid feedforward/feedback control.

In the feedforward approach the parameters of the primary excitation signal must be either known in advance or measured. The information on the disturbance is fed to the input of the control system which respond in a pre-defined manner. In this case total local cancellation of noise or vibrations is theoretically possible. The description and examples of implementations of such systems can be found in [35–38]. In the feedback approach the response of the controlled structure is measured and fed back to the input. The control performance of such system depends on its open-loop feedback gain, which is in practice limited by the stability issues. The detailed theoretical background and mathematical preliminaries regarding such systems can be found, for example, in [39, 40]. The hybrid approach combines the described features of the feedback and feedforward control. The description of the hybrid control systems and examples of implementations are presented in [41–43].

The state variables describing the vibrations of the controlled structure are usually chosen in such a manner that their unforced behavior can be considered independently. Such an approach is called modal control [44]. In active noise and vibration systems the state variables are often related to the eigenforms of vibrations. However, an important problem connected with this form of description of the system arises due to the fact that the dynamic response of the structure is approximated by a finite number of modal components. If the assumed number of modes is not large enough, the effect called *spillover* will occur, significantly affecting the control performance [45]. On the other hand, a too large number of the included harmonic components can increase the computational time and cost above the limits imposed by the hardware specifications and demands of the real-time operation. The objective function in the active noise and vibration control systems is usually a quadratic function and the control process is performed by linear-quadratic regulators (LQR, LQG) [32, 46]. Other approaches presented in the literature are based on various kinds of PID controllers [32, 47–49]. Depending on the architecture, the control system may be either centralized (with a single data processing unit) or decentralized (with a number of independent control loops). As it is shown in [50, 51], both approaches can achieve a similar efficiency in noise and vibration reduction.

Vibrations of thin beam and plate structures

2.1 Theoretical considerations

The purpose of the present chapter is to introduce the assumptions, theoretical preliminaries, and the notation which are used in the following parts of this study to describe vibrations of various considered structures. The information contained herein is of a fundamental importance from the point of view of the analysis of acoustic radiation, modal parameters of piezoelectric sensors and actuators and the active control theory presented further, as the quality of the results concerning the vibrational parameters will significantly affect the results of subsequent computations. Theoretical foundations underlying the mathematical and physical models describing vibrations of thin beam and plate structures were developed as far back as in 18th and 19th century and now fall within the basic problems of continuum mechanics. The relevant issues are discussed in details, for example in [11, 13, 52, 53].

Although the investigations on active vibroacoustic control system presented in this study concern rectangular plates, some parts of related theoretical, numerical and experimental considerations are also devoted to vibrations of thin beams. Due to a simpler formal description of those structures and availability of analytical solutions of the relevant equations, the thin beams were chosen to verify some concepts regarding possibilities of sensing and exciting vibrations with piezoelectric transducers. Those issues are discussed in detail in Chapter 4.

The geometry of the considered problem is presented in Figure 2.1. The length a and width b of the plate are assumed to be much greater than its thickness h_s . Analogously, the length a_p and width b_p of the piezotransducer attached to the surface of the structure are assumed to be much greater than the thickness h_p . The orientation of the global Cartesian coordinate system is chosen in such a way that the edges of the plate are parallel to the relevant axes.

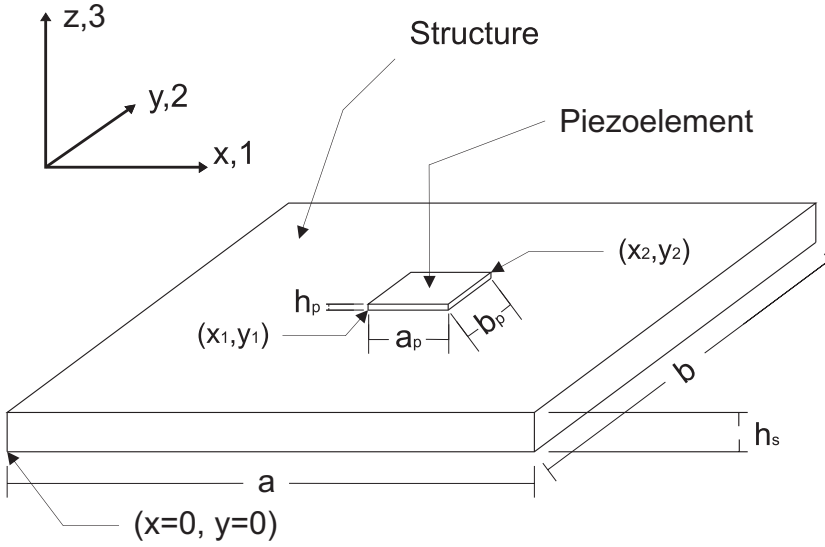


Figure 2.1. Geometry of the considered problem

Vibrational motion of the structures is assumed to occur only in the z direction, hence, only one, corresponding component of the displacement field is considered, namely, the deflection $w = w(x, y, t)$. In the case of the so-called beam structures it is assumed that the length a of a structure is much greater than its width b and its thickness h_s . The flexural waves propagate along the x direction only and the deflection w is constant along the y direction, i.e.: $\frac{\partial w}{\partial y} = 0$. The vibrations are described using the classical Euler-Bernoulli beam theory and the following equation (see, for example, [52]):

$$EI \frac{\partial^4 w}{\partial x^4} + \rho S \frac{\partial^2 w}{\partial t^2} = F_{Be}, \quad (2.1)$$

where E is the Young modulus of the isotropic material of the beam, I is the cross-sectional moment of inertia, ρ is the density of the material, S is the constant cross-section area of the beam, and finally, $F_{Be} = F_{Be}(x, t) \left[\frac{\text{N}}{\text{m}} \right]$ is the external load applied per length of the beam. The solutions of Equation 2.1 can be obtained analytically for arbitrarily chosen boundary conditions and presented as a sum of trygonometric and hyperbolic functions. The relevant formulas are presented, for example, in [52].

The solutions to the beam equation (2.1) can be written in a following,

general form [52]:

$$w(x) = C_1^B \sin(\alpha^B x) + C_2^B \cos(\alpha^B x) + C_3^B \sinh(\alpha^B x) + C_4^B \cosh(\alpha^B x), \quad (2.2)$$

where C_1^B, \dots, C_4^B , and α^B are constants whose values are determined by solving Equation (2.2) for a given set of boundary conditions. The modal shape functions of a beam structure obtained in such a manner are orthogonal, i.e., functions $\Phi_m(x)$ and $\Phi_n(x)$ describing shapes of vibrational modes m and n , respectively, obey the following condition:

$$\int_0^a \Phi_n(x)\Phi_m(x)dx = \begin{cases} 0 & \text{for } m \neq n \\ \int_0^a \Phi_n^2(x)dx & \text{for } m = n \end{cases} \quad (2.3)$$

Similarly, plate structures considered in this study are thin in the sense of the classical Kirchhoff's plate theory. They are assumed to be made of homogeneous, isotropic material (thus, in the case of composites, such an approach can be applied provided that the relevant effective material constants are known). Their vibrations are then described by the following equation of motion (see, for example, [52]):

$$D \left(\frac{\partial^4 w}{\partial x^4} + 2 \frac{\partial^4 w}{\partial x^2 \partial y^2} + \frac{\partial^4 w}{\partial y^4} \right) + \rho h_s \frac{\partial^2 w}{\partial t^2} = F_{ext}, \quad (2.4)$$

where $D = \frac{Eh_s^3}{12(1-\nu^2)}$ is the flexural rigidity of the plate which depends on its thickness h_s , as well as on Young's modulus E and Poisson's ratio ν of the material, while $F_{ext} = F_{ext}(x, y, t) [\frac{N}{m^2}]$ is the function of the external load applied per surface area of the plate.

It is assumed that each of the considered structures is subjected to an external harmonic excitation with an arbitrary spatial distribution. The system is linear and the structural damping is neglected, therefore, the response of the structure is also harmonic, with the same frequency and phase as the excitation. The present study focuses only on the low-frequency range (up to about 500 Hz), since higher frequency vibrations can be rather easily suppressed using the well-known passive techniques – like thin soft liners, a porous core of panel (see for example [54]). Taking all these assumptions into account, the response of a structure can be approximated by a finite sum of N structural modes as follows:

$$w(\mathbf{x}, t) \cong \sum_{n=1}^N \Phi_n(\mathbf{x})w_n(t) = e^{i\omega t} \sum_{n=1}^N \Phi_n(\mathbf{x})W_n \cong e^{i\omega t} \tilde{w}(\mathbf{x}), \quad (2.5)$$

where $(\mathbf{x}) \equiv (x)$ in the case of beam structures and $(\mathbf{x}) \equiv (x, y)$ in the case of plate structures, while Φ_n is the normalized shape function of mode n and w_n is the corresponding time-varying coefficient. When a harmonic motion is considered – with $\omega = 2\pi f$ as the angular frequency of the external excitation force (f being the frequency) – these coefficients are time-harmonic and can be expressed as $w_n(t) = e^{i\omega t}W_n$, where W_n are the (frequency-dependent) modal amplitudes; $\tilde{w}(\mathbf{x})$ is the (frequency-dependent) amplitude function of harmonic vibrations.

Modal shape functions Φ_n are found by solving the corresponding eigen-problems to the equations of motion (2.1) or (2.4), i.e., by setting their right-hand-side terms to zero and seeking non-trivial (i.e., non-zero) solutions in the form $e^{i\omega t}\tilde{w}(\mathbf{x})$. In the case of beams, regardless of their boundary conditions (and, as a matter of fact, because of their ‘unidimensional’ simplicity), it is always possible to find analytical solution consisting of a sum of trigonometric and hyperbolic functions [52]. In the case of plate structures, however, even when they are rectangular in shape, the analytical solutions can be found only for some specific (‘geometrically-homogeneous’) boundary conditions and – in general – it is required to use numerical methods, such as the Finite Element Method, in order to solve such problems.

The function describing an external harmonic excitation force acting on a plate can be expressed as follows:

$$F_{ext} = F_{ext}(x, y, t) = \tilde{F}_{ext}e^{i\omega t}, \quad (2.6)$$

where $\tilde{F}_{ext} = \tilde{F}_{ext}(x, y)$ denotes the spatial distribution of the amplitudes of pressure on the surface of the plate. This function can also be decomposed into an infinite series of modal components Φ_n of vibrations of the structure and approximated by a finite number N of them:

$$\tilde{F}_{ext} = \sum_{n=1}^N \Phi_n(x, y)F_n. \quad (2.7)$$

The modal shape functions Φ_n are assumed to be orthogonal, thus:

$$\int_0^a \int_0^b \Phi_n(x, y)\Phi_m(x, y)dxdy = \begin{cases} 0 & \text{for } m \neq n, \\ \int_0^a \int_0^b \Phi_n^2(x, y)dxdy & \text{for } m = n. \end{cases} \quad (2.8)$$

Taking into account the orthogonality property (2.8) the modal amplitudes can

be expressed as follows:

$$W_n = \frac{\int_0^a \int_0^b \tilde{w}(x, y) \Phi_n(x, y) dx dy}{\int_0^a \int_0^b \Phi_n^2(x, y) dx dy}, \quad (2.9)$$

$$F_n = \frac{\int_0^a \int_0^b \tilde{F}_{ext}(x, y) \Phi_n(x, y) dx dy}{\int_0^a \int_0^b \Phi_n^2(x, y) dx dy}. \quad (2.10)$$

The relation describing the modal amplitudes of vibrations of a plate induced by an external, harmonic excitation force with the given angular frequency ω and spatial pressure distribution \tilde{F}_{ext} is sought. First, the unforced vibrations are considered. Equation (2.4) is rewritten in the following form, with right-hand side equal to 0:

$$\nabla^4 \tilde{w}(x, y) - k_s^4 \tilde{w}(x, y) = 0, \quad (2.11)$$

where:

$$\frac{\rho h_s \omega^2}{D} = k_s^4. \quad (2.12)$$

The coefficient $k_s = \frac{\omega}{c_s}$ is the structural wavenumber and c_s denotes the wave propagation velocity in the considered plate.

Equation (2.11) is satisfied for the eigenmodes of vibrations of the plate and the corresponding structural wavenumber values. Substituting relation (2.5) into (2.11) the following formula is obtained:

$$\nabla^4 W_n \Phi_n(x, y) - k_n^4 W_n \Phi_n(x, y) = 0, \quad (2.13)$$

where k_n is the wavenumber of mode n , equal:

$$k_n = \frac{\omega_n}{c_s}, \quad (2.14)$$

ω_n is the angular eigenfrequency of mode n .

Getting back to the forced vibrations of plate structures, equation (2.4) after including relations (2.5)–(2.10) can be rewritten in the following form:

$$\nabla^4 \tilde{w}(x, y) e^{i\omega t} - \rho h_s \omega^2 \tilde{w}(x, y) e^{i\omega t} = \frac{1}{D} \tilde{F}_{ext}(x, y) e^{i\omega t}. \quad (2.15)$$

After dividing both sides of Equation (2.15) by $e^{i\omega t}$ and substituting the amplitude distribution functions with their modal decomposition coefficients, the following relation is obtained:

$$\sum_{n=1}^N [W_n \nabla^4 \Phi_n(x, y) - k_e^4 W_n \Phi_n(x, y)] = \frac{1}{D} \sum_{n=1}^N [\Phi_n(x, y) F_n]. \quad (2.16)$$

Both sides of Equation (2.16) are multiplied by a shape function $\Phi_m(x, y)$ of a structural mode number m and integrated over the surface of the plate:

$$\int_0^a \int_0^b \left(\sum_{n=1}^N [W_n \nabla^4 \Phi_n(x, y) - k_e^4 W_n \Phi_n(x, y)] \right) \Phi_m(x, y) dx dy = \quad (2.17)$$

$$\frac{1}{D} \int_0^a \int_0^b \left(\sum_{n=1}^N \Phi_n(x, y) F_n \right) \Phi_m(x, y) dx dy.$$

Looking back at the plate equation (2.11) and substituting the modal decomposition factors instead of the displacement amplitude distribution function $\tilde{w}(x, y)$ one can obtain:

$$\sum_{n=1}^N W_n \nabla^4 \Phi_n(x, y) = \sum_{n=1}^N k_n^4 W_n \Phi_n(x, y). \quad (2.18)$$

Substituting Equation (2.18) into Equation (2.17) one can obtain:

$$\sum_{n=1}^N \left[W_n (k_n^4 - k_e^4) \int_0^a \int_0^b \Phi_n(x, y) \Phi_m(x, y) dx dy \right] = \quad (2.19)$$

$$\frac{1}{D} \sum_{n=1}^N F_n \int_0^a \int_0^b \Phi_n(x, y) \Phi_m(x, y) dx dy,$$

Taking into account the orthogonality property of the modal shape functions (2.8), Equation (2.19) can be rewritten in the following form:

$$W_n = \frac{F_n}{D (k_n^4 - k_e^4)}. \quad (2.20)$$

Substituting the relations (2.10) and (2.12) into Equation (2.20), the following formula is eventually obtained:

$$W_n = \frac{1}{\rho h_s} \frac{\int_0^a \int_0^b \tilde{F}_{ext}(x, y) \Phi_n(x, y) dx dy}{(\omega_n^2 - \omega^2) \int_0^a \int_0^b \Phi_n^2(x, y) dx dy}. \quad (2.21)$$

Equation (2.21) connects the amplitude of vibrations of a structural mode n with the frequency and amplitude distribution of an external, harmonic excitation force. Thus, if the parameters of the excitation are known, then the response of the plate can be computed as a sum of amplitudes of modal components vibrating at the imposed angular frequency ω . The only exception is the situation when the excitation frequency is equal to any of the eigenfrequencies of vibrations of the plate. In such a case the amplitude of the corresponding mode, computed using relation (2.21) would theoretically reach the infinity. This conclusion obviously disagrees with observations, because the amplitudes of vibrations of real-life structures are always finite. The reason for this discrepancy is the fact that – according to the assumptions described previously – in the considered, simple model damping and nonlinear effects are neglected. The problem of determining the amplitudes of resonant vibrations and the results of relevant experimental investigations are presented in Section 4.7 of this study.

2.2 Numerical simulations

Due to the undertaken assumptions, the methods, algorithms, and solutions concerning active vibroacoustic control of plate structures developed and presented in this study should be applicable to plates with arbitrary boundary conditions. Since there are no known analytical solutions of Equation (2.4) in such a general case, the problem has to be solved numerically. Various kinds of thin, rectangle shaped plates are considered in the present study. However, no specific computational schemes that could be beneficial to use for special cases of boundary conditions were employed, so the presented approaches can be easily generalized into any mounting conditions.

The parameters of structural modes of vibrations of the considered plate were determined using the Finite Element Method and the Comsol Multiphysics software. A mapped mesh of rectangular elements was used to discretize the surface of the structure. The simulations were performed for various meshes consisting of from few dozens up to several thousands of elements. Some aspects

regarding the influence of resolution of the discretization on the obtained results are introduced in Section 2.3.

The mode shapes and eigenfrequencies of vibrations of the 20 cm wide, 30 cm high, and 1 mm thick rectangle shaped aluminum plate structure determined numerically are presented in Table 2.1. The results of simulations were verified experimentally. The plate was clamped by a 6 cm long middle section of one of its shorter edges, using a provided for this purpose protruding part. The plate was excited to vibrate by a pair of piezoelectric actuators (the issues regarding the use of piezoelectric transducers are described in detail in Chapter 4 of this study). Very sharp resonant characteristics, with high amplitudes of vibrations occurring only for specific excitation frequencies (which were assumed to be the actual eigenfrequencies of the structure) were observed. The laser vibrometer was used to determine the vibrational pattern in all cases (i.e., determine locations of points with minimum and maximum amplitudes of vibrations on the surface of the plate). The overall agreement between the measurements and results of simulations was fair. The shape functions of all of the considered structural modes matched the corresponding patterns determined numerically. However, some discrepancies between the measured and predicted values of eigenfrequencies are also observed. The comparison of the results is presented in Table 2.1. The accuracy of simulations varies for different structural modes, with errors ranging from about 1 to 3 Hz (modes no. 1, 2, 3, 15) up to even over 20 Hz in extreme cases (modes no. 9 and 12). The most important factor which is probably responsible for the differences between experiments and simulations are the mounting imperfections. For the computational purposes, the plate was assumed to be perfectly clamped by a part of the shorter edge, while the holders used in a laboratory stand were never perfectly stiff and carried some of the energy of vibrations.

The precise reconstruction of the actual boundary conditions in the numerical model is crucial from the point of view of the obtained results. Figure 2.2 presents mode shapes and eigenfrequencies of six first forms of vibrations of 20 cm wide, 30 cm high, and 2 mm thick aluminum plate, for two various mounting types (different than the one considered in Table 2.1). Mounting „A” denotes cantilevered plate, while in the case of mounting „B” the plate is clamped only by a 5 x 1 cm rectangular shaped middle section, at its shorter edge. As it can be seen, most of the mode shapes are quite the same in both cases, however, the change in boundary conditions from „A” to „B” results in occurrence of a new form of vibrations (mounting „B”, 5th mode, eigenfrequency 260,35 Hz). The influence of such a change on the eigenfrequency values is selective - 2nd and 4th modes (with frequencies 36,04 Hz and 213,42 Hz in case „A” and 54,71 Hz

and 177,98 Hz in case „B”, respectively) seem to be the most sensitive to the considered modification, while some other forms of vibrations are almost not affected at all.

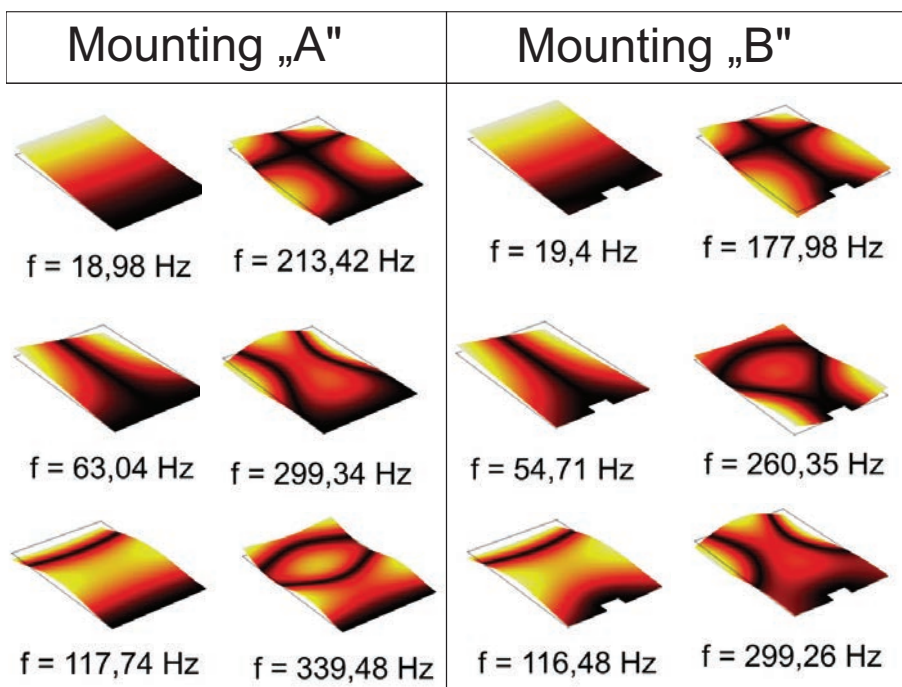


Figure 2.2. Mode shapes and eigenfrequencies of aluminum plate structure with dimensions 20 cm x 30 cm x 2 mm determined numerically using a 2-D plate model for two different types of mountings. Mounting „A”: cantilevered plate; Mounting „B”: plate clamped by a part of one of its shorter edges.


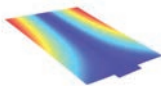
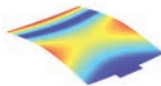
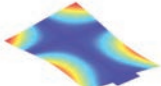
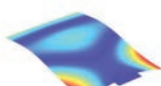
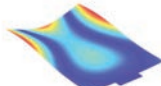
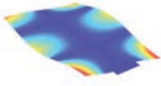
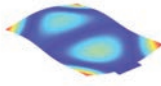
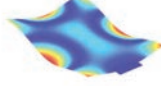
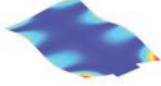
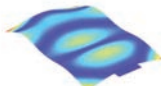
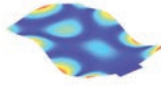

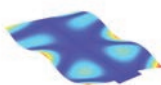
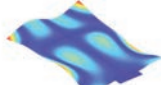
Mode no. 1		Mode no. 2		Mode no. 3	
					
Eigenfrequency [Hz]		Eigenfrequency [Hz]		Eigenfrequency [Hz]	
Computed: 8	Measured: 7,1	Computed: 24,6	Measured: 27,1	Computed: 50,3	Measured: 51,7
Mode no. 4		Mode no. 5		Mode no. 6	
					
Eigenfrequency [Hz]		Eigenfrequency [Hz]		Eigenfrequency [Hz]	
Computed: 82,3	Measured: 90,7	Computed: 127,2	Measured: 120	Computed: 144,9	Measured: 155
Mode no. 7		Mode no. 8		Mode no. 9	
					
Eigenfrequency [Hz]		Eigenfrequency [Hz]		Eigenfrequency [Hz]	
Computed: 160,2	Measured: 172,4	Computed: 199	Measured: 183	Computed: 247,6	Measured: 269
Mode no. 10		Mode no. 11		Mode no. 12	
					
Eigenfrequency [Hz]		Eigenfrequency [Hz]		Eigenfrequency [Hz]	
Computed: 261,4	Measured: 276,6	Computed: 337,8	Measured: 320	Computed: 383,9	Measured: 406
Mode no. 13		Mode no. 14		Mode no. 15	
					
Eigenfrequency [Hz]		Eigenfrequency [Hz]		Eigenfrequency [Hz]	
Computed: 386,5	Measured: 380	Computed: 404,6	Measured: 411	Computed: 467,9	Measured: 471

Table 2.1. Mode shapes and eigenfrequencies of aluminum plate structure with dimensions 20 cm x 30 cm x 1 mm determined numerically using a 2-D plate model, compared to the resonant frequencies determined experimentally.

2.3 Orthogonality of the eigenfunctions

In the case of plate structures with arbitrary boundary conditions the mode shape functions cannot be obtained analytically and they have to be determined with numerical methods, such as the Finite Element Method used in this study. However, the results of numerical simulations only approximate the exact solution and the obtained eigenshape functions do not have to be strictly orthogonal. The accuracy of computations depends, among other factors, on the resolution of discretization. Due to the fact that the orthogonality property (2.8) underlies the derived formulas describing the behavior of plate structures (2.21), the possible discrepancies at this point strongly affect the results presented in the other parts of this study. For this reason it has been decided to investigate the influence of the resolution of discretization on the compatibility between the assumed and true properties of the obtained mode shapes. The forms of vibrations of the considered plate (presented in Table 2.1) were determined using several different mesh resolutions, predefined in the Comsol Multiphysics software, ranging from „extremely coarse” (150 elements) up to „extremely fine” (10000 elements). Then, using a Matlab script the absolute values of products (2.8) of each with each shape functions were determined and normalized with respect to the value $\int_0^a \int_0^b \Phi_n^2(x, y) dx dy$ for every considered mode n . The results concerning the first eight forms of vibrations of the plate are presented in Tables 2.2–2.5.

Mode no.	1	2	3	4	5	6	7	8
1	1	0.015	0.238	0	0.259	0.066	0.017	0.252
2	0.015	1	0.003	0.229	0.026	0.025	0.163	0.042
3	0.238	0.003	1	0.003	0.038	0.002	0.007	0.291
4	0	0.229	0.003	1	0.024	0.014	0.011	0.019
5	0.259	0.026	0.038	0.024	1	0.069	0.007	0.032
6	0.066	0.025	0.002	0.014	0.069	1	0.034	0.269
7	0.017	0.163	0.007	0.011	0.007	0.034	1	0.017
8	0.252	0.042	0.291	0.019	0.032	0.269	0.017	1

Table 2.2. Normalized absolute values of products of shape functions determined using the extremely coarse mesh resolution (150 elements)

In the ideal case, if all of the approximated shape functions would satisfy the condition (2.8), then the values in all of Tables 2.2–2.5 should be equal to 1 on the diagonal and 0 everywhere else. In fact, many among the off-diagonal elements in all of the presented tables are greater than zero. The higher the

Mode no.	1	2	3	4	5	6	7	8
1	1	0	0.04	0.001	0.041	0.046	0.001	0.065
2	0	1	0.001	0.042	0.001	0	0.056	0.002
3	0.04	0.001	1	0.001	0.002	0.003	0.001	0.056
4	0.001	0.042	0.001	1	0	0.001	0.005	0
5	0.041	0.001	0.002	0	1	0.011	0	0.056
6	0.046	0	0.003	0.001	0.011	1	0	0.047
7	0.001	0.056	0.001	0.005	0	0	1	0.003
8	0.065	0.002	0.056	0	0.056	0.047	0.003	1

Table 2.3. Normalized absolute values of products of shape functions determined using the coarse mesh resolution (1500 elements)

Mode no.	1	2	3	4	5	6	7	8
1	1	0	0.021	0	0.024	0.034	0.001	0.047
2	0	1	0	0.033	0	0	0.043	0.001
3	0.021	0	1	0.001	0.007	0.014	0	0.041
4	0	0.033	0	1	0	0	0.003	0.001
5	0.024	0	0.007	0	1	0.019	0.001	0.041
6	0.034	0	0.014	0	0.019	1	0	0.037
7	0.001	0.043	0	0.003	0	0	1	0.003
8	0.047	0.001	0.041	0.001	0.041	0.037	0.003	1

Table 2.4. Normalized absolute values of products of shape functions determined using the normal mesh resolution (2300 elements)

Mode no.	1	2	3	4	5	6	7	8
1	1	0.005	0.003	0	0.003	0.005	0.001	0.012
2	0.005	1	0.003	0.013	0.001	0.001	0.016	0
3	0.003	0.003	1	0.004	0.015	0.02	0.003	0.014
4	0	0.013	0.004	1	0.001	0.003	0.003	0.001
5	0.003	0.001	0.015	0.001	1	0.018	0.003	0.008
6	0.005	0.001	0.02	0.003	0.018	1	0.001	0.018
7	0.001	0.016	0.003	0.003	0.003	0.001	1	0
8	0.012	0	0.014	0.001	0.008	0.018	0.001	1

Table 2.5. Normalized absolute values of products of shape functions determined using the extremely fine mesh resolution (10000 elements)

value, the worse the orthogonality criterion between the two corresponding shape

functions is fulfilled. The worst situation is observed for the lowest („extremely coarse”) mesh resolution - the products of some pairs of the eigenfunctions are equal almost 0.3. In such case the corresponding modal components could not be separated in the process of decomposition (2.9). Fortunately, the quality of the obtained results improves significantly with the increasing of the mesh resolution. For the „normal” mesh, consisting of 2300 elements, all of the off-diagonal values are less than 0.05 and more than half of them is not greater than 0.01. In this case, the results of numerical simulations can be regarded as acceptable for further calculations. The approximation of the orthogonality property of the modal shape functions is even better for the „extremely fine” mesh, consisting of 10000 elements. In such case the higher off-diagonal value is equal to 0.018, while more than two-thirds of the rest of them is less than 0.01. However, the number of elements with the lowest values, below 0.001, is lower than in the case of the less dense, „normal” mesh. This is probably due to the numerical errors whose importance increases with the resolution.

The presented results clearly indicate that the denser the mesh used to discretize the surface of the plate (at least, in the considered range of resolutions) is, the better the orthogonality criterion between the determined modal shape functions is fulfilled. On the other hand, increasing the number of elements in simulations also increases the computational time and cost. However, due to the simplicity of the considered problem and the fact that only limited number of low-frequency forms of vibrations are of interest, even simulations carried out using the „extremely fine” mesh take less than one minute on a standard personal computer. The results of such simulations, with a relatively dense mesh, are used for further computations described in the present study.

Acoustic radiation of vibrating plate structures

3.1 Introduction

Acoustic radiation of different vibrating structures is a topic of great interest and has been the subject of numerous theoretical and experimental scientific investigations. The importance of this phenomenon is implied by the fact, that actually most of the sounds observed in the nature or generated – intentionally or not – by people or machines result as a coupling between vibrating surfaces and the acoustic medium. Thus, it is highly desirable to be able to accurately model the distribution of the acoustic pressure generated in this manner in the space surrounding the considered structures. Such predictions allow to control the ambient sound field by controlling the vibrations of the sources and can be used in countless practical applications. In this context, one of the most commonly considered types of vibrating elements are the plate structures, due to their usefulness in modeling many real-world mechanical systems on the one hand and the ease of description on the other.

The very first attempts of creating formal description of dependencies between some mechanical properties of different structures and parameters of sounds emitted by those structures during vibrations actually took place as far back as in ancient times. In the 6th century BC Pythagoras was investigating sounds emitted by strings of different lengths and created the mathematical foundations of determining pitch [55]. However, it was not until the 19th century when Lord Rayleigh developed and described the mathematical models concerning acoustical properties of vibrating pistons placed in an infinite, rigid baffle [56]. His works initiated research on the acoustic radiation characteristics of various vibrating plate structures (see, for example, [11, 53, 57]). The methods of determining the distribution of the acoustic pressure generated in this manner are still being intensively developed.

Theoretical considerations and results of numerical simulations concerning the far-field acoustic radiation characteristics of baffled plates will be presented in Section 3.3 of this chapter. The differences between radiation patterns of various vibrational modes in the low-frequency range will be introduced and discussed. As it will be shown, in the case of structures relatively small, as compared to the acoustic wavelength, the forms of vibrations may be divided into two categories, basing on the computed distributions of generated sound pressure levels: the „monopole” and the „dipole” modes. According to the properties of elementary acoustic sources, the latter are weak radiators.

The presence of the acoustic medium which is necessary for acoustic waves to propagate, influences the vibrational characteristics of the considered structure which is the source of the radiation. The problem of determining the eigenfrequencies and corresponding modal shape functions of vibrating plate structures submerged in different media has been the topic of numerous scientific investigations (see, for example, [58–62]), which resulted in the development of various computational methods and algorithms suitable for different systems and boundary conditions. Despite the fact that in many cases the influence of the acoustic medium cannot be neglected (this is particularly true for heavy fluids, such as water), if the vibrating thin plate structures are relatively small as compared to the acoustic wavelength and the surrounding medium can be treated as a light fluid - such as, for example, air - then it can be shown [63] that in such case the eigenfrequencies and vibrational mode shapes of the plate are not significantly affected by the presence of the medium. This means that the mechanical analysis of the vibrational characteristics can be decoupled from the acoustic analysis and performed independently for the *in vacuo* case. The obtained results may be then used for the computation of the distribution of generated acoustic pressure by introducing them as the boundary conditions on the surface of the considered structure. The issues concerning the influence of different acoustic media on vibrational characteristics of plates will be discussed more in detail in Section 3.2.

Sections 3.4 and 3.5 concern free-field vibroacoustic emission of thin, rectangle-shaped plate structures. Analytical solutions describing either selected vibrational characteristics or parameters of the generated acoustic pressure field are known only for a limited number of some special cases of prescribed boundary conditions for such structures, as, for example, simply-supported, baffled plates [11, 53]. In the general case such exact solutions cannot be given and the considered problem has to be solved numerically. Taking into account that the considered ambient medium is air, the eigenfrequencies and the corresponding vibrational mode shapes are determined independently from the acoustic anal-

ysis using the Finite Element Method. The acoustic pressure field distribution could also be computed using the same method but it would require to expand the mesh of elements into a large area of space surrounding the vibrating plate and would significantly increase the computational cost. Moreover, due to the fact that the discretized area has a finite volume and the considered domain is unbounded, some special techniques for solving the exterior acoustic problems, such as *Perfectly Matched Layers* or *Infinite Elements*, should be implemented additionally. For that reason the Boundary Element Method was chosen as a more appropriate tool for the acoustic analysis in the specified case.

The Boundary Element Method has been extensively developed since the sixties of the last century for the purposes of various research and engineering fields. Some preliminaries of this method with examples of applications in mechanics, acoustics, and electromagnetics can be found in [64–67]. In the considered case of the free-field acoustic radiation of the thin, rectangular plate two of the specific features of the Boundary Element Method make it particularly convenient to use. First, the dimension of the discretized domain is reduced by one, compared to the Finite Element Method model, and includes only the flat surface of the plate. Second, the fundamental solution of the problem which is used for the formulation of the solved equations obeys the Sommerfeld radiation condition at infinity. This means that there is no need in implementing any additional computational techniques to take into account the unbounded character of the acoustic domain. On the other hand, some complexities in the computational process arise due to the fact that the considered problem is an exterior acoustic problem with an open boundary surface for which the only applicable version of the chosen numerical method is the Indirect Variational Boundary Element Method [68] which will be referred to further on as the IVBEM. The variational computational scheme introduces double surface integrals and highly singular terms to the solved equations. In the relevant literature similar issues concerning plate structures have already been described (see, for example, [69]). However none of the sources include the detailed information about the implementation of the procedures for solving the derived equations. The importance of such information is associated with some significant simplifications that can be introduced at this stage by taking into account the simple geometry and some special features of the considered problem. For that reason these important issues are included in the present study. In order to efficiently deal with the mentioned difficulties a dedicated algorithm has been developed and implemented using the Matlab environment. The results of the numerical simulations are compared with the results of the experimental investigations performed in an anechoic chamber to validate the accuracy of the predictions.

3.2 Structural-acoustic coupling

3.2.1 Outline

Most of the scientific investigations devoted to the problem of acoustic radiation of vibrating structures focus on vibroacoustic emission in air, considering simple but representative structural elements, such as membranes, beams, and plates with different boundary conditions. Due to the relatively low density of air, the vibration characteristics of structures are not significantly altered by the inertial loading introduced by a medium and the problem of determining eigenfrequencies and corresponding mode shapes can be simplified to the in-vacuo case. A similar procedure applied to a structural element submerged in a heavy fluid, such as water, would result in a total discrepancy between predictions and measurements, as the influence of the medium is in this case crucial.

The influence of fluid loading on the acoustic radiation characteristics of the structural elements has been investigated by many scientists. Some analytical solutions for specific cases were developed by Maidanik and Kerwin [58] and Stuart [59, 60]. Many authors considered the impact of the submersion in water on the plate's eigenfrequencies and eigenmode shapes. Different methods have been developed to solve this problem. Some of them assume that the structural mode shapes remain unchanged and focus only on the alteration of the natural frequencies of the plates [70, 71]. Additional factors are often introduced to model the inertial loading by mass incrementation of the vibrating structure [70–73]. Other, more general approaches, use Rayleigh-Ritz method to compute both mode shapes and eigenfrequencies [72, 74]. The influence of fluid loading is different for plates having contact with water on one or both sides.

One of the main areas in which hydroacoustic emission is crucial is military technology. In past decades a lot of effort has been put into reducing noise generated by marine and navy vessels. This is especially true of the submarines, for which stealth operation is the most desirable. Knowledge of the vibrational characteristics of the hulls of vessels is also an important issue for the safety reasons [75]. The operating parameters of the powertrains of the vessels must meet the criteria resulting from the eigenfrequency analysis of the hulls having contact with water.

3.2.2 Numerical model

The solution of the eigenvalue problem of vibrations of a fluid-loaded structure will be analyzed on the example of a rectangle-shaped, 20 cm wide, 30 cm high, and 1 mm thick aluminum plate placed in an infinite, rigid baffle, having

contact with various kinds of acoustic media on the one side. Notwithstanding the fact, that only air is in the scope of interest of the present study, heavy-fluid case (represented by water) is also considered in this section in order to better evaluate the influence of medium parameters on the vibrational characteristics of a submerged structure. Free boundary conditions are assigned to all the four edges of the plate. Damping is neglected and only transverse motion of the structure is taken into account. The solid domain - represented by the plate - is described with the following constitutive equation:

$$\rho\omega^2 w + \mathbf{n}\nabla\cdot\underline{\underline{\sigma}} = -F_{ext}, \quad (3.1)$$

where ρ is the density of the plate, ω is angular frequency of vibrations, w is the displacement in direction perpendicular to the plate's surface, $\underline{\underline{\sigma}}$ is the stress tensor, \mathbf{n} is the unit vector normal to the plate's surface and pointing towards the fluid, and F_{ext} denotes external pressure applied to the structure.

The liquid domain is described with the following pressure acoustics equation:

$$\Delta p + \frac{\omega^2}{c_w^2} p = 0, \quad (3.2)$$

where ρ_w and c_w denote the density and acoustic wave velocity of the considered medium.

Equations (3.1) and (3.2) are coupled via following boundary conditions assigned on the solid-fluid interface:

$$\mathbf{n} \cdot \nabla \frac{p}{\rho_w} = \frac{\partial^2 w}{\partial t^2} \quad (3.3)$$

$$\underline{\underline{\sigma}} \cdot \mathbf{n} = p \mathbf{n} \quad (3.4)$$

Equation (3.3) implies the equality of normal accelerations between the adjoining areas of plate and the medium, while Equation (3.4) imposes the equality of action and reaction force values between the domains.

Equations (3.1) and (3.2) with boundary conditions (3.3) and (3.4) were solved to find the natural frequencies of the submerged plate and corresponding structural mode shapes. Numerical simulations have been performed for three different situations: plate with surrounding water, plate with surrounding air, and for plate without any external load assumed. The low-frequency range only was considered, taking into account the first eight eigenmodes (without rigid body motion solution at frequency $f = 0$).

The problem has been solved using the Finite Element Method and the COMSOL Multiphysics software. The acoustic domain was represented by a

hemisphere with a radius large enough to approximate the free-field environment and plane wave radiation boundary condition set on the surface. The base plane of the hemisphere represented an infinite baffle with a rigid wall boundary condition. The plate was positioned in the center of the base plane with all of the edges free and was in contact with the acoustic medium on the one side. The geometry and discretization of the problem are presented in Figure 3.1. The assumption of far-field approximation by the hemisphere was validated by comparing the results of simulations obtained for different radii values.

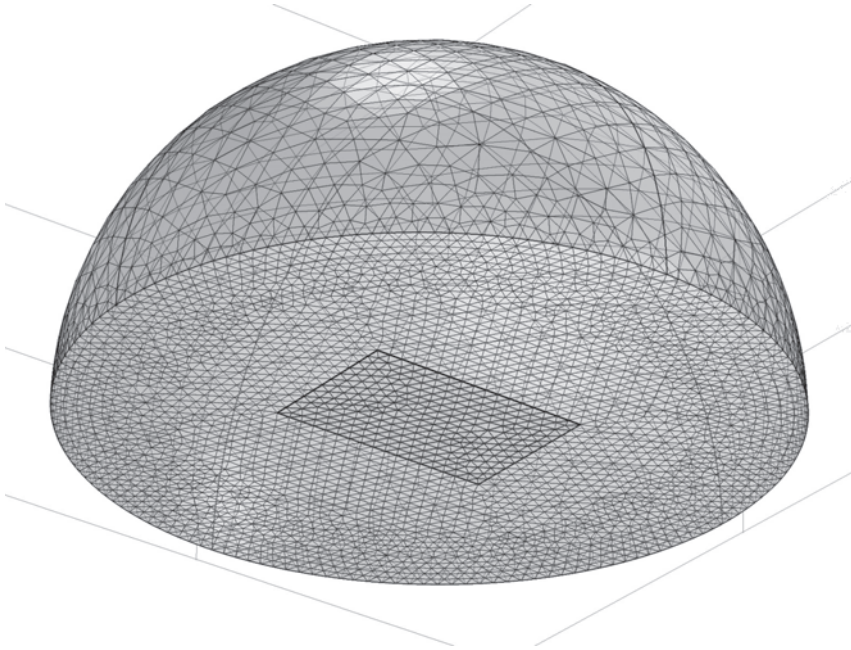


Figure 3.1. Baffled plate in contact with water on its one side: geometry and discretization.

3.2.3 Results and discussion

Numerical simulations have been performed for three different situations: plate with surrounding water, plate with surrounding air, and plate without any external load assumed. The latter involved a simple, two-dimensional model of the structure without a medium and baffle. It has been found that the shapes of the corresponding structural modes in all three considered cases - for air, water and the in vacuo case - showed no significant differences. The obtained results are presented in figure 3.2. The corresponding eigenfrequencies, determined for

each case, are presented in Table 3.1.

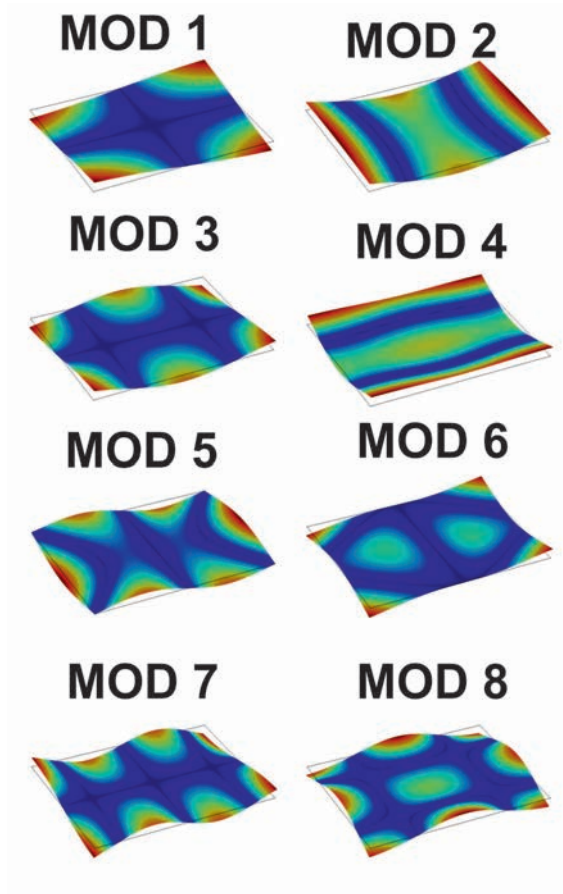


Figure 3.2. Mode shapes of the first eight forms of vibrations of the plate with all edges free (without rigid body motion solution at frequency $f = 0$).

Eigenfrequencies computed for the air and for the in vacuo case are almost the same, the differences are small enough to be considered as numerical errors - especially taking into account the fact that higher values were obtained for the case without inertial loading. This conclusion confirms that omitting the influence of the acoustic medium does not significantly affect the results of the vibrational analysis performed for relatively small plate structures submerged in a light fluid in the low-frequency range.

Submerging the plate in water causes a reduction of the values of natural frequencies by the factor of approximately 3, as compared to the results obtained

Mode number	Eigenfrequency [Hz]		
	No load	Air	Water
1	54,77	54,55	15,57
2	58,44	58,26	15,97
3	126,46	126,74	40,01
4	136,47	136,4	42,63
5	157,95	161,33	51,73
6	183,43	184,38	60,61
7	234,9	239,5	82,54
8	269,98	274,75	97,07

Table 3.1. Eigenfrequencies determined numerically for three different cases.

for two other considered cases. This observation implies the fact that if the acoustic medium is a heavy fluid, then the influence of a inertial loading cannot be omitted and the numerical model has to include the coupling between the structure and the environment. Solving such a problem is numerically expensive and requires discretization of large volume of the ambient space.

The described numerical model can also be used to determine the acoustic radiation characteristics of the vibrating plate. Basing on the solution of Equation (3.2) in the fluid domain, the distribution of the acoustic pressure in ambient space can be computed. The results concerning the plate having contact with water on one side for four selected eigenmodes are presented in figure 3.3.

As it can be seen, close to the surface of the structure the sound field distribution is complex and radiation characteristics vary significantly for different forms of vibrations. Numerous local maxima and minima of the amplitude of acoustic pressure are observed. The further from the surface, the acoustic radiation pattern becomes more regular. The sound propagation velocity in water is over four times greater than in air and thus the dimensions of the submerged plate compared to the wavelength in the considered low-frequency range are low. For that reason the plate - regarded as an acoustic antenna - reveals no significant directivity gain. The far-field radiation characteristics of baffled plate structures are described more in detail in the following section.

3.3 Far-field acoustic radiation of a baffled plate

Far-field acoustic radiation of a rectangle-shaped plate structure placed in an infinite, rigid baffle is considered. Such structures and boundary conditions

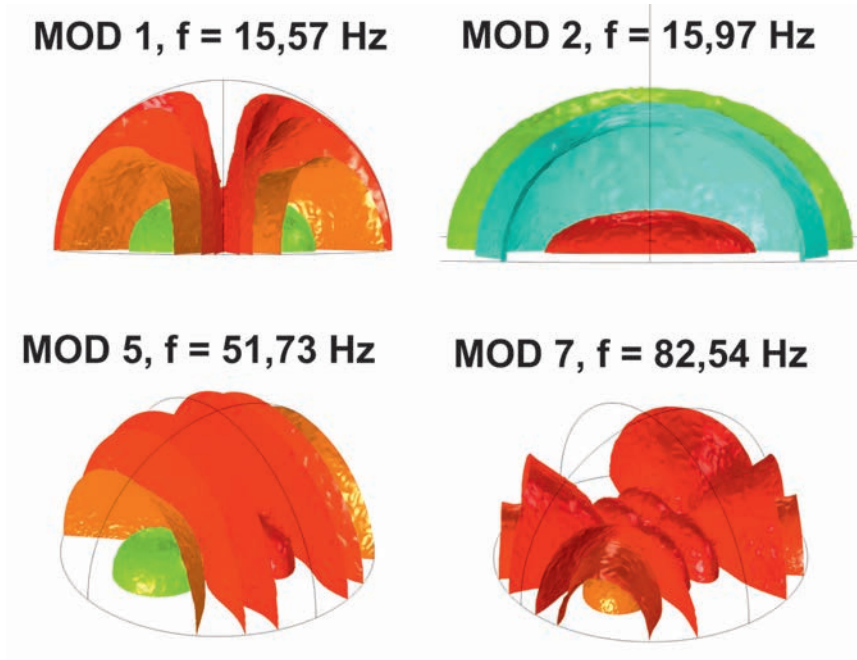


Figure 3.3. Distribution of the amplitude of acoustic pressure in the near-field zone of the vibrating plate structure submerged in water.

provide a starting point for numerous scientific investigations devoted to active vibroacoustic control systems and methods (see, for example, [11, 26, 29]). This is due to the fact that the sound field distribution in this case can be described with relatively simple analytical formulas. The foundations of the relevant mathematical model have been developed as far back as in the eighteenth century by Lord Rayleigh [56]. However, the experimental validation of the results may in general turn out to be troublesome. This is especially true in the considered case of arbitrary boundary conditions, as, for example, the assumption of mechanically free edges of the structure is hardly compatible with the requirement of no acoustic gap between the plate and the baffle. For that reason, the described approach is only briefly introduced in the present study and exemplified with the results of relevant numerical simulations, in order to exhibit some specific features of the generated sound field distribution in the low-frequency range and to demonstrate the contrast in the computational complexity as compared to a more general case of unbaffled plate that will be described in the following sections. Additionally, the presented formulas may also be used in deriving the modal radiation coefficients, introduced in Section 5.1, for computation of the

cost function in the control equations.

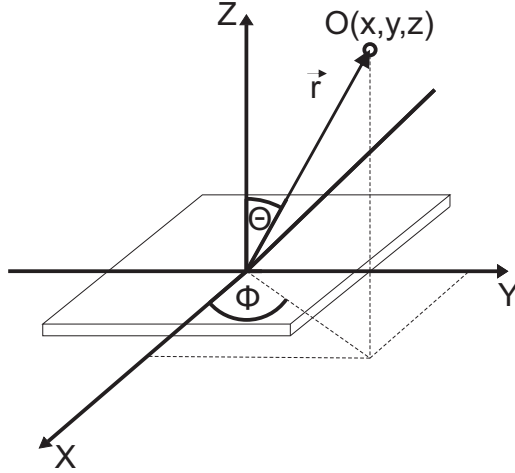


Figure 3.4. Acoustic radiation of a baffled plate – geometry of the problem.

It is assumed that the plate is excited to vibrate by a harmonic force. Due to the structural-acoustic coupling the induced flexural waves in the structure cause the radiation of the acoustic waves in air (which is assumed to be the acoustic medium of the ambient space). The geometry of the considered problem is illustrated in Figure 3.4. The acoustic pressure p in any point \mathbf{r} of the far-field ambient half-space with given radial coordinates (r, ϕ, Θ) is described using the Rayleigh's integral with following equation [11, 53, 76]:

$$p(\mathbf{r}) = \frac{i\omega\rho_a e^{ik_a|\mathbf{r}|}}{2\pi|\mathbf{r}|} \sum_{n=1}^N \left(W_n \int_0^a \int_0^b \Phi_n(x, y) e^{ik_a\Delta r} dx dy \right), \quad (3.5)$$

where k_a is the wavenumber of the acoustic wave, ρ_a is the density of air, W_n is the amplitude of the vibrational mode n with the shape function Φ_n and Δr is approximated by the following relation:

$$\Delta r \approx -x \sin \Theta \cos \phi - y \sin \Theta \sin \phi \quad (3.6)$$

Considering the vibrating plate as an acoustic antenna, the far-field radiation beam pattern describing its directional characteristics may be introduced. The relevant function is defined as a ratio of the amplitude of the generated acoustic

pressure in a given direction (ϕ, Θ) to the value of the amplitude of the acoustic pressure in antenna boresight direction (ϕ_B, Θ_B) :

$$\Xi(\phi, \Theta) = \left[\frac{p(r, \phi, \Theta)}{p(r, \phi_B, \Theta_B)} \right]_{r=\text{const}}. \quad (3.7)$$

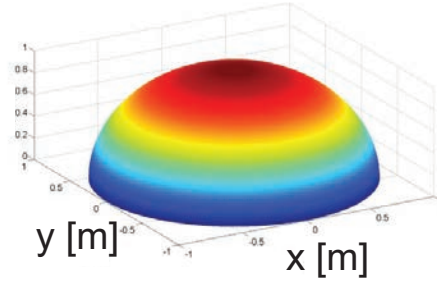
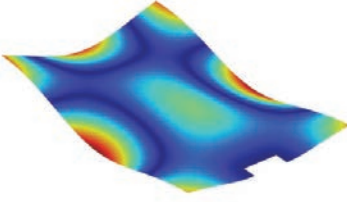
The radiation beam pattern is frequency-dependent, hence, in order to compute the far-field acoustic directional characteristics of the baffled, vibrating plate, both the amplitudes of the involved modal components and the excitation frequency have to be known.

The acoustic beam patterns of the considered structures have been determined numerically on an example of a thin, plate structure made of aluminum placed in an infinite, rigid baffle. The plate is 40 cm long, 25 cm wide, and 1 mm thick. It is assumed that the structure is clamped at some part of one of its shorter edges and all the other boundaries are free. The computations were carried out in two stages. First, the eigenfrequencies and the shapes of the corresponding structural vibration modes had been determined using the finite element analysis. To this end, COMSOL MULTIPHYSICS software had been used and the solutions obtained for the two-dimensional plate model had been saved in a file. Based on the computed vibrational characteristics, the far-field acoustic pressure distribution was determined using the relations (3.5) and (3.6). The results from the file were imported by a MATLAB script and numerical integration over the relevant regions as carried out for different structural modes and vibration frequencies.

Some exemplary results of the numerical simulations are presented in Figure 3.5. Three-dimensional acoustic beam patterns for two exemplary structural modes of the thin plate structure vibrating at frequency 400 Hz are shown. As it can be seen, the results may differ significantly for various forms of vibrations.

The examples presented in Figure 3.5 are the representative class of solutions of the described problem. Due to the relatively small dimensions of the considered plate structure as compared to the acoustic wavelength in the low-frequency range, all the modes reveal either acoustic monopole- or dipole-like radiation beam patterns. The “dipole” modes are found to be weak acoustic radiators and are in general connected with the antisymmetric shape functions of the corresponding forms of vibrations. In contrast, the efficiency of far-field sound radiation of the “monopole” modes may be very high. Such observations are essential in terms of view of the active vibroacoustic control of the considered structures.

Structural mode nr 10



Structural mode nr 14

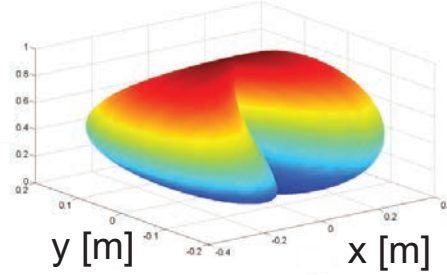
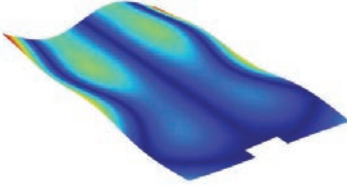


Figure 3.5. Three-dimensional acoustic radiation beam patterns of two exemplary structural modes of the thin plate structure vibrating at frequency 400 Hz.

3.4 Free-field acoustic radiation – BEM model

3.4.1 Theoretical background

The geometry of the considered problem is presented in Figure 3.6. It is assumed that the considered rectangular plate is positioned in the plane $z = 0$ of the global XYZ coordinate system and that one of its edges has the coordinates (x, y) equal $(0, 0)$. The plate is thin and its thickness is neglected in further considerations. Due to the harmonic character of the considered excitation force and taking into account the fact that the system is linear and undamped, the acoustic pressure p at any point \mathbf{r} of the surrounding space satisfies the Helmholtz equation:

$$\Delta p + k^2 p = 0, \quad (3.8)$$

where k is the wavenumber of the radiated acoustic wave.

We solve the equation (3.8) for Neumann boundary conditions imposed on the whole surface Ω of the considered plate:

$$\left. \frac{\partial p}{\partial n} \right|_{(x,y)} = -i\omega\rho_a V_n(x, y) \quad \text{for } (x, y) \in \Omega. \quad (3.9)$$

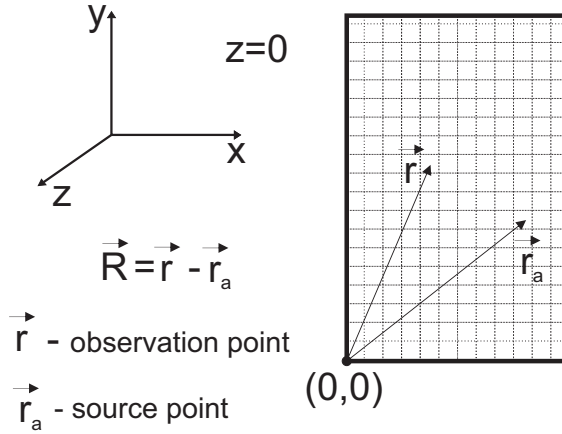


Figure 3.6. The geometry of the considered problem: plate domain.

Here $V_n(x, y)$ is the amplitude of the normal velocity of the surface of the plate at a point with coordinates (x, y) and ω is the angular frequency of the radiated acoustic wave. For the sake of brevity the coordinates will be omitted in the formulas presented further, unless they are important for clarity of the description. The distribution of the amplitude value of the normal velocity on the surface Ω is computed directly from the Finite Element Method model of the plate vibrations and scaled to the results of measurements carried out using a laser vibrometer.

The considered problem of the plate radiation in the free space is an exterior acoustic problem with an open boundary surface. It may be regarded as a special case of an exterior problem with a closed boundary by considering both sides of the plate as separate surfaces denoted Ω^+ and Ω^- , where $\Omega = \Omega^+ \cup \Omega^-$. We now introduce the following quantities:

- the single layer potential:

$$\sigma(\mathbf{r}_a) = \frac{\partial p(\mathbf{r}_a^+)}{\partial n} - \frac{\partial p(\mathbf{r}_a^-)}{\partial n}, \tag{3.10}$$

- the double layer potential:

$$\mu(\mathbf{r}_a) = p(\mathbf{r}_a^+) - p(\mathbf{r}_a^-), \tag{3.11}$$

where r_a^+ and r_a^- denote the position of the acoustic point sources at surfaces Ω^+ and Ω^- , respectively. We can now rewrite the boundary conditions (3.9) as

follows:

$$\frac{\partial p(\mathbf{r}_a^-)}{\partial n} = -i\omega\rho_a V_n(\mathbf{r}_a^-) \quad \text{on } \Omega^-, \quad (3.12)$$

$$\frac{\partial p(\mathbf{r}_a^+)}{\partial n} = -i\omega\rho_a V_n(\mathbf{r}_a^+) \quad \text{on } \Omega^+. \quad (3.13)$$

By assuming for thin plate $\Omega^+ \approx \Omega^- \approx \Omega$ and substituting Equations (3.12) and (3.13) into Equation (3.10) we obtain:

$$\sigma = 0 \quad \text{and} \quad \frac{\partial p}{\partial n} = -i\omega\rho_a V_n \quad \text{on } \Omega. \quad (3.14)$$

The acoustic pressure at any point of the ambient space indicated by a vector \mathbf{r} is described with the following boundary integral formulation [68]:

$$p(\mathbf{r}) = \int_{\Omega} \mu(\mathbf{r}_a) \frac{\partial G(\mathbf{r}, \mathbf{r}_a)}{\partial n} d\Omega(\mathbf{r}_a) \quad (3.15)$$

where G is the Green's function, which satisfies the following equation:

$$\Delta G(\mathbf{r}, \mathbf{r}_a) + k^2 G(\mathbf{r}, \mathbf{r}_a) = \delta(\mathbf{r} - \mathbf{r}_a), \quad (3.16)$$

where $\delta(\cdot)$ denotes the Dirac delta function. The considered fundamental solution should also satisfy Sommerfeld radiation condition:

$$\lim_{|\mathbf{r} - \mathbf{r}_a| \rightarrow \infty} |\mathbf{r} - \mathbf{r}_a| \left(\frac{\partial G(\mathbf{r}, \mathbf{r}_a)}{\partial |\mathbf{r} - \mathbf{r}_a|} + ikG(\mathbf{r}, \mathbf{r}_a) \right) = 0. \quad (3.17)$$

Fulfillment of the condition (3.17) ensures that the obtained solution is valid for the free-field acoustic environment. The considered Green's function in the three-dimensional space has the form:

$$G(\mathbf{r}, \mathbf{r}_a) = \frac{e^{-ik|\mathbf{r} - \mathbf{r}_a|}}{4\pi |\mathbf{r} - \mathbf{r}_a|}. \quad (3.18)$$

By taking into account the boundary conditions (3.14) the integral equation (3.15) can be rewritten as:

$$-i\omega\rho_a V_n = \int_{\Omega} \mu(\mathbf{r}_a) \frac{\partial^2 G(\mathbf{r}, \mathbf{r}_a)}{\partial n(\mathbf{r}) \partial n(\mathbf{r}_a)} d\Omega(\mathbf{r}_a). \quad (3.19)$$

Equation (3.19) has to be solved for the unknown double layer potential μ on Ω . To this end, the equivalent variational statement is used, namely, the solution μ will minimize the following functional [68]:

$$\mathfrak{J} = 2 \int_{\Omega} i\omega\rho_a\mu(\mathbf{r}) V_n(\mathbf{r}) d\Omega(\mathbf{r}) + \int_{\Omega} \int_{\Omega} \mu(\mathbf{r}) \mu(\mathbf{r}_a) \frac{\partial^2 G(\mathbf{r}, \mathbf{r}_a)}{\partial n(\mathbf{r}) \partial n(\mathbf{r}_a)} d\Omega(\mathbf{r}) d\Omega(\mathbf{r}_a), \quad (3.20)$$

The properties of the Green's function and the continuity of μ allow to rewrite the second, highly singular integral in an equivalent, less singular form, better suited for numerical calculations [68, 69]:

$$\begin{aligned} & \int_{\Omega} \int_{\Omega} \mu(\mathbf{r}) \mu(\mathbf{r}_a) \frac{\partial^2 G(\mathbf{r}, \mathbf{r}_a)}{\partial n(\mathbf{r}) \partial n(\mathbf{r}_a)} d\Omega(\mathbf{r}) d\Omega(\mathbf{r}_a) = \\ & \int_{\Omega} \int_{\Omega} G(\mathbf{r}, \mathbf{r}_a) [k^2 \mu(\mathbf{r}) \mu(\mathbf{r}_a) (\mathbf{n}(\mathbf{r}) \cdot \mathbf{n}(\mathbf{r}_a)) - \\ & - ((\nabla \times \mu(\mathbf{r})) \cdot (\nabla \times \mu(\mathbf{r}_a)))] d\Omega(\mathbf{r}) d\Omega(\mathbf{r}_a), \end{aligned} \quad (3.21)$$

where:

$$\nabla \times \mu = \mathbf{n} \times \nabla \mu \quad (3.22)$$

and \mathbf{n} is the unit vector normal to the surface of the boundary plate.

The considered area Ω is discretized into a number n_e of small boundary elements with corresponding areas Ω^e , $e \in \{1, 2, \dots, n_e\}$ and n_n nodes defined at some particular locations of the elements. n_{en} is the number of nodes belonging to a single element. Note that the elements may (and usually do) share common nodes, so, in general, $n_n \neq n_e n_{en}$. It is assumed that the sought double layer potential at every single element can be approximated by a product of the unknown nodal values μ_i and the element shape functions N_i^e (which take the value of 1 in the corresponding node i and are 0 in all other nodes), namely:

$$\mu(\mathbf{r}) \approx \hat{\mu}(\mathbf{r}) = \sum_{i=1}^{n_{en}} N_i^e(\mathbf{r}) \mu_i \quad (\mathbf{r} \in \Omega^e). \quad (3.23)$$

The discretized form of the functional (3.20) can be now written as:

$$\mathfrak{J} = \sum_{i=1}^{n_n} \sum_{j=1}^{n_n} \mu_i B_{ij} \mu_j - 2 \sum_{i=1}^{n_n} \mu_i C_i, \quad (3.24)$$

where:

$$B_{ij} = \int_{\Omega_i} \int_{\Omega_j} G(\mathbf{r}, \mathbf{r}_a) [k^2 N_i(\mathbf{r}) N_j(\mathbf{r}_a) - (\nabla N_i(\mathbf{r}) \times \mathbf{n}) \cdot (\nabla N_j(\mathbf{r}_a) \times \mathbf{n})] d\Omega_i(\mathbf{r}) d\Omega_j(\mathbf{r}_a) \quad (3.25)$$

and

$$C_i = -i\omega\rho_a V_n^i \int_{\Omega_i} N_i(\mathbf{r}) d\Omega_i(\mathbf{r}), \quad (3.26)$$

where V_n^i denotes the normal velocity at point i . The global shape functions $N_i(\mathbf{r})$ are defined in the whole boundary surface Ω . Inside every element to which node i belongs functions N_i are identical to the corresponding local shape functions N_i^e and are zero in all other domains. Thus, the integration surfaces Ω_i and Ω_j include all of the elements that contain interpolation nodes i and j respectively.

To find the double layer potential values in the specified nodes using the variational scheme the following equation is solved:

$$\frac{\partial \mathfrak{J}}{\partial \mu} = 0, \quad (3.27)$$

which yields:

$$\underline{\underline{B}} \mu = \mathbf{C}, \quad (3.28)$$

where $\underline{\underline{B}}$ is the $(n_n \times n_n)$ size matrix composed of elements B_{ij} described by relation (3.25), \mathbf{C} is the $(n_n \times 1)$ vector composed of elements C_i described by relation (3.26) and μ is the $(n_n \times 1)$ vector of unknown nodal values of the double layer potential.

Now, the acoustic pressure in any point of the ambient space is given with the following relation:

$$p(\mathbf{r}) = \mathbf{D}^T \mu, \quad (3.29)$$

where the elements of vector \mathbf{D} are given with the following formula [68]:

$$D_i = \int_{\Omega} N_i(\mathbf{r}_a) \frac{\partial G(\mathbf{r}, \mathbf{r}_a)}{\partial \mathbf{n}(\mathbf{r}_a)} d\Omega(\mathbf{r}_a). \quad (3.30)$$

Assuming that the observation point indicated by the vector \mathbf{r} has coordinates (x, y, z) and the source point on the plate indicated by the vector \mathbf{r}_a has coor-

dinates $(x_a, y_a, 0)$ the normal derivative of Green's function is equal:

$$\frac{\partial G(\mathbf{r}, \mathbf{r}_a)}{\partial \mathbf{n}(\mathbf{r}_a)} = \frac{ze^{-ik\sqrt{(x-x_a)^2+(y-y_a)^2+z^2}} \left(-1 - ik\sqrt{(x-x_a)^2+(y-y_a)^2+z^2} \right)}{\left(\sqrt{(x-x_a)^2+(y-y_a)^2+z^2} \right)^3}. \quad (3.31)$$

After solving Equation (3.28) with the coefficients (3.25) and (3.26) for the unknown nodal values μ_i of the double layer potential in the whole considered plate domain Ω , Equation (3.29) is solved only for those points of the ambient space in which the values of the acoustic pressure are sought.

3.4.2 Implementation – the algorithm

An original, dedicated algorithm for computation of the free-field acoustic radiation characteristics of vibrating rectangular thin plate structures has been developed and tailored to exploit the simple geometry of the considered problem (see Fig. 3.6). The algorithm is based on the IVBEM method and allows to significantly reduce computational time and cost, as compared to a straightforward implementation of the relevant formulas. The details of the proposed approach are described further.

The domain Ω is divided into n_e identical, first-order rectangular boundary elements. The elements are arranged in n_{row} rows and n_{col} columns. The resolution of the division can be adapted to the considered form of vibrations with an adequate reserve as the computation time and cost will be significantly reduced by taking the advantage of the occurring symmetries. Inside every single element a local coordinate system (ξ, η) , $\xi \in \langle -1; 1 \rangle$, $\eta \in \langle -1; 1 \rangle$ is defined, with axes parallel to the X and Y axes of the global coordinate system respectively.

The application of the linear shape functions definitely ensures the convergence of solution, as they satisfy the completeness and compatibility conditions for the considered problem [68]. The chosen functions defined for any boundary element e are as follows:

$$\begin{aligned} N_1^e(\xi, \eta) &= \frac{1}{4}(1 - \xi)(1 - \eta), \\ N_2^e(\xi, \eta) &= \frac{1}{4}(1 + \xi)(1 - \eta), \\ N_3^e(\xi, \eta) &= \frac{1}{4}(1 + \xi)(1 + \eta), \\ N_4^e(\xi, \eta) &= \frac{1}{4}(1 - \xi)(1 + \eta). \end{aligned} \quad (3.32)$$

Basing on the chosen element shape functions and taking into account the fact that due to the considered geometry and mesh properties a single interpolation node can belong to one, two or four neighbouring boundary elements, the coefficients B_{ij} , C_i , and D_i are computed using equations (3.25), (3.26) and (3.31). The surface integrals are determined numerically using the four-point Gauss integration scheme, except for the cases in which the integration surfaces overlap over the same boundary element. In such a situation the results obtained with the standard numerical method would be burdened with a significant error due to singularities in the integrand. To avoid this obstacle the special algorithm for dealing with such double surface integrals with $\frac{1}{R}$ singularity proposed by Wang and Atalla [69, 77] has been implemented. The algorithm is briefly described below.

Taking into account the form of the Green's function for the considered problem, given with Equation (3.18) and transforming Equation (3.25) into the local coordinate system, the double surface integral over the same boundary element may be expressed as follows:

$$\begin{aligned}
 & \int_{\Omega_i^e} \int_{\Omega_j^e} G(\mathbf{r}, \mathbf{r}_a) [k^2 N_i^e(\mathbf{r}) N_j^e(\mathbf{r}_a) - \\
 & - (\nabla N_i^e(\mathbf{r}) \times \mathbf{n}) \cdot (\nabla N_j^e(\mathbf{r}_a) \times \mathbf{n})] d\Omega_i^e(\mathbf{r}) d\Omega_j^e(\mathbf{r}_a) = \\
 & = \int_{-1}^1 \int_{-1}^1 \int_{-1}^1 \int_{-1}^1 \frac{e^{-ik\mathbf{r}-\mathbf{r}_a}}{4\pi |\mathbf{r} - \mathbf{r}_a|} [k^2 N_i^e(\mathbf{r}) N_j^e(\mathbf{r}_a) - \\
 & - (\nabla N_i^e(\mathbf{r}) \times \mathbf{n}) \cdot (\nabla N_j^e(\mathbf{r}_a) \times \mathbf{n})] J_i J_j d\xi_i d\eta_i d\xi_j d\eta_j,
 \end{aligned} \tag{3.33}$$

where J_i and J_j are the Jacobians of the transformation of the local coordinate system to the global coordinate system which satisfy the following relation:

$$d\Omega_i^e = J_i d\xi_i d\eta_i, \quad d\Omega_j^e = J_j d\xi_j d\eta_j. \tag{3.34}$$

Taking into account the considered geometry:

$$J_i = J_j = \frac{a^e b^e}{4}, \tag{3.35}$$

where a^e and b^e are the length of the edges of the rectangular boundary element e parallel to the X and Y axis of the global coordinate system respectively.

Equation (3.33) can be now rewritten in the following form:

$$\begin{aligned} & \int_{-1}^1 \int_{-1}^1 \int_{-1}^1 \int_{-1}^1 \frac{e^{-ik(\mathbf{r}-\mathbf{r}_a)}}{4\pi|\mathbf{r}-\mathbf{r}_a|} [k^2 N_i^e(\mathbf{r}) N_j^e(\mathbf{r}_a) - \\ & - (\nabla N_i^e(\mathbf{r}) \times \mathbf{n}) \cdot (\nabla N_j^e(\mathbf{r}_a) \times \mathbf{n})] J_i J_j d\xi_i d\eta_i d\xi_j d\eta_j = \\ & = \int_{-1}^1 \int_{-1}^1 \int_{-1}^1 \int_{-1}^1 \frac{f(\xi_i, \eta_i, \xi_j, \eta_j)}{r^e} d\xi_i d\eta_i d\xi_j d\eta_j, \end{aligned} \quad (3.36)$$

where

$$\begin{aligned} f(\xi_i, \eta_i, \xi_j, \eta_j) &= \frac{e^{-ikR}}{4\pi} [k^2 N_i^e(\mathbf{r}) N_j^e(\mathbf{r}_a) - \\ & - (\nabla N_i^e(\mathbf{r}) \times \mathbf{n}) \cdot (\nabla N_j^e(\mathbf{r}_a) \times \mathbf{n})] J_i J_j \frac{r^e}{R}, \end{aligned} \quad (3.37)$$

$$R = |\mathbf{R}| = |\mathbf{r} - \mathbf{r}_a| = \sqrt{(x_i - x_j)^2 + (y_i - y_j)^2}, \quad (3.38)$$

and

$$r^e = \sqrt{(\xi_i - \xi_j)^2 + (\eta_i - \eta_j)^2}. \quad (3.39)$$

The integration variables are converted as follows:

$$x_i = x_p + \frac{a^e(1 + \xi_i)}{2}, \quad (3.40)$$

$$x_j = x_p + \frac{a^e(1 + \xi_j)}{2}, \quad (3.41)$$

$$y_i = y_p + \frac{b^e(1 + \eta_i)}{2}, \quad (3.42)$$

$$y_j = y_p + \frac{b^e(1 + \eta_j)}{2}, \quad (3.43)$$

where (x_p, y_p) are coordinates of the center point of element e . Thus:

$$R(\xi_i, \eta_i, \xi_j, \eta_j) = \sqrt{\left[\frac{a^e}{2}(\xi_i - \xi_j)\right]^2 + \left[\frac{b^e}{2}(\eta_i - \eta_j)\right]^2}. \quad (3.44)$$

The integral (3.36) is computed using four-point numerical scheme described in [77]:

$$\int_{-1}^1 \int_{-1}^1 \int_{-1}^1 \int_{-1}^1 \frac{f(\xi_i, \eta_i, \xi_j, \eta_j)}{r^e} d\xi_i d\eta_i d\xi_j d\eta_j = \sum_{m=1}^{M_m} \sum_{n=1}^{M_n} \sum_{o=1}^{M_o} \sum_{p=1}^{M_p} f(\xi_m, \eta_n, \xi_o, \eta_p) W_{mnop}, \quad (3.45)$$

where:

$$M_m = M_n = M_o = M_p = 4 \quad (3.46)$$

denote the Wang's integration order. The values of weight coefficients W_{mnop} and the coordinates of the integration points $\xi_m, \eta_n, \xi_o, \eta_p$ are given in [77].

The proposed algorithm for determination of the free-field acoustic radiation characteristics of the vibrating plate structure includes the following steps:

1. Generation of a mesh consisting of identical, rectangular elements covering the whole surface of the considered plate with a given resolution,
2. Interpolation of the values of the normal velocities in the nodes basing on the scaled results of the FEM analysis of the eigenvalue problem for the considered plate.
3. Computation of the elements of matrix $\underline{\underline{B}}$ and vectors \mathbf{C} and \mathbf{D} using formulas (3.25), (3.26), (3.30), and (3.31).
4. Solution of Equation (3.28) for the unknown double layer potential values in the interpolation nodes.
5. Solution of Equation (3.29) for the unknown values of the acoustic pressure in selected points of the ambient space.
6. Postprocessing and visualization of the results.

Notice that step 3 is crucial from the point of view of the computational time and cost. It involves each with each element double surface integrals for every corresponding interpolation node to compute the coefficients B_{ij} , and for that reason it is the bottleneck of the whole process, as the number of the required operations increases dramatically with increasing resolution of discretization. Moreover, due to the fact that the coefficients B_{ij} are frequency-dependent, this step of the algorithm has to be repeated for every single considered frequency of vibrations. Thus, it is highly desirable to reduce the duration of this step as much as possible. The following features concerning this problem should be taken into account:

- The Green's function for the considered problem (3.18) is symmetrical with respect to its arguments \mathbf{r} and \mathbf{r}_a .
- The unit vector \mathbf{n} is constant on the whole surface of the boundary plate.
- The Jacobians (3.35) are equal for all elements.
- The values of the double surface integral over a single boundary element (3.36) concerning the same pairs of the shape functions are equal for all elements of the mesh.

Basing on the observations mentioned above two important conclusions regarding the solved equations may be derived. The first, quite obvious, an attribute of the matrix $\underline{\underline{B}}$ that should be noticed is that it is symmetrical. This property actually results from the variational formulation used for the problem and is common for all IVBEM based models. The symmetry of the matrix allows to reduce the number of the computed elements, however, the overall computational cost is still high as the number of required operations increases rapidly with increasing resolution (n_e) of discretization. A more significant reduction of the computational time and cost may be obtained by taking advantage of the simple geometry of the plate domain and the properties of the regular mesh of elements. The second important conclusion is that the value of the double surface integral over two surfaces of the boundary elements in Equation (3.25) in the considered case depends only on the absolute distance between the elements.

Basing on the above observations and conclusions the following algorithm for computation of the elements of matrix $\underline{\underline{B}}$ given with equation (3.25) is proposed:

1. A single mesh element s , $1 \leq s \leq n_e$, in the corner of the rectangular domain is chosen. The values of the following expression are computed for all mesh elements e , $e \in \{1, 2, \dots, n_e\}$ and for all possible pairs of the element shape functions (N_i^s, N_j^e) , $i \in \{1, \dots, 4\}$, $j \in \{1, \dots, 4\}$:

$$\int_{\Omega^s} \int_{\Omega^e} G(\mathbf{r}, \mathbf{r}_a) [k^2 N_i^s(\mathbf{r}) N_j^e(\mathbf{r}_a) - (\nabla N_i^s(\mathbf{r}) \times \mathbf{n}) \cdot (\nabla N_j^e(\mathbf{r}_a) \times \mathbf{n})] d\Omega^s(\mathbf{r}) d\Omega^e(\mathbf{r}_a). \quad (3.47)$$

The results are stored in memory. In the case when $s = e$ the described above four-point special integration scheme (3.33) is used to deal with singularities.

2. For every pair of the mesh interpolation nodes with indices (i, j) , $i \in \{1, \dots, n_n\}$, $j \in \{1, \dots, i\}$ the numbers of the boundary elements to which the nodes belong, distance between the elements, and the corresponding numbers of the element shape functions are determined. The adequate values of the expression (3.47) computed in the previous step of the algorithm are loaded from the memory and added to the values of the corresponding elements B_{ij} .
3. Using the symmetry property of the matrix $\underline{\underline{B}}$ the values from the upper diagonal part are copied to the corresponding elements in the lower diagonal part.

The first step of the algorithm requires $n_{en}^2 n_n$ times computation of the double surface integral given by the expression (3.47). The two following steps are computationally cheap and do not affect significantly the total duration of the process. If only the symmetry property of the matrix $\underline{\underline{B}}$ was used the complexity of the algorithm would be $O(n_{en}^2 n_n^2)$. Taking into account the fact that in practical applications $n_{en} \ll n_n$ and the total number of interpolation nodes is usually of the order 10^2 or greater the savings of computational time and cost associated with the use of the presented algorithm are significant.

The developed algorithm has been implemented using the Matlab environment and tested on a standard PC with a 4-core processor. The total computational time of determining the value of acoustic pressure in a single point of space was less than one minute for a mesh consisting of one thousand elements.

3.5 Experimental investigations, results, and discussion

The experimental investigations regarding the free-field acoustic radiation characteristics have been carried out in an anechoic chamber using a 20 cm wide, 30 cm high, and 1 mm thick rectangular plate made of aluminum. The plate was clamped in the central part of one of its shorter edges while all other edges were free, as presented in Figure 3.7.

The plate was excited to vibrate by a pair of piezoelectric transducers, mounted symmetrically on both sides of the structure and driven with reversely polarized harmonic voltage signal from an amplifier connected to a generator. Low-order vibrational modes with corresponding eigenfrequencies up to 400 Hz were examined. The plate revealed sharp resonant characteristics and acoustic radiation for off-resonant frequencies turned out to be very low.

The amplitude of the acoustic pressure in selected points of the ambient space was measured using a half-inch condenser microphone by Brüel&Kjær (type 4193 with preamplifiers type 2664) connected to the Nexus 2690 conditioning amplifier, from the same manufacturer. The output of the amplifier was connected to an oscilloscope (Tektronix TDS 2004C).

The amplitude of the acoustic pressure was measured along the axis perpendicular to the surface of the plate and passing through its center and in several planes parallel to the plate's surface for different excitation frequencies equal to several selected eigenfrequencies of vibrations. The results of the measurements are presented in Figures 3.8–3.14. Figures 3.8–3.11 present the computed and measured sound pressure level values in the z -axis as functions of the distance from the center point of the plate. The measurements were taken at distances

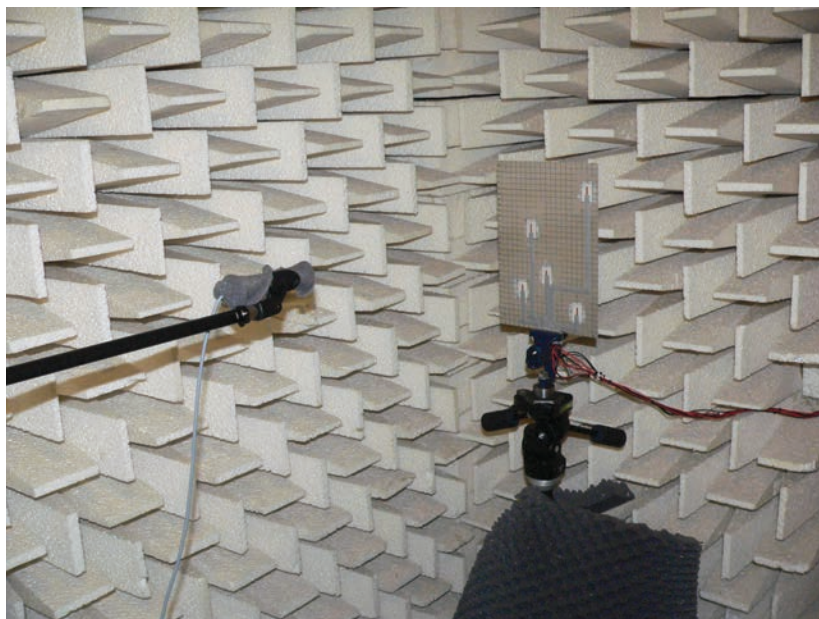


Figure 3.7. Aluminium plate structure used in the experimental investigations in an anechoic chamber.

varying from 1 cm to 1 m. However, in the case of the fifth structural mode (Figure 3.8) the maximum range was shortened to 20 cm due to the low level of the observed amplitude of acoustic pressure. Figures 3.12–3.14 present the computed and measured sound pressure level values in the plane $z=2$ cm. The color graphs illustrate the results of the numerical simulations, while the blue circles show values measured experimentally in the corresponding points of space.

One should notice that to compute the correct, absolute values of the acoustic pressure the normal velocity values introduced as the boundary conditions in the IVBEM model (see Equation (3.9)) should correspond to the true normal velocity amplitudes of the vibrations excited during the experiments. However, by solving the eigenproblem for an undamped system the velocity field is determined with an accuracy of a scalar scaling factor. For that reason the results from the Finite Element Method model of plate vibrations have been scaled to the maximum amplitudes of velocities measured using the laser vibrometer for each vibrational mode, with specified excitation conditions.

The comparison of the measured and computed results reveals a fair agreement between the experiments and numerical predictions. The computed distribution of the sound pressure level in the ambient space and the values of the

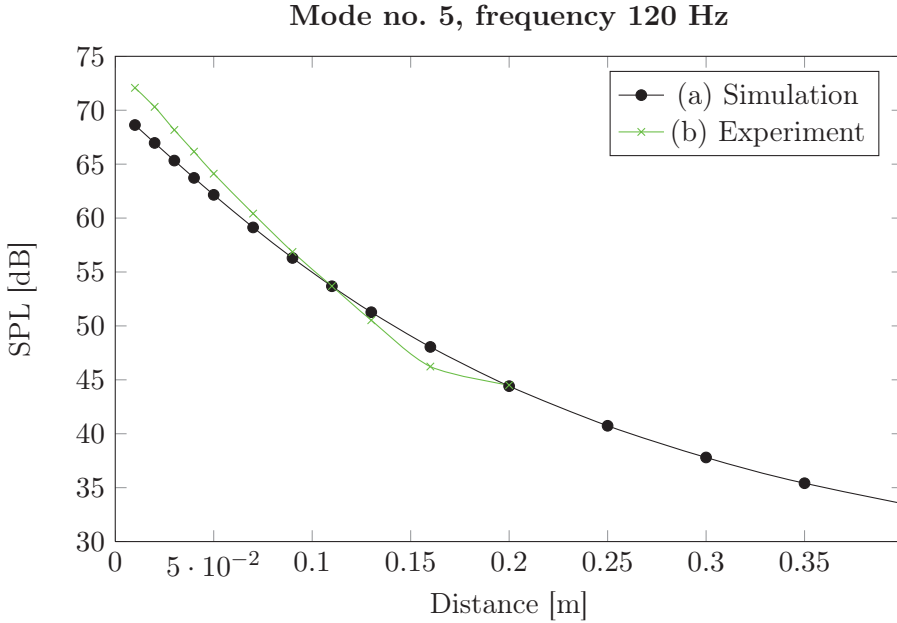


Figure 3.8. Sound pressure level as a function of the distance in the z -axis from the center of the investigated plate structure vibrating in the 5th mode: (a) numerical simulation, (b) measurements.

amplitude of the acoustic pressure have been largely proved correct. However, some significant discrepancies between the simulations and measurements may be also observed (especially see Figures 3.9 and 3.10). The errors result from imperfections in the both laboratory stand (worse low-frequency performance of the anechoic chamber, propagation of vibrations through fastening elements, sound reflections from the measurement equipment) and the developed mechanical and acoustic numerical models (assumption of ideal boundary conditions and material properties, disregarding the influence of the piezoelectric transducers and electrical connections attached to the surface of the plate). The accuracy of the simulations can be probably further increased by improving the described issues.

The agreement between the values obtained numerically and experimentally in general improves with the distance from the plate. This effect is caused by the fact that the complex character of the sound field distribution in the near-field zone promotes the intensification of errors caused by the mentioned imperfections. The results of the measurements carried out in a XY -plane, 2 cm from the surface of the plate (Figures 3.12–3.14) generally agree well with the compu-

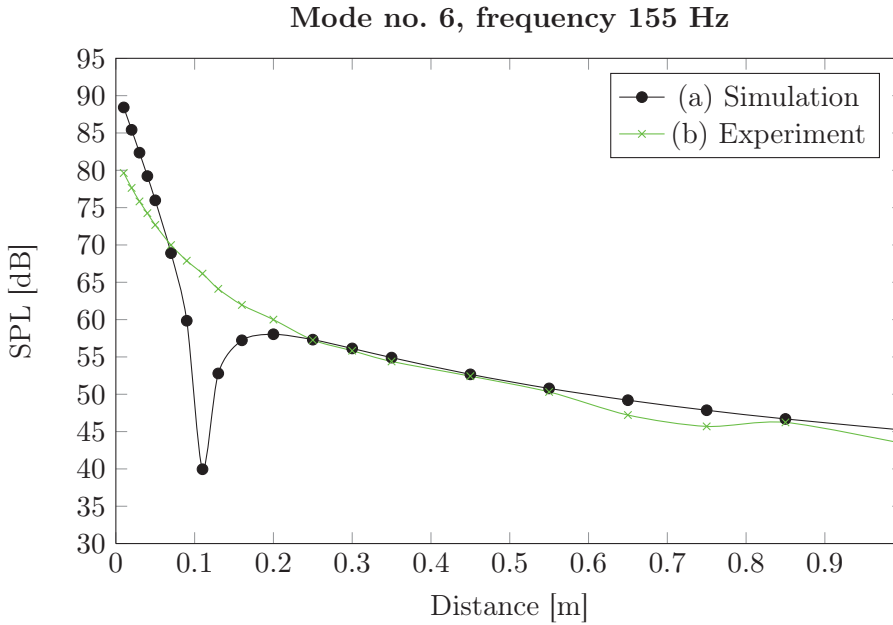


Figure 3.9. Sound pressure level as a function of the distance in the z -axis from the center of the investigated plate structure vibrating in the 6th mode: (a) numerical simulation, (b) measurements.

tations. Significant discrepancies reaching up to few dB are observed in several isolated points (especially close to the edges), but the character of the distribution of the sound pressure level in the immediate vicinity of the structure is in all cases reflected correctly. The numerical predictions become most reliable at distances greater than about 10–20 cm from the surface of the considered structure. Beyond this range about 6 dB drop in the sound pressure level with doubling the distance is observed (see Figures 3.9–3.14). This corresponds to the free-field spherical wave propagation.

3.6 Conclusions

Various issues regarding the structure-borne sound generation have been discussed in the present chapter. The mechanism underlying the acoustic radiation from vibrating plates is the coupling between the structure and the surrounding acoustic medium. Detailed formal description and modeling of the occurring phenomena is complex, due to the bidirectional interaction between solid and

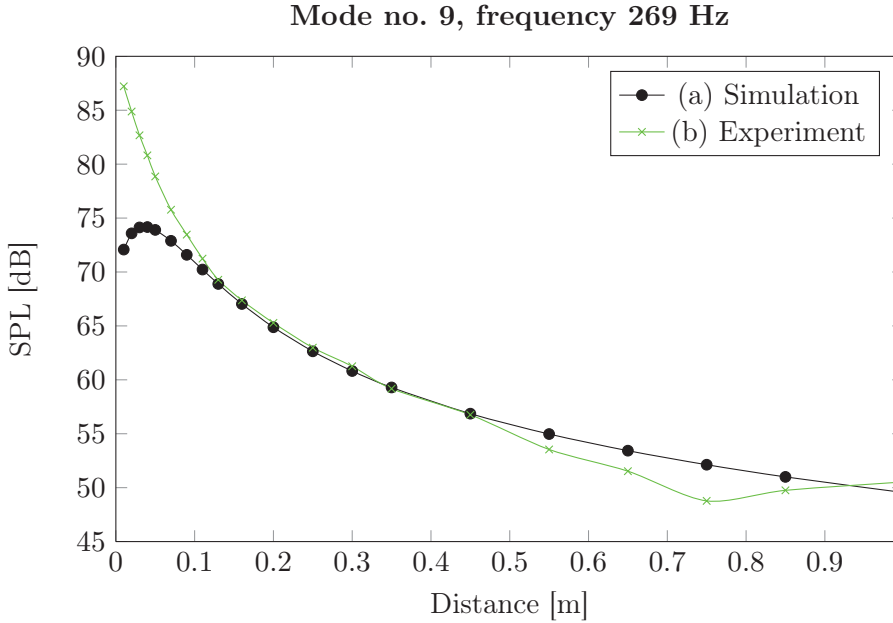


Figure 3.10. Sound pressure level as a function of the distance in the z -axis from the center of the investigated plate structure vibrating in the 9th mode: (a) numerical simulation, (b) measurements.

acoustic domains. However, as it has been shown in Section 3.2 in the case of relatively small structures (as compared to the radiated acoustic wavelength) submerged in light fluids (such as, for example, air) the influence of the inertial loading introduced by the medium is small and can be neglected. This conclusion allows for a significant simplification of the considered problem, by carrying out an independent analysis for the vibration and acoustic radiation characteristics.

Two important cases of structure-born sound generation have been discussed and analyzed, namely, free-field acoustic radiation of baffled and unbaffled vibrating plate structures. As it has been shown in Section 3.3, in the first case the distribution of acoustic pressure in the far-field can be modeled using relatively simple analytical formulas, given with Equations (3.5) – (3.6). In contrast, in the latter case no analytical solutions are known and the problem has to be solved numerically. The relevant procedure has been described in Section 3.4.1. Among a variety of numerical methods capable of handling the considered problem the Indirect Variational Boundary Element Method has been chosen as the most appropriate one. A novel, dedicated algorithm of implementation of this method has been proposed in section 3.4.2. The algorithm allows for a signifi-

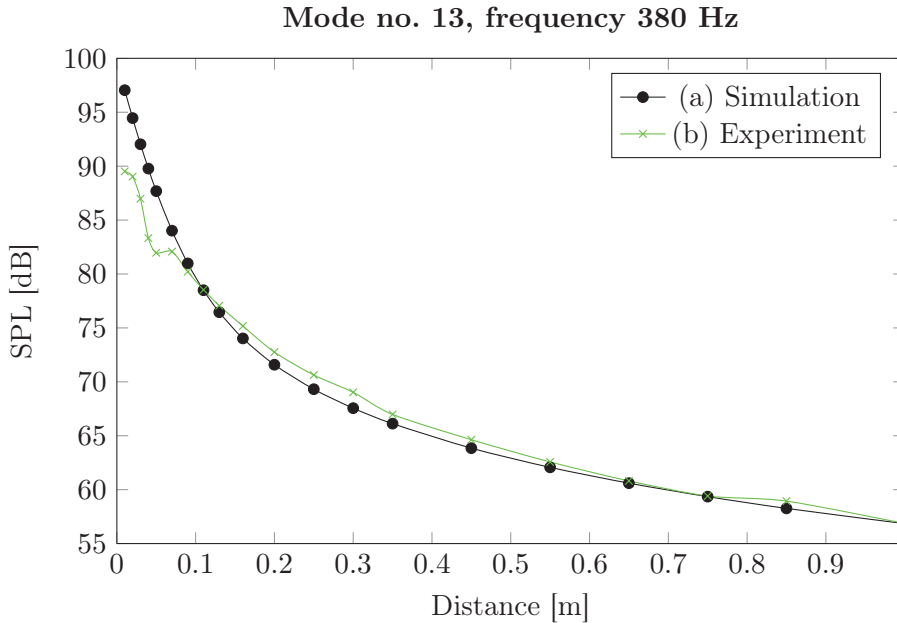


Figure 3.11. Sound pressure level as a function of the distance in the z -axis from the center of the investigated plate structure vibrating in the 13th mode: (a) numerical simulation, (b) measurements.

cant reduction of computational time and cost, as compared to straightforward implementation of the relevant formulas by taking the advantage of a simple geometry of the considered problem and the symmetries between the elements of matrices.

The results of the numerical simulations on the free-field acoustic radiation characteristics of a thin, rectangle-shaped vibrating plate have been validated experimentally. The empirical investigations were carried out in an anechoic chamber and regarded different forms of vibrations excited at the corresponding eigenfrequencies of the examined structure. The amplitude of the acoustic pressure was measured at different points of the ambient space using microphone and the proper conditioning and amplifying electronics. The results of the measurements in general agreed with the numerical predictions, however, some significant discrepancies have also been observed at points close to the surface of the plate. The reason for that is the fact that the complex character of the acoustic pressure distribution in the near-field region promotes the influence of the imperfections in both the laboratory stand and numerical models. Nevertheless, taking into account the overall fair agreement between the results

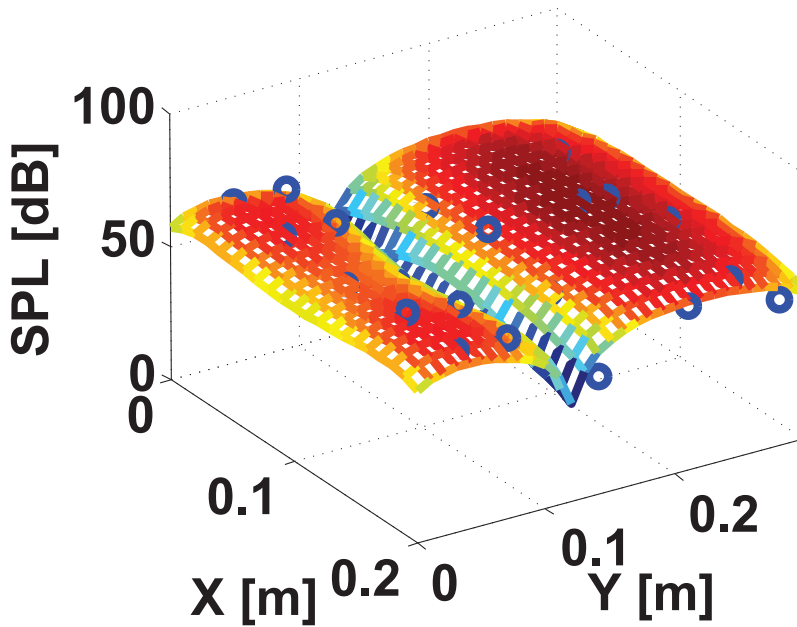


Figure 3.12. The distribution of sound pressure levels [dB] in the plane $z = 2$ cm for vibrational mode no. 5 with frequency $f = 120$ Hz. The color graph illustrates the results of the numerical simulations, while the blue circles show the values measured experimentally in corresponding points of space.

and a high performance of the developed algorithm, it may be regarded as a useful and effective tool in analysis of the free-field acoustic radiation characteristics of vibrating plate structures with arbitrary boundary conditions.

The results and conclusions presented in this chapter are crucial from the point of view of the whole study, as they allow to associate the vibrational characteristics of the structure with the parameters of the generated acoustic pressure field in the ambient space.

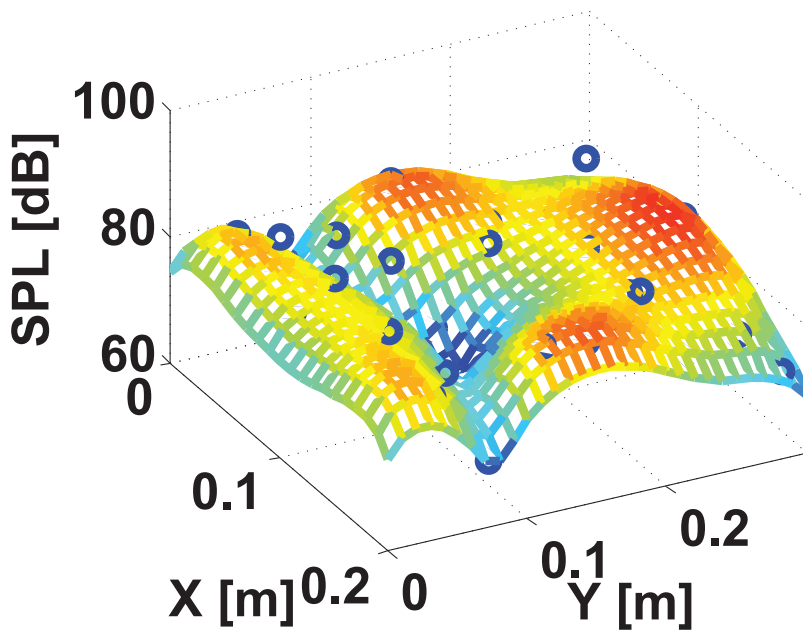


Figure 3.13. The distribution of sound pressure levels [dB] in the plane $z = 2$ cm for vibrational mode no. 9 with frequency $f = 269$ Hz. The color graph illustrates the results of the numerical simulations, while the blue circles show the values measured experimentally in corresponding points of space.

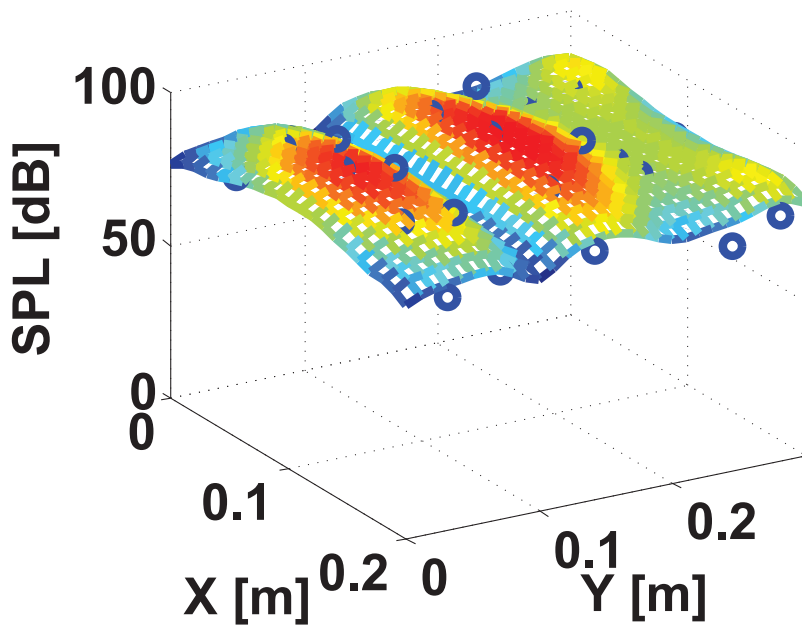


Figure 3.14. The distribution of sound pressure levels [dB] in the plane $z = 2$ cm for vibrational mode no. 11 with frequency $f = 320$ Hz. The color graph illustrates the results of the numerical simulations, while the blue circles show the values measured experimentally in corresponding points of space.

Piezoelectric sensors and actuators

4.1 State of the art, assumptions, and general description

Sensors and actuators are the necessary elements of all closed-loop control systems. In the applications considered in the present study, concerning active vibroacoustic control systems, sensors allow to determine a current state of vibrating structures (or some parameters of the generated acoustic field), whereas actuators are used to apply the control loads. Among a variety of available techniques of implementation, one of the most commonly used are piezoelectric transducers attached to the surface of structures under control. Such a solution preserves compactness of the controlled system while providing good electro-mechanical properties. The electric signals from sensors are processed by a control unit and, based on the results, the optimal parameters of the excitation signals driving actuators are determined. However, assuming that the parameters of the external excitation – which is the primary source of the vibrations – are unknown, the information obtained from the sensors is never complete, that is: as the number of sensors and their areas are limited to some reasonable (finite) values, the gathered data would not allow to possess a complete knowledge about the parameters of the vibrations of the considered structure in any possible case. On the other hand, for the very similar reasons, the control system is not able to excite any arbitrarily chosen form of vibrations using the finite number of actuators.

The present chapter focuses on issues regarding the utilization of small rectangle-shaped piezoelectric transducers as both sensors and actuators in active vibration and vibroacoustic control systems of beam, plate and panelled structures. A new form of a theoretical description, suitable for further derivation of the control equations, is proposed. The modal sensitivity functions of sensors and the modal selectivity functions of actuators are introduced to describe their ability for sensing and exciting specific structural modes of the structures. The presented approach – in contrast to most studies described in

literature – is elaborated and tested for plates with arbitrary (non-homogeneous) boundary conditions; moreover, due to a high level of generality of the proposed form of description it should work for structures of more complex geometries than rectangular plates. The introduced functions are used to model and analyze performance and stability of the active vibroacoustic control system presented in Chapter 5. A relevant theoretical background for sensors and actuators is presented in Sections 4.2 and 4.3, respectively.

Many of the studies devoted to the field of active vibration and vibroacoustic control focus on specific types of structures, which may be accurately described using analytic formulas – like, for example, beams or simply supported plates. Solutions obtained for such cases allowed to design piezoelectric sensors and actuators sensitive only to specific sets of structural modes [11] or even to a single structural mode [78, 79] by changing the shapes, sizes and/or locations of the transducers. However, the results of these investigations cannot be easily generalized into a more general case of plates with arbitrary boundary conditions of support.

Taking into account the parameters of a closed-loop feedback control system it is desirable to use collocated piezoelectric sensor-actuator pairs. Two different solutions which ensure this feature can be found in literature. The first one – which is simpler and more practical, yet not always feasible due to the possible lack of access to both sides of a structure – is to attach the transducers symmetrically to the both surfaces of a thin beam or plate [11, 80]. The second solution involves the use of a single piezoelectric element as sensor and actuator simultaneously [46, 81–84]. The advantages of such a solution with respect to the functionality of the control system are significant, but the necessary complications of the corresponding electronic circuits together with a requirement to meet very stringent parameters make it impractical.

The shapes of the piezoelectric transducers and their locations on the surface of the structure determine the sets of the vibrational mode components available by changing the gains of the feedback loops in a specified, limited range of values. Optimization algorithms for the placement of sensors and actuators may be based on various cost functions depending on the type of structure, its purpose, and also some restrictions related with the usage of various types of transducers. The state of the art in this field is well documented in corresponding review papers (see, for example, [85–87]). Again, the majority of relevant scientific investigations is focused on thin beams [88, 89] and plates with specific boundary conditions (simply supported [90, 91], clamped [92, 93], cantilevered [92, 94]). Other approaches also usually impose some restrictions on the structure mounting parameters, like, for example, plates with arbitrary

but homogeneous boundary conditions along the edges [95]. The optimization problem is usually solved numerically with different iterative algorithms. Due to the fact that the piezo-transducers are permanently bound to the surfaces of the controlled structures and their locations have to be chosen at the stage of the control system design, it is necessary to analyze in advance their parameters and probable control strategies.

Results of analytical solutions and numerical simulations concerning modal parameters of piezoelectric sensors and actuators are compared to the results of experimental investigations and presented in Section 4.6. It is assumed that the structures and the piezoelectric transducers attached to their surfaces are rectangle in shape and that their edges are parallel to the axes of the global coordinate system. The typical geometry of the problem is depicted in Figure 2.1. Vibrational motion of the structures is assumed to occur only in the z direction, thus, only one, corresponding component of the displacement field is considered, namely, the deflection $w = w(x, y, t)$. In the case of the so-called beam structures it is assumed that the length a of a structure is much greater than its width b and its thickness h_s . The flexural waves propagate along the x direction only and the deflection w is constant along the y direction, that is: $\frac{\partial w}{\partial y} = 0$. The vibrations of the beams are modeled using the classical Euler-Bernoulli beam theory. Similarly, the considered plate and panelled structures are thin in the sense of the classical Kirchhoff's plate theory. They are considered to be made of homogeneous, isotropic material (thus, in the case of composites, such an approach can be applied provided that the relevant effective material constants are known). The equations of motions for the considered structure models are presented in Chapter 2. The results of theoretical predictions are compared with the results of experiments carried out on various beam, plate and panelled structures made up of aluminium or composite materials including the actual materials used in aviation. The drawn conclusions are of great importance in developing active vibroacoustic control systems.

4.2 Piezoelectric sensors

The behavior of piezoelectric transducers is governed by the constitutive equations which include coupling between mechanical and electrical phenomena. Assuming that the summation convention is used (i.e., the summation is carried out over the repeating indices $i, j, k, l = 1, 2, 3$) these equations can be presented

as follows, for example, in the so-called stress-charge form:

$$T_{ij} = c_{ijkl}S_{kl} - e_{kij}E_k, \quad (4.1)$$

$$D_k = e_{kij}S_{ij} + \epsilon_{ki}E_i, \quad (4.2)$$

where T_{ij} $\left[\frac{\text{N}}{\text{m}^2}\right]$ is the second-order stress tensor, S_{ij} $\left[\frac{\text{m}}{\text{m}}\right]$ is the second-order strain tensor, c_{ijkl} $\left[\frac{\text{N}}{\text{m}^2}\right]$ is the fourth-order elasticity tensor, e_{kij} $\left[\frac{\text{C}}{\text{m}^2}\right]$ is the third-order tensor of piezoelectric coefficients (for the so-called stress-charge form), D_k $\left[\frac{\text{C}}{\text{m}^2}\right]$ is the electric displacement vector, E_k $\left[\frac{\text{V}}{\text{m}}\right]$ is the electric field vector, and ϵ_{ki} $\left[\frac{\text{F}}{\text{m}}\right]$ is the second-order tensor of dielectric constants.

It is assumed that a sensor electrode covers the whole relevant surface S of the transducer and that the polarization of the material is constant. The electric charge which appears on the electrodes of a piezoelectric sensor fixed to the surface of a vibrating thin plate or beam structure is computed as follows:

$$Q = - \iint_S D_3 dS. \quad (4.3)$$

The piezoelectric transducers are made up of transversely-isotropic piezoceramics, which involves that: $e_{311} = e_{322}$ which now will be denoted by e_3 , whereas $e_{312} = e_{321} = 0$. In the absence of external electric field, and having also noticed that $S_{33} \approx 0$, the relevant component of the dielectric displacement vector (4.2) can be expressed as follows:

$$D_3 = e_{3ij}S_{ij} = e_{311}S_{11} + e_{322}S_{22} + e_{333}S_{33} \simeq e_3(S_{11} + S_{22}). \quad (4.4)$$

It is assumed that (because of a very good bonding) the in-plane deformation of piezoelectric element is consistent with the deformation of the underlying structure, thus, the relevant components depend on the corresponding curvatures and the distance between the mid-planes of the piezo-element and the structure, namely:

$$S_{11} = \frac{h_p + h_s}{2} \frac{\partial^2 w}{\partial x^2}, \quad S_{22} = \frac{h_p + h_s}{2} \frac{\partial^2 w}{\partial y^2}. \quad (4.5)$$

Here, h_p and h_s are the thickness of the piezo-element and the structure, respectively. Obviously, in the case of beam structures $S_{22} = 0$.

Substituting (4.5) into (4.4) and (4.3), the electric charge induced on the shunted piezoelectric sensor attached to the surface of the plate structure can be expressed as follows:

$$Q = \frac{-(h_p + h_s)}{2} e_3 \int_{x_1}^{x_2} \int_{y_1}^{y_2} \left(\frac{\partial^2 w}{\partial x^2} + \frac{\partial^2 w}{\partial y^2} \right) dx dy, \quad (4.6)$$

where x_1, y_1, x_2, y_2 are given in Figure 2.1.

We would like to obtain the sensitivity function of piezoelectric sensor to specific structural modes. To this end, we first compute the amplitude of the electric charge induced on a transducer by substituting the time-harmonic form (2.5) into Equation (4.6) to obtain:

$$Q = e^{i\omega t} \tilde{Q} = -e^{i\omega t} \frac{(h_p + h_s)}{2} e_3 \sum_{n=1}^N W_n \left[\int_{x_1}^{x_2} \int_{y_1}^{y_2} \left(\frac{\partial^2 \Phi_n}{\partial x^2} + \frac{\partial^2 \Phi_n}{\partial y^2} \right) dx dy \right]. \quad (4.7)$$

Here, \tilde{Q} denotes the amplitude of the harmonically varied sensor charge.

It is assumed that the piezoelectric sensors are connected to the charge-to-voltage transducers circuits. Hence, the resulting voltage signal which is fed to the active control system is proportional to the charge given by equation (4.7), and so the desired sensitivity function $\tilde{S}_m \left[\frac{V}{m} \right]$ of a sensor to the structural mode m can be defined as follows:

$$\tilde{S}_m = \tilde{R} \frac{\tilde{Q}_m}{W_m} = -\tilde{R} \frac{(h_p + h_s)}{2} e_3 \left[\int_{x_1}^{x_2} \int_{y_1}^{y_2} \left(\frac{\partial^2 \Phi_m}{\partial x^2} + \frac{\partial^2 \Phi_m}{\partial y^2} \right) dx dy \right], \quad (4.8)$$

where \tilde{Q}_m is the electric charge amplitude induced by the mode m , and $\tilde{R} \left[\frac{V}{C} \right]$ is the gain of the signal conditioning circuit attached to the piezoelectric transducer.

4.3 Piezoelectric actuators

The external loading introduced by the rectangle-shaped piezoelectric actuator situated in such a way that its edges are parallel with the relevant axes of the global coordinate system (see Figure 2.1) can be approximated by linear (i.e., per length) moments acting along these edges. The excitation function $F_a(x, y)$ describing the spatial distribution of the introduced pressure acting on the structure can be then expressed as follows [11]:

$$F_a(x, y) = EIK^f s_a [\delta'(x - x_1) - \delta'(x - x_2)] [H(y - y_1) - H(y - y_2)] + EIK^f s_a [\delta'(y - y_1) - \delta'(y - y_2)] [H(x - x_1) - H(x - x_2)], \quad (4.9)$$

where $\delta'(\cdot)$ is the derivative of the Dirac delta function, $H(\cdot)$ is the Heaviside step function, E is the Young's modulus of the structure, K^f is the material-geometric constant dependent on material properties of the piezo-ceramics and

type of actuator (symmetric or antisymmetric) [11], and s_a is the strain of the actuator (the same in the x - and y -direction, because of the transversal-isotropy in the xy -plane) caused by the applied driving voltage V which generates within the piezo-element a uniform electric field in the z -direction, $E_3 = V/h_p$, therefore:

$$s_a = \frac{d_3 V}{h_p}, \quad (4.10)$$

where d_3 is the relevant piezoelectric material constant ($d_3 \equiv d_{311} = d_{322}$ from the strain-charge form of piezoelectric constitutive relation). The effects of added mass and stiffness introduced by the actuator as well as a longitudinal strain of the structure (resulting from the transverse asymmetry of the actuator) are neglected in the present considerations.

While considering the response of a structure to an external harmonic excitation, it is very convenient to perform the decomposition of the loading force into the eigenmodes of the structure. Due to the orthogonality property of the mode shape functions Φ_n , the amplitude of the mode number m excited by the external loading F_a can be expressed as (see Equation (2.21)):

$$W_m = \frac{\iint_S F_a(x, y) \Phi_m dS}{\rho h_s (\omega_m^2 - \omega^2) \iint_S \Phi_m^2 dS}, \quad (4.11)$$

where ρ is the density of the structure and ω_m is the angular eigenfrequency of the considered mode m . To compute the modal decomposition coefficients A_m of the excitation introduced by the actuator driven with the harmonic voltage V , relations (4.9) and (4.10) are used in Equation (4.11), which yields the following result:

$$A_m(V, \omega) = \frac{EIK^f d_3 V}{h_p \rho_s h_s (\omega_m^2 - \omega^2) \iint_S \Phi_m^2 dS} \left[\int_{x_1}^{x_2} \int_{y_1}^{y_2} \left(\frac{\partial^2 \Phi_m}{\partial x^2} + \frac{\partial^2 \Phi_m}{\partial y^2} \right) dx dy \right]. \quad (4.12)$$

We now introduce the actuator selectivity function to the structural mode m , defined as:

$$\tilde{A}_m = \tilde{A}_m(\omega) = \frac{A_m(V, \omega)}{V}. \quad (4.13)$$

The selectivity of a piezo-actuator to the structural mode m describes the amplitude of mode m excited by the actuator driven with a harmonic signal of unit voltage amplitude with the angular frequency ω (in absence of other excitation forces). It should be pointed out that – in contrast to the modal sensitivity

function of a piezo-sensor, defined previously – the modal selectivity is a function of the frequency of driving signal and strongly depends on the difference between this frequency and the eigenfrequency of mode m . The singularity in Equation (4.12) occurring in the case when $\omega_m = \omega$ results obviously from the assumptions of negligible damping and linearity of the system, which are not valid for large amplitude vibrations. When the Equations (4.12) and (4.13) are compared with the relation defining the sensor sensitivity function (4.8) an important remark should be made, namely: the surface integrals are the same and depend only on the transducer's coordinates (x_1, y_1) and (x_2, y_2) . This means that the efficiency of a piezoelectric transducer with respect to a particular structural vibration mode is similar both for the mode sensing and actuating. These considerations of course lead in the formal way to the result consistent with the reciprocal principle regarding the direct and inverse piezoelectric effects.

4.4 Signal conditioning

Piezoelectric sensors used for vibration monitoring convert the displacement of their surfaces into electric charge, accordingly to the formulas (4.2)–(4.7) describing relevant underlying phenomena. Therefore, they may be classified as self-generating sensors and, as so, theoretically, applied in passive detection systems (i.e., not requiring an external power supply to operate). However, due to a very low current efficiency of sensor-based sources, such solutions are impractical and not suitable for the considered applications. In order to achieve a strong and reliable output signal the transducers should be connected to dedicated conditioning circuits with a very high input impedance.

In the present study concerning low-frequency vibrations and relatively small amplitudes of displacement, the piezoelectric sensor is modeled as charge or voltage source with parallel or series capacitor C_p representing the electric capacitance of the transducer resulting from its dielectric properties - see Figure 4.1. Similar simple models are commonly used to describe the behavior of piezoelectric sensors in practical applications – see, for example, [82, 96–99]. The parallel resistance representing the current leakage has been omitted, as it is assumed that the sensor is always connected to a balanced input amplifier and no DC signals are considered.

Among a variety of types of electronic circuits capable of effective processing of signals from piezoelectric sensors one of the most popular are simple devices based on operational amplifiers, namely charge and voltage mode amplifiers whose exemplary wiring diagrams are presented in Figure 4.2. The theory of

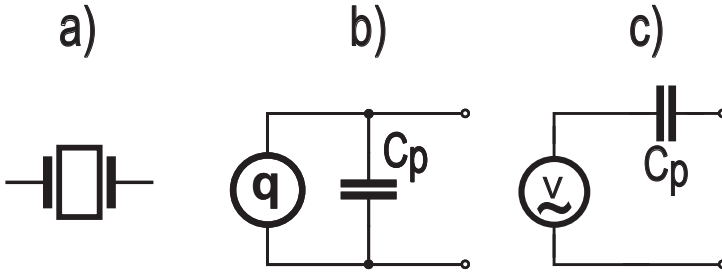


Figure 4.1. Piezoelectric sensor: a) schematic symbol, b) charge model, c) voltage model.

operation of such devices has been well described in literature – see, for example [96, 100]. The frequently encountered name „charge amplifier” can be slightly misleading, because the circuit it concerns is rather a charge-to-voltage converter and it does not amplify electric charge in the literal sense. However, due to the fact that such nomenclature is commonly used in scientific and technical literature, it is also adopted in the present study.

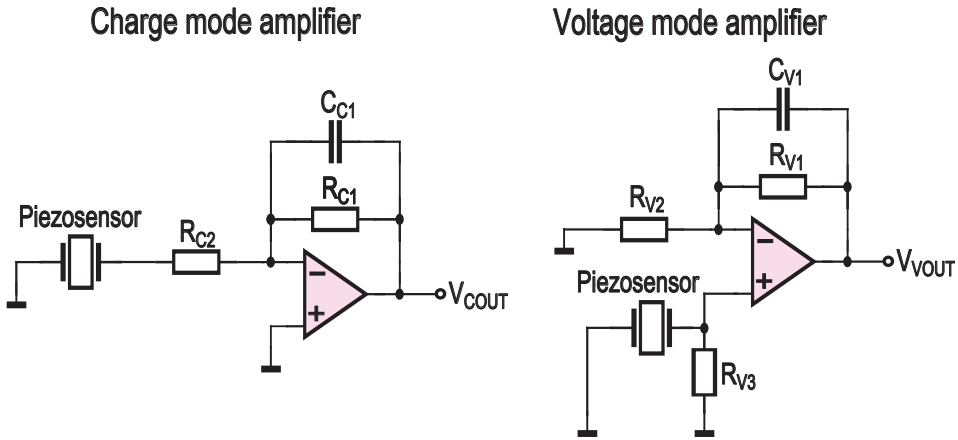


Figure 4.2. Typical signal conditioning circuits for piezoelectric sensors: charge mode amplifier (left) and voltage mode amplifier (right).

The operational amplifiers used in construction of the signal conditioning circuits for piezoelectric sensors should have as high input impedance as possible in order to minimize the current leakage. For that reason, the good choice is to use components with FET transistor inputs whose parameters usually meet this criterion well. The values of the elements connected to the operational amplifiers

(resistances, capacities) determine the gain and cutoff frequencies of the whole device. The desired characteristics should be specified at the design stage.

Assuming that the operational amplifiers used to construct the circuits presented in Figure 4.2 may be modeled as the ideal ones (with infinitely high input impedances, zero output impedances and infinitely high open-loop gains), the gain of the charge amplifier (defined as the ratio of output voltage amplitude to the amplitude of electric charge induced on a piezoelectric sensor modeled as in Figure 4.1, picture b) is given with the following formula:

$$G^C = \frac{1}{C_{C1}} \left[\frac{\text{V}}{\text{C}} \right]. \quad (4.14)$$

The lower and upper cutoff frequencies of the amplifier are computed with the following equations, respectively:

$$f_L^C = \frac{1}{2\pi R_{C1} C_{C1}} \quad [\text{Hz}], \quad (4.15)$$

$$f_H^C = \frac{1}{2\pi R_{C2} (C_{C1} + C_p)} \quad [\text{Hz}], \quad (4.16)$$

where C_p is the capacity of the piezoelectric sensor – see Figure 4.1.

Analogously, the gain of the voltage mode amplifier (defined as the ratio of output voltage amplitude to the amplitude of electric charge induced on a piezoelectric sensor modeled as in Figure 4.1, picture b) is given with the following formula [96]:

$$G^V = \frac{1}{(C_{C1} + C_{CAB})} \left(1 + \frac{R_{V1}}{R_{V2}} \right) \left[\frac{\text{V}}{\text{C}} \right], \quad (4.17)$$

where C_{CAB} is the capacity of the wires connecting sensor with the amplifier. The lower and upper cutoff frequencies of the amplifier are computed with the following equations, respectively:

$$f_L^V = \frac{C_{C1} + C_{CAB}}{2\pi R_{C1} C_{C1} C_{CAB}} \quad [\text{Hz}], \quad (4.18)$$

$$f_H^V = \frac{1}{2\pi R_{V3} (C_{V1})} \quad [\text{Hz}]. \quad (4.19)$$

The gain of the charge amplifier depends only on the capacity C_{C1} , while the gain of voltage mode amplifier is also a function of the capacity of the connecting wires C_{CAB} , which also influences the lower cutoff frequency of the

latter device. This means that the mentioned parameters of the voltage amplifiers might drift in time due to changes in configuration or replacements of the interface cables. For that reason and according to the fact that the stable gain in the low-frequency range is crucial for the considered applications, the charge mode amplifier has been chosen as the type of a signal conditioning circuit for piezoelectric sensors used in the present study.

For the sake of the conducted experimental research a dedicated signal conditioning circuit has been developed and constructed. The relevant wiring diagram is presented in Figure 4.3. The circuit is based on AD745 FET input operational amplifier from Analog Devices, which provides a high input impedance and low biasing current together with a low noise performance. Due to the fact that the considered measurements of plate vibrations carried out using piezoelectric sensors require a wide gain control range as the amplitudes of vibrations vary significantly for resonant and off-resonant frequencies, the values of the feedback loop capacitors and resistors can be modified using two multikey switches. At the same time, in the same way, the lower cutoff frequency is set. The series resistor R_{C2} from Figure 4.2, whose function is to protect the operational amplifier against the electrostatic discharges, has been omitted in the present design.

One of the constructed prototypes of the signal conditioning circuits is presented in Figure 4.4. The printed circuit board was etched from one-sided copper laminate. The maximum allowable supply voltage range, which also limits the maximum available output signal level, is $\pm 18V$. A large number of similar devices have been built and tested with various piezoelectric transducers, proving good performance and low level of introduced noise.

The behavior of piezoelectric transducers used as actuators for exciting vibrations of thin plate structures has been described in Section 4.3. As it results from Equation (4.12), they are voltage driven, i.e., the amplitudes of the induced structural modes are proportional to the amplitude of the applied harmonic voltage signal. From the point of view of the output amplifier, the piezoelectric actuators are a high-impedance capacitive load. For that reason they should not be driven with standard audio amplifiers, which are intended for an entirely different type of low-impedance inductive loads (namely, loudspeakers). Dedicated electronic circuits, suitable for the considered applications, have been developed and constructed. The corresponding specifications and wiring diagrams are presented in Chapter 5, Section 5.5 together with the description of the complete active control system.

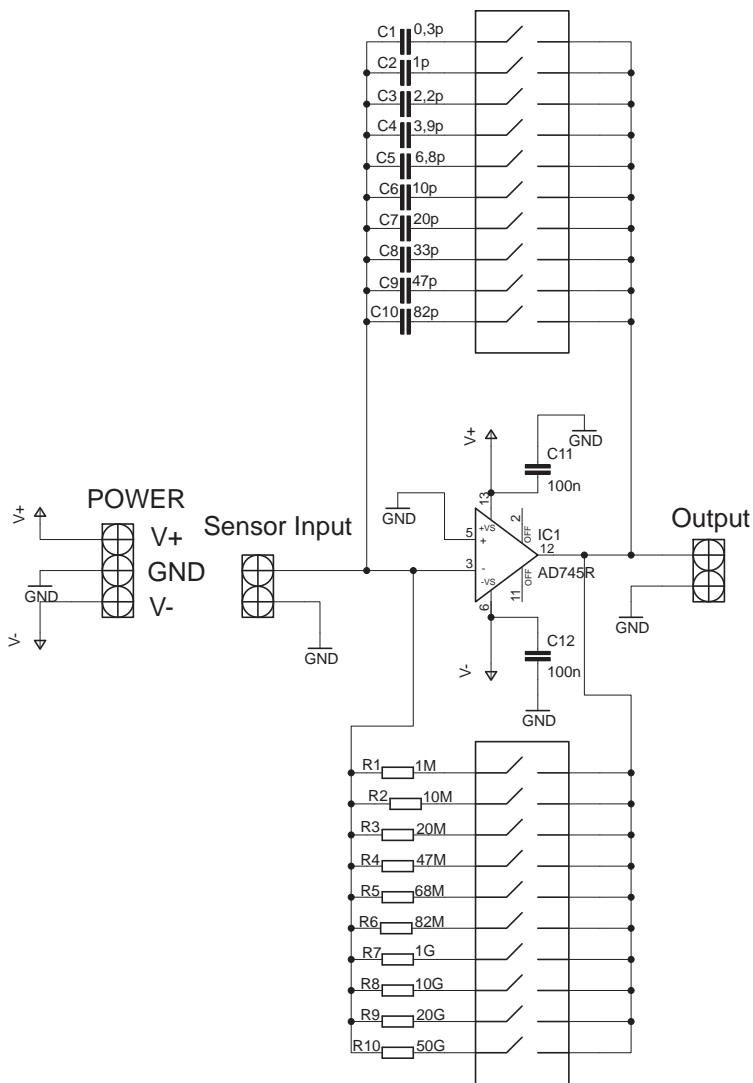


Figure 4.3. Electric scheme of designed and constructed charge amplifier with adjustable gain and cutoff frequency, based on AD745 low noise, FET input operational amplifier.

4.5 Some technical aspects on the preparation of the composite structures for active control systems

The piezoelectric transducers used in the active vibration or vibroacoustic control systems usually take the form of very thin and small plates (patches)

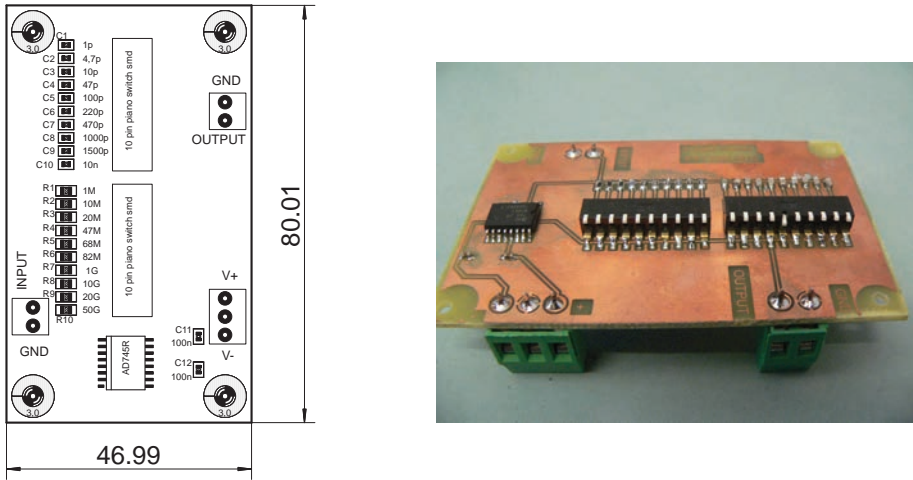


Figure 4.4. Developed and constructed charge amplifier with adjustable gain and cutoff frequency: printed circuit board assembly scheme (left) and a picture of an exemplary built device (right)

with electrodes sputtered on their both faces. Due to the fact that one of those faces needs to be attached to the surface of a controlled structure, the problem of ensuring electrical connectivity arises. Most of the kinds of glues typically used in bonding the piezo-elements are very good insulators, while the structures are typically made up of excellent conducting materials: metals (like aluminum) or carbon-fiber composites. A few solutions to cope with this issue are described in literature. Some of them require drilling a hole in the structure through which a wire is connected to the piezo-element. However, such a violation of the controlled element is often not possible and creates additional problems in the case of collocated sensor/actuator pairs. Another way to ensure the access to the bottom electrode of a piezo-element is to use additional pads between the transducer and the structure, but then the mass, thickness and mechanical properties of the attached system change significantly. Yet another approach suggests to use some kind of conductive glue providing both a very good bonding and electrical contact; however, one must be very careful during manufacturing, since the squeezed-out glue may cause a short-circuiting of the electrodes of transducer. To avoid this situation, a combined method using two kinds of glue can be used, as it is illustrated in Figure 4.5. This technique was successfully applied and tested during the experiments carried out on various aluminum beams and plates.

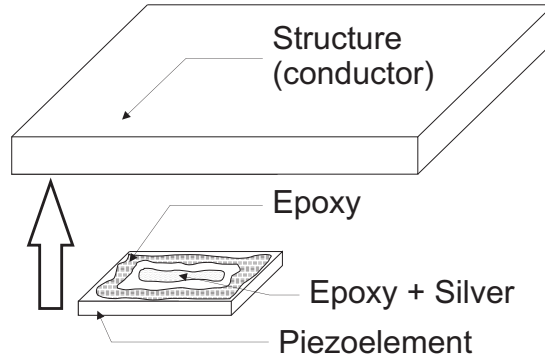


Figure 4.5. Technique of attaching a piezoelectric element to a structure made of conductive material, ensuring the electric contact between these elements and avoiding short-circuiting the electrodes.

4.6 Numerical and experimental investigations

Modal sensitivity/selectivity functions of small, rectangle-shaped piezoelectric transducers attached to the surfaces of beam, plate, and panelled structures are investigated in this section. The solutions obtained using analytical formulas and numerical simulations are compared to the results of experiments. The research described in the present section of the study concerned several different aluminum and composite structures, including structures made of actual materials used in aviation (carbon fiber sandwich structures with nomex-honeycomb core). Such a variety of test objects allows to draw some conclusions regarding the scope of applicability of the proposed approach and to bring the obtained results closer to the actual, real-life practical uses.

The numerical finite-element analyses were used to solve eigen-problems of the investigated plate and panelled structures, however, it must be emphasized here that in the proposed line of investigation only eigenmode shapes were of interest since this part of the study subject is the modal sensitivity and selectivity. Thus, the mass and stiffness properties of structures were not important when carrying out these analyses, and in case of composite structures very approximative values could be taken. Such approach, however, requires that the investigated plate and beam composite structures can be considered as macroscopically homogeneous and macroscopically isotropic (in their planes), so that the mode shapes should be the same whatever the stiffness and mass density are, and they depend only on the structure geometry and conditions of support. This entails also the fact that the effect of small piezoelectric patches fixed to their

faces can be neglected. However, this latter assumption – important also for aluminium structures and usually valid at lower frequencies – is rather standard and should be also valid in the case of stiffer composites.

The assumption of in-plane isotropy may at first appear as disputable in case of composites, however, one should notice that although the carbon-fibers for the composite plate faces were woven in an orthogonal pattern (see Figure 4.7), exactly the same fibers were used in both mutually perpendicular directions, and that results in the so-called structural isotropy (in plane) of both faces. In other words, the carbon fabric is a plain weave and thus isotropic in the plane of the weave. The honeycomb core is also isotropic in the plane of the cell pattern under three loading mechanisms as explained in [101], since it is formed from cells of regular hexagons.

Nevertheless, the final confirmation of the validity of both assumptions of macroscopic homogeneity and isotropy is confirmed by the results of the proposed approach which compares and utilises in conjunction numerical and experimental investigations.

4.6.1 Beam structures

Due to the undertaken assumptions the classical Euler-Bernoulli thin beam theory is used to describe the vibrational motion of the considered beam structures. Under such conditions the vibration mode shapes can be computed analytically, as the sum of harmonic and hyperbolic functions, with coefficients depending on the boundary conditions [52]. Based on such a formula, the modal sensitivity function was computed for a piezoelectric sensor (of known dimensions) attached to the clamped beam structure. Some results of these computations, obtained for a 3 cm long piezo-element on a 58 cm long beam (with one end clamped and the other free) are shown in Figure 4.6. According to the considerations discussed in Sections 4.2 and 4.3, piezoelectric sensors and actuators are bounded with a reciprocal relation, which implies that the sensitivity and ability of exciting specific structural modes depend only on the location of the transducer on the surface of structure.

The presented results were used for positioning piezoelectric transducers on thin beams made of aluminium and glass-fiber which were examined during further experimental research. For homogeneous beams the modal shape functions do not depend on the material; they are the same for every thin beam of the same length and boundary conditions and the material properties affect only the eigenfrequencies. In the presented case, the piezo-element location that allows to sense or excite every mode is close to the clamped end of the beam.

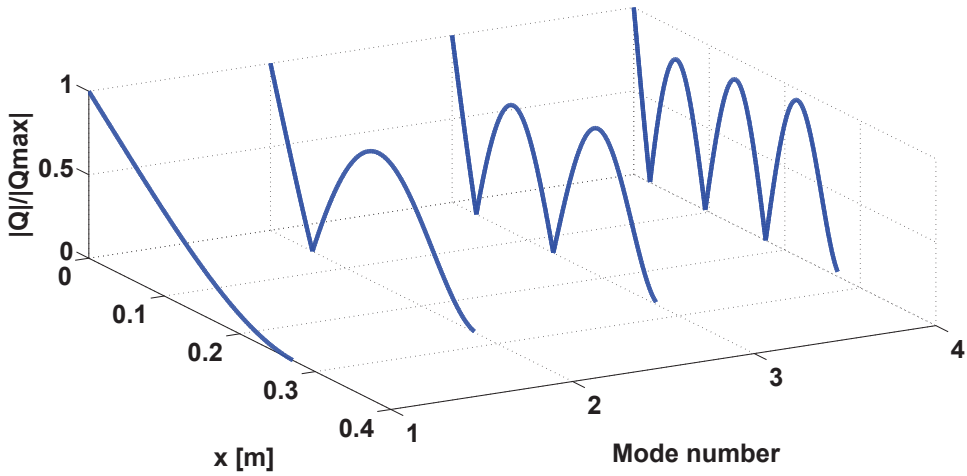


Figure 4.6. Normalized sensitivity functions for the rectangle-shaped piezoelectric sensor attached to a cantilevered beam of length 58 cm as a function of the structural mode number and the distance of the sensor from the clamped end of the beam.

The transducers may be positioned so that they will not respond or induce any specific structural modes but they still will be sensitive to most of the modes in the considered low-frequency range.

The experimental investigations were performed using 1 mm thick, 28 cm long, and 2 cm wide aluminium beams and a single glass-fiber composite beam 58 cm long, 3 cm wide, and 2.3 mm thick. The piezo-elements were made of Pz29 piezoceramics and were 2 cm wide, 3 cm long, and 0.3 mm thick. The values of important relevant parameters of the utilized piezoceramic material are as follows: $e_3 = 21, 2 \frac{C}{m^2}$, $d_3 = 5, 74 \cdot 10^{-10} \frac{C}{N}$. The beam structures that were used in experimental investigations are shown in Figure 4.7.

The experimental examination of the vibrations of beam structures revealed an excellent agreement with the theoretical predictions. The vibrations were excited by a single piezoelectric actuator positioned close to the clamped end of beam, while the other piezo-elements, fixed at different distances along the beam, were used as sensors. The electrodes of the sensors were connected to a charge-to-voltage converters. It is worth to notice that for aluminium beams – for which the material constants are known – the predicted and measured first three eigenfrequencies of the bending modes (i.e., all eigenfrequencies of the bending modes in the considered low-frequency range below 400 Hz) at 11, 65 and 185 Hz agreed with an accuracy better than 1 Hz. That observation jus-

tifies the assumption to neglect the stiffness and mass influence of the attached piezoelectric elements to the vibration characteristics of beam structures.

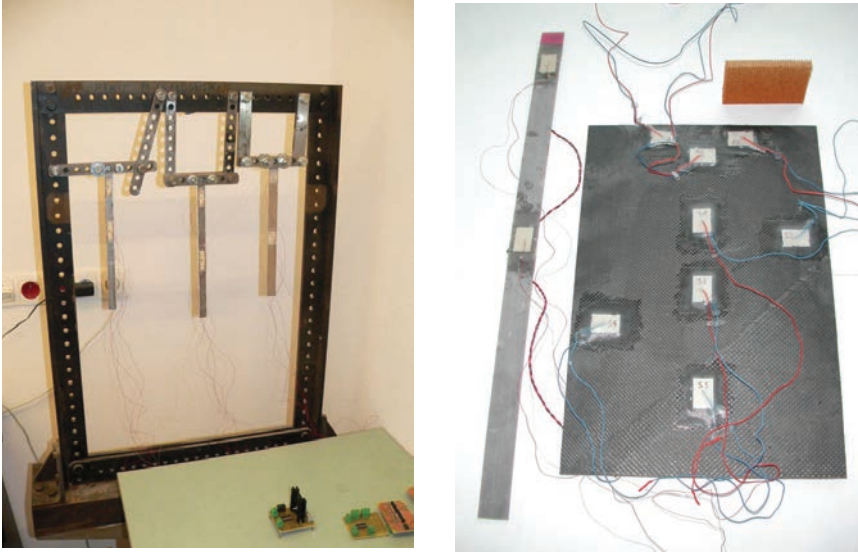


Figure 4.7. Three thin aluminium beams fixed to an experimental stand (left); a glass-fiber composite beam and a sandwich panel made up from the carbon-fiber composite liners with the *Nomex*-honeycomb core (right) used in the experimental investigations.

In the case of the beam made of glass-fiber composite, no material constants were known. Two rectangle-shaped piezoelements were attached to the surface of the structure: the first one – fixed 4 cm from the clamped end – served as actuator simulating the external source of vibrations. The second transducer was located 29 cm from the clamped end and it was used as a sensor. Due to the numerical simulations, the sensor should be insensitive to the structural modes No. 3 and 5. The resonant frequencies were found experimentally and the mode shapes were identified using a laser vibrometer. The results are presented in Table 4.1; the modes No. 3 and 5 were not sensed by the sensor which agrees with the theoretical predictions.

If a thin beam (of length L and the rectangular cross-section of height h_s) is elastic, isotropic, and homogeneous – or can be approximately treated as such – its eigenfrequencies can be calculated using the following formula [52]:

$$f_n = \frac{\beta_n^2 h_s}{2\pi L^2 \sqrt{3}} v_b, \quad (4.20)$$

Frequency [Hz]	Number of nodes in the mode shape function	Identified mode number
95.8	3	4
235.5	5	6
318.6	6	7
448.5	7	8
562.1	8	9

Table 4.1. Measured resonant frequencies and the corresponding parameters of structural mode shapes for the glass-fiber composite beam.

where $v_b = \sqrt{E_b/\rho_b}$ is the velocity of the plane wave in the (supposedly elastic and isotropic) material of the beam (E_b and ρ_b are the Young's modulus of the material and its density, respectively) and β_n is the coefficient dependent on the boundary conditions and the mode number [52]. Equation (4.20) and the results of measurements given in Table 4.1 were used to estimate the ("effective", average) speed of sound for the composite material from which the examined beam was made. The mean value found using the measured eigenfrequencies listed in Table 4.1 was 2553 m/s. Then, this value was used in Equation (4.20) with the coefficient $\beta_2^2 = 22,034$ [52] appropriate for the 2nd mode (not used in the previous calculations) to estimate the eigenfrequency of this mode. The computed result of 17.7 Hz agrees well with the resonant frequency of 18.2 Hz measured for this mode.

The presented results clearly conclude that in the case of thin beams made from different materials the ability of sensing or exciting specific forms of vibrations with small, rectangle shaped piezoelectric transducers can be accurately determined with simple analytical formulas. The optimal locations of sensors and actuators should be chosen in order to maximize (or minimize) the modal sensitivity and selectivity values for modes most significant in the considered cases. However, as it can be seen from Figure 4.6, such transducers will always be sensitive to most of the forms of vibrations. This conclusion is especially important when considering off-resonant vibrations with many modal components involved.

4.6.2 Plate and panelled structures

The modal sensitivity and selectivity functions (4.8) and (4.13) of small rectangle-shaped piezoelectric transducers attached to the surfaces of plate or sandwich-panel structures are investigated in this section. In general, for arbitrary (non-homogeneous) boundary conditions of support, the rectangle plate

mode-shape functions Φ_n cannot be found analytically. Therefore, the finite element analysis was applied to determine the eigenfrequencies and the corresponding eigenvectors of the investigated structures. Experimental investigations were carried out on the sandwich composite panel made up of two carbon-fiber faces and a *Nomex*-honeycomb core (see Figure 4.7) and a thin aluminium plate (see Figure 4.9). The aluminium plate was 300 mm long, 200 mm wide, and 1 mm thick, while the sandwich plate was 402 mm long, 272 mm wide, and 5 mm thick. The structures were clamped by a part of their shorter edges and all the other edges were free.

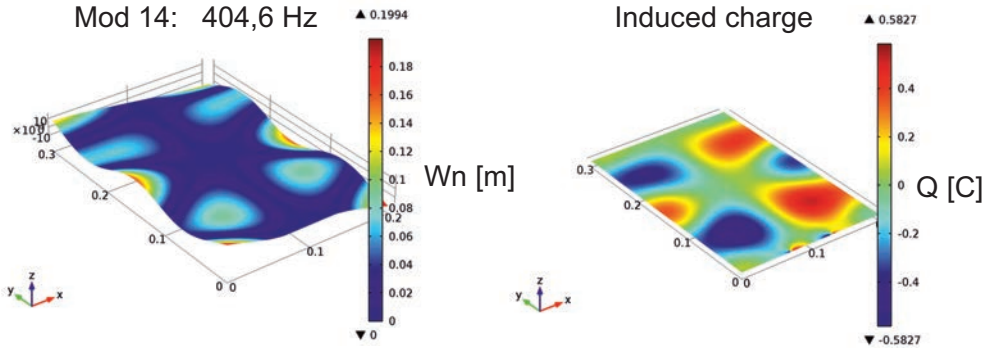


Figure 4.8. Results of the numerical simulations: the shape of an exemplary vibrational mode of the considered plate structure made of aluminium (left) and the corresponding distribution of the induced electric charge induced on the theoretical point-sensors made of the considered piezoceramics (right).

Eight 0.3 mm-thick rectangle-shaped piezoelectric transducers with dimensions 20 mm \times 30 mm were attached to one face of the sandwich panel. Three of them were fixed close to the clamped boundary and served as actuators which simulated the external excitation sources. The other five acted as sensors. In the case of the aluminium plate, five pairs of such piezotransducers were used. In each pair, the two piezotransducers were attached symmetrically to both sides of the plate, with polarization and wires connected in such a way so that an asymmetric bimorph actuator/sensor was formed. From five pairs one served as the source of the excitation force while the others were used as sensors.

The COMSOL Multiphysics software was used for the numerical simulations. Two different models of the considered structures were developed and compared: a simple two-dimensional thin plate model and a three-dimensional model of plate with five pairs of asymmetrically-attached piezoelectric sensors/actuators. In the second case the transducers were assumed to be made of transversally



Figure 4.9. Thin aluminium plate with attached piezoelectric transducers in the laboratory stands used in the experimental investigations.

isotropic piezoceramics, for which the material parameters were taken from the manufacturer's data catalog. The main reason for using two different models was to investigate the influence of the added mass and stiffness introduced by the transducers on the vibrational characteristics of the considered structures. The comparison between the obtained results indicates that – in the considered low-frequency range – including the comparatively small transducers in the simulations had no significant effect either on the shape functions of the eigenmodes, or on the eigenfrequencies. The experimental investigations revealed that the mode shapes – determined using the laser vibrometer – were exactly as predicted, but the measured eigenfrequencies were not that consistent with the simulations. The results are presented in Table 4.2.

The modal sensitivity functions of the piezoelectric sensors attached to the considered structures were investigated numerically and experimentally. The normalized absolute values of the obtained results for the first several vibration modes are given in Tables 4.3 and 4.4 for the sandwich plate, and in Tables 4.5 and 4.6 for the aluminium plate. The value 1 in a cell of the Table indicates that the specific transducer is the most sensitive to the specific mode of all the piezo-elements (thus, the sensitivities are relative with respect to the result of

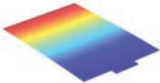
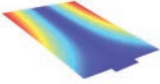
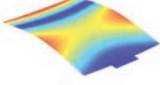
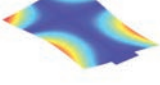
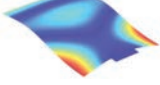


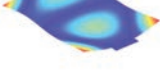
Eigenfrequency [Hz]			Mode shape
2D plate model	3D model	Measured	
8	8.1	7.1	
24.6	25	27.1	
50.3	50.5	51.7	
82.8	83.1	90.1	
127.2	129.2	123.5	
144.9	143.4	155.1	
160.2	163.5	172.4	
199	199	183	

Table 4.2. Resonant frequencies determined numerically (using a 2D plate model and the 3D structure model with piezoelements) and experimentally, and the corresponding mode shapes.

the “best” sensor), while the value 0 indicates that it is not sensitive to this mode at all.

The locations of the piezo-elements were chosen based on the results of the numerical simulations described in the previous section. The exemplary results are presented in Figure 4.8. To determine the modal sensitivity or selectivity values the computed charge should be integrated over the desired surface corre-

Mode number	Sensor 1	Sensor 2	Sensor 3	Sensor 4	Sensor 5
1	1	0.678	0.468	0.28	0.055
2	0.008	0.329	0.01	1	0
3	0.317	0.846	1	0.969	0.28
4	0.001	1	0.09	0.29	0
5	0.6	0.105	1	0.72	0.68

Table 4.3. Values of the normalized sensitivity function of piezoelectric sensors attached to the sandwich panel obtained from the numerical simulations.

Mode number	Sensor 1	Sensor 2	Sensor 3	Sensor 4	Sensor 5
1	1	0.5	0.634	0.2	0.062
2	0.089	0.523	0.178	1	0.103
3	0.662	0.625	1	0.6	0.185
4	0.465	0.922	1	0.52	0.367
5	0.052	0.091	0.973	1	0.445

Table 4.4. Values of the normalized sensitivity function of piezoelectric sensors attached to the sandwich panel obtained from the experimental investigations.

Mode number	Sensor 1	Sensor 2	Sensor 3	Sensor 4
1	1	0.34	0.9	0.03
2	0.29	0.6	0.07	1
3	0.24	1	0.68	0.22
4	1	0.3	0.02	0.88
5	0.25	1	0.22	0.37
6	0.56	0.65	1	0.34
7	0.52	1	0.02	0.09
8	0.56	0.34	1	0.16

Table 4.5. Values of the normalized sensitivity function of piezoelectric sensors attached to the aluminium plate obtained from the numerical simulations.

sponding to a chosen transducer location. The purpose was to ensure a negligible or high sensitivity to the selected structural modes. Once again, it can be seen that a relatively small, rectangle-shaped piezo-element can be placed in locations that ensure a very high or, in other case, negligible sensitivity to one or two selected structural modes, but that the transducer will also respond to most of the other modes in the considered low-frequency range.

The comparison of the results given in Tables 4.3-4.6 reveals that the experimental and numerical results are in general similar, though some significant dis-

Mode number	Sensor 1	Sensor 2	Sensor 3	Sensor 4
1	1	0.42	0.91	0.08
2	0.17	0.99	0.55	1
3	0.4	1	0.68	0.33
4	1	0.19	0.05	0.75
5	0.1	1	0.4	0.27
6	0.69	0.14	1	0.42
7	0.34	1	0.1	0.05
8	0.56	0.34	1	0.2

Table 4.6. Values of the normalized sensitivity function of piezoelectric sensors attached to the aluminium plate obtained from the experimental investigations.

crepancies between the predicted and measured values are observed too. For example, in the case of the sandwich structure sensors 3 and 5 were in fact sources of the electric signal at the *all* considered resonant frequencies, although their locations were deliberately chosen in such a way that the transducers should be – theoretically – insensitive or almost insensitive to some selected modes. As a matter of fact, none of the sensitivity values in Table 4.4 is close to zero.

The results are in general more consistent between the numerical predictions and experiments for the aluminium plate. For some vibrational modes of this structure – see, for example the mode No. 8 in Tables 4.5 and 4.6 – the results are in fact almost exact. The main reason for this better agreement is obviously the exactness in modelling the material for the isotropic aluminium plate, and also a seemingly lower structural damping than in the case of the sandwich plate; a better adhesion of the transducers to the surfaces of the aluminium plate might also have its effect. The methods of mounting the piezoelements to the considered structures were different due to a need to ensure the electrical contact to the both electrodes of a transducer – including the ‘bottom’ electrode that is the one in contact with the plate. In the case of electrically conductive aluminium the plate was used as a common ground so that the whole bottom side of a transducer could be thoroughly and fully glued to the plate with a conductive glue; in the case when the piezoelements were attached to the sandwich plate additional electric wires had to be glued to the ‘bottom’ electrodes making the attachment not sufficiently complete.

4.7 Excitation of resonant vibrations

Vibrations of plates excited by a harmonic force at a frequency equal to one of the eigenfrequencies of the structure are particularly important in the scope of the present study. It has been observed that the investigated structures have very sharp resonant characteristics, which is connected with a low structural damping, and due to that the significant emission of sound occurs only for the mentioned types of harmonic excitation. In the assumed model of vibrations, described in Chapter 2, the amplitudes of specific modes are inversely proportional to the differences between squared excitation frequency and squared corresponding eigenfrequency. If those two frequencies are equal, the value of the expression cannot be determined – it theoretically reaches infinity. Such a conclusion argues obviously with the observations, as the amplitudes of vibrations of real structures are always limited. The limitations result from damping and nonlinear effects, which have not been taken into account in the used simple form of the formal description of the considered problem. For that reason, the amplitudes of resonant vibrations of the investigated structures are in the present study determined experimentally, using a laser vibrometer. It is assumed, that due to the observed sharp resonant characteristics all of the structural modes with corresponding eigenfrequencies not equal to the given excitation frequency can be neglected in such case. This assumption has been actually validated by determining the shape functions of the excited forms of resonant vibrations which agreed well with the shapes of the corresponding eigenmodes determined numerically.

However, an important question arises: are the amplitudes of resonant vibrations excited by a piezoelectric actuator in the considered cases limited primarily by the internal damping or by occurring nonlinear effects? In other words, are those amplitudes linearly proportional to the amplitude of the harmonic voltage signal applied to the transducer? This issue is of a fundamental importance for the carried out experimental research, as it decides whether the results obtained for various levels of the driving signals can be easily scaled and compared to each other. To answer this question, the following investigation has been performed using thin aluminium plate described in section 4.6. For each of the eigenmodes shape functions presented in Table 4.2 the coordinates of points of maximum vibration amplitudes have been determined using a Matlab script. Then, the plate was excited to vibrate at corresponding eigenfrequencies by one pair of piezoelectric transducers attached symmetrically on both sides of the structure. The amplitudes of induced vibrations were measured with a laser vibrometer at specified points for each structural mode as functions of the amplitudes of

voltage signals driving actuators. The exemplary results are presented in Tables 4.7–4.10.

Excitation voltage amplitude [V]	Measured velocity amplitude [m/s]	Displacement amplitude [m]
5	0,002	$2,58 \times 10^{-6}$
10	0,00405	$5,22 \times 10^{-6}$
15	0,006	$7,73 \times 10^{-6}$
20	0,008	$1,03 \times 10^{-5}$

Table 4.7. Maximum amplitudes of vibrations of thin aluminium plate structure excited to vibrate at its eigenfrequency corresponding to the structural mode no. 5.

Excitation voltage amplitude [V]	Measured velocity amplitude [m/s]	Displacement amplitude [m]
5	0,0106	$1,1 \times 10^{-5}$
10	0,0215	$2,23 \times 10^{-5}$
15	0,0318	$3,29 \times 10^{-5}$
20	0,042	$4,36 \times 10^{-5}$

Table 4.8. Maximum amplitudes of vibrations of thin aluminium plate structure excited to vibrate at its eigenfrequency corresponding to the structural mode no. 6.

Excitation voltage amplitude [V]	Measured velocity amplitude [m/s]	Displacement amplitude [m]
5	0,0101	$9,4 \times 10^{-6}$
10	0,0203	$1,88 \times 10^{-5}$
15	0,0303	$2,82 \times 10^{-5}$
20	0,04	$3,72 \times 10^{-5}$

Table 4.9. Maximum amplitudes of vibrations of thin aluminium plate structure excited to vibrate at its eigenfrequency corresponding to the structural mode no. 7.

The presented results concern four subsequent forms of vibrations with corresponding eigenfrequencies ranging from 123 Hz to 183 Hz. For the excitation amplitudes up to 20 V the maximum vibration amplitudes are of the order of $10^{-6} - 10^{-5}$ m. To investigate the linearity of relation between the applied voltage levels and induced modal amplitudes the ratios of the considered parameters related to the lowest values have been computed. The results are presented in Table 4.11.

The presented results indicate that the investigated relation is almost ideally linear. Therefore, the nonlinear effects are not the primarily factor limiting the

Excitation voltage amplitude [V]	Measured velocity amplitude [m/s]	Displacement amplitude [m]
5	0,0068	$5,89 \times 10^{-6}$
10	0,0136	$1,18 \times 10^{-5}$
15	0,0208	$1,8 \times 10^{-5}$
20	0,0275	$2,38 \times 10^{-5}$

Table 4.10. Maximum amplitudes of vibrations of thin aluminium plate structure excited to vibrate at its eigenfrequency corresponding to the structural mode no. 8.

Excitation voltages ratio	Velocities ratio		Velocities ratio		Velocities ratio	
	mode no. 5	mode no. 6	mode no. 7	mode no. 8	mode no. 8	mode no. 8
1	1	1	1	1	1	1
2	2,025	2,028	2,005	2,004	2,004	2,004
3	3	2,995	2,995	3,051	3,051	3,051
4	4	3,962	3,96	4,044	4,044	4,044

Table 4.11. Ratios of the maximum vibration amplitudes for four different structural modes excited at their corresponding eigenfrequencies as functions of ratios of amplitudes of the exciting voltages.

amplitudes of resonant vibrations. The maximum observed deviations are less than 2% in all cases, which may be assumed as considerably low. This allows to conclude that scaling and comparing the results of measurements carried out with different levels of excitation voltages should not be misleading.

4.8 Conclusions

Various issues regarding the utilization of small, rectangle-shaped piezoelectric transducers as sensors and actuators for sensing and exciting vibrations of beam, plate and panelled structures have been discussed in the present chapter. A new form of a theoretical description introducing modal sensitivity and selectivity functions, suitable for structures with arbitrary boundary conditions has been proposed. The elaborated approach allows for a simple evaluation of usefulness of given sensors and actuators in controlling specified forms of vibrations and simplifies the determination of optimal placement of the transducers on the surfaces of the controlled structures.

The modal parameters of piezoelectric sensors and actuators were determined numerically and experimentally using various beam, plate, and panelled structures, including sandwich composite made of carbon-fiber liners with

nomex-honeycomb core – an actual material used in aviation applications. The agreement of the comparison between the results of simulations and the results of measurements was almost perfect in the case of beams, slightly worse for the thin aluminium plate, and the worst (but still generally fair) for the sandwich structure. The differences in the accuracy of predictions occur probably due to the varying degree of simplifications in relevant models and imperfections in construction of the investigated structures.

An independent part of considerations has been devoted to the problem of resonant vibrations. The assumed models of thin beam and plate vibrations, used to describe the behavior of the investigated structures, do not take into account damping and so are unable to determine the modal amplitudes for cases in which the external harmonic excitation force has frequency equal to one of the eigenfrequencies of the structure. The carried out experiments clearly indicated that the amplitudes of the resonant vibrations are linearly proportional to the amplitudes of the voltage signals driving actuator. Thus, scaling and comparing results obtained for different levels of excitation should not be misleading.

Various technical aspects regarding practical implementation of the piezoelectric sensors and actuators have been described. A developed technique of attaching transducers to conductive surfaces that ensures electrical contact with both electrodes and prevents short-circuiting between them has been presented. Such a method was successfully applied to construct the composite structures used in the present study. For the sake of practical implementations the electric signal from piezoelectric sensors needs to be amplified with an adequate conditioning circuit. The parameters of the most commonly used types of such circuits have been discussed. The charge amplifier was pointed out as most suitable for the considered applications. The description of an exemplary developed device of such type has been presented together with relevant wiring diagrams. The constructed amplifiers proved very good effectiveness and demonstrated a low noise performance in numerous experiments.

Piezoelectric sensors and actuators are basic and necessary components of the developed active vibroacoustic control system which is the main topic of the present study. The presented conclusions regarding various aspects of their utilization in the considered applications form the basis for investigations described in the next chapter.

Active vibroacoustic control system

5.1 Aim and methods

General assumptions regarding the considered problem are presented in Section 1.1. The aim of the present study is to develop, construct, and evaluate an active control system capable of reducing the amplitude of the acoustic pressure $|p|$, generated by a vibrating plate structure in any given point of the ambient space, indicated by a vector \mathbf{R} . It is assumed that the considered system uses piezoelectric transducers attached to the surface of the plate as both sensors and actuators. The system has decentralized feedback architecture, i.e., all of the sensor-actuator pairs are connected independently with feedback amplifiers. The number of such pairs included in the system is denoted as M . The gain G_m of the feedback loop number m , where $1 \leq m \leq M$, can be adjusted in the range from 0 to G_m^{max} , where G_m^{max} denotes the maximum available gain value for feedback loop number m . For the sake of brevity it is convenient to write the control parameters as a vector, in the following form:

$$\mathbf{G} = \begin{bmatrix} G_1 \\ G_2 \\ \vdots \\ G_M \end{bmatrix}, \quad (5.1)$$

where each of the elements of the vector satisfies the following condition:

$$\forall_{m=\{1,2,\dots,M\}} \quad 0 \leq G_m \leq G_m^{max}. \quad (5.2)$$

By changing the feedback gains, the characteristics of the secondary excitation sources, namely, the actuators, are altered and, consequently, so are the modal components of vibrations of the plate. Due to the assumption of the linearity of the considered phenomena, neglectation of the structural damping and due to the fact that only steady state, low frequency harmonic vibrations are

considered, the acoustic pressure in a given point of space \mathbf{R} , for a given angular frequency of the excited vibrations ω can be expressed as a function of the modal amplitudes:

$$p(\mathbf{R}, \omega) = p(W_1, \dots, W_N)|_{(\mathbf{R}, \omega)}, \quad (5.3)$$

where N is the number of considered structural modes of vibrations. The form of the function $p(W_1, \dots, W_N)$, linking the acoustic pressure with the amplitudes of the modal components of vibrations of the plate, depends on the assumed boundary conditions. In a general case such a problem has no analytical solution and the acoustic pressure distribution has to be computed numerically. The relevant issues have been described in detail in Chapter 3 of this study.

The acoustic pressure p is a complex value and for the considered, steady-state problem it can be unambiguously defined by its real and imaginary components, which are in this case also functions of the modal amplitudes of vibrations. Thus, the amplitude of the acoustic pressure can be expressed as:

$$|p| = \sqrt{p_{re}^2(W_1, \dots, W_N) + p_{im}^2(W_1, \dots, W_N)}, \quad (5.4)$$

where $p_{re}(W_1, \dots, W_N)$ and $p_{im}(W_1, \dots, W_N)$ denote the real and imaginary part, respectively.

In order to determine the optimal control strategy, the aim of the control has to be defined in terms of a relevant cost function whose value should be minimized. The optimization process is restricted by limited values of gains of feedback amplifiers. In practice such restrictions result from parameters of the electronic components included in the control system and parameters of the power supplies. However, due to the fact that the gain adjustments within the available ranges do not significantly influence the system hardware characteristics and that the issues related to power consumption have no practical meaning from the point of view of the addressed problem, introduction of a control cost term penalizing amplifications was considered redundant. Given the above conclusions and taking into account the fact that the value of amplitude of the acoustic pressure (5.4) is always non-negative, for the computational purposes the assumed form of the cost function is the squared acoustic pressure amplitude. Thus, according to (5.4), for a specified point of the surrounding space and a given excitation force, the cost function can be expressed as:

$$f_c(W_1, \dots, W_N) = p_{re}^2(W_1, \dots, W_N) + p_{im}^2(W_1, \dots, W_N). \quad (5.5)$$

The real and imaginary components can be written in the following forms:

$$p_{re}(W_1, \dots, W_N) = \sum_{n=1}^N P_n^{re} W_n \quad (5.6)$$

and

$$p_{im}(W_1, \dots, W_N) = \sum_{n=1}^N P_n^{im} W_n, \quad (5.7)$$

where P_n^{re} and P_n^{im} are modal radiation coefficients, linking the values of the real and imaginary components of the acoustic pressure in a given point of space with the modal amplitudes of vibrations of the plate. The values of those coefficients have to be in general determined numerically, using, for instance, the methods described in Chapter 3 of the present study. The cost function can be thus written in the following form:

$$f_c(W_1, \dots, W_N) = \left[\sum_{n=1}^N P_n^{re} W_n \right]^2 + \left[\sum_{n=1}^N P_n^{im} W_n \right]^2, \quad (5.8)$$

The goal of the optimization process is to find a gain vector \mathbf{G} satisfying the condition (5.2), for which the vibrational pattern of the plate will be altered in such a way that for the given point of space, given excitation parameters and specified boundary conditions, the value (5.8) will be as low as possible. The introduced cost function is actually a sum of two quadratic functions, one related to real and the other to imaginary part of the acoustic pressure. The following notations are introduced:

$$f_{re} = \left[\sum_{n=1}^N P_n^{re} W_n \right]^2, \quad (5.9)$$

$$f_{im} = \left[\sum_{n=1}^N P_n^{im} W_n \right]^2. \quad (5.10)$$

From the computational point of view, in the control optimization process it is convenient to consider both of those components separately. As it will be shown in the following sections of the present chapter, in such cases it is possible to introduce very fast and efficient algorithms for determining optimal feedback control gains, which will ensure achieving the lowest possible values

of the components given with Equations (5.9) and (5.10). However, what is obvious, such a procedure cannot ensure that the global minimum of the cost function (5.8) will be achieved, as the optimal gain values and the resulting optimal vibrational patterns determined for both squared real and imaginary parts of the acoustic pressure independently do not have to coincide for the same sets of control parameters.

Let the f_c^{min} denote the sought, global minimum of the cost function (5.8), achievable for a vector of permitted, optimal gain values \mathbf{G}_c^{opt} (the issues regarding connection between the feedback gains vector and resulting modal amplitudes of vibrations are temporarily omitted at this point - they will be described in details in the following sections of the present chapter). Similarly, the f_{re}^{min} and f_{im}^{min} will denote the global minimums of the squared real and imaginary acoustic pressure components (5.9) and (5.10), achievable for gain vectors \mathbf{G}_{re}^{opt} and \mathbf{G}_{im}^{opt} , respectively. In the most favorable case, if $\mathbf{G}_{re}^{opt} = \mathbf{G}_{im}^{opt}$, then, obviously also $\mathbf{G}_c^{opt} = \mathbf{G}_{re}^{opt} = \mathbf{G}_{im}^{opt}$ and, consequently: $f_c^{min} = f_{re}^{min} + f_{im}^{min}$. However, in the general case, the \mathbf{G}_{re}^{opt} does not have to be equal to \mathbf{G}_{im}^{opt} and, consequently, all the three introduced optimal feedback gain vectors can be different. Thus, the sought global minimum f_c^{min} cannot be determined using the described procedure. Whatever is the case, following relation is always satisfied:

$$f_c^{min} \leq f_{re}^{min} + f_{im}^{min}. \quad (5.11)$$

Thus, for any chosen vector of feedback gains G it is always possible to estimate, how close the achieved cost function value is to the theoretically best possible (although not necessarily achievable) global minimum. Such quality factor can be formally defined as the efficiency of the selected set of control parameters:

$$E_f^c(G) = \frac{f_{re}^{min} + f_{im}^{min}}{f_{re}(G) + f_{im}(G)}, \quad (5.12)$$

where $f_{re}(G)$ and $f_{im}(G)$ denote the values of functions (5.9) and (5.10), obtained for a vector of feedback gains G . In the first step of the assumed optimization procedure, the efficiency value (5.12) is computed for the determined gain vectors \mathbf{G}_{re}^{opt} and \mathbf{G}_{im}^{opt} . If any of the results is sufficiently close to 1, then the achieved value of the cost function can be regarded as the acceptable approximation of the actual global minimum within the permitted range of control parameters, and the optimization process finishes until the change of excitation parameters is detected. In the unfavorable case, if the computed efficiency values are relatively low, the control optimization problem is solved numerically. Whatever the case, the relevant procedures, in order to be time-effective and

computationally reasonable, require fast algorithms for determining the values of components (5.9) and (5.10), related to the real and imaginary parts of the acoustic pressure. The relevant issues are the subject of the further sections of the present chapter.

5.2 Single feedback loop

In order to develop an optimal control algorithm for the considered problem, the components of the cost function, given with Equations (5.9) and (5.10) have to be formulated as functions of control parameters, which are the feedback gains (5.1). For the sake of brevity, in the first step a simplified control system, with only one feedback loop (one sensor-actuator pair) will be considered. The results of the present considerations will be further developed in the following section to address the case of the control system with multiple feedback loops.

Two sources of vibrations are present in the considered system. The primary source is the external, harmonic excitation force, with the angular frequency ω and spatial distribution F_{ext} . At this point it is assumed that those parameters are known in advance - the methods of determining them will be described in Section 5.4, devoted to the problem of adaptation of the control system. The modal amplitudes of vibrations of the plate structure excited by the external force itself - i.e. in the absence of the forces introduced by the control system - can be computed using Equation (2.21):

$$\mathfrak{F}_n = \frac{\iint_S F_S(x, y) \Phi_n dS}{\rho_s h_s (\omega_n^2 - \omega^2) \iint_S \Phi_n^2 dS}, \quad (5.13)$$

where \mathfrak{F}_n denotes the amplitude of the vibrational mode number n , excited by the external disturbance in the absence of the forces introduced by the control system.

The second source of excitation is the piezoelectric actuator. The modal amplitudes of vibrations of the plate, excited by the actuator driven with the harmonic voltage V are given with Equation (4.12). In the considered control system, the actuator is fed with electric voltage signal induced on the sensor, via the signal conditioning circuit and feedback amplifier with adjustable gain G .

The whole system is assumed to be linear, so all the considered phenomena occur with the imposed angular frequency ω and, accordingly to Equation (2.21), the response of the structure to multiple excitation sources can be considered as a sum of responses to each of the forces independently. Thus, the following

relation concerning any vibrational mode number a , where $1 \leq a \leq N$, with a corresponding modal amplitude W_a can be stated:

$$W_a = \mathfrak{F}_a + |V| \tilde{A}_a, \quad (5.14)$$

where $|V|$ is the amplitude of the driving, harmonic voltage V , which, in the considered, steady state operating conditions is equal:

$$V = -G e^{i\omega t} \sum_{n=1}^N \tilde{S}_n W_n, \quad (5.15)$$

where \tilde{S}_n is the modal sensitivity of the sensor to mode n . Thus, substituting (5.15) into (5.14):

$$W_a = \mathfrak{F}_a - G \tilde{A}_a \sum_{n=1}^N \tilde{S}_n W_n. \quad (5.16)$$

The relation (5.16) can be converted into the following form:

$$W_a = \frac{\mathfrak{F}_a}{1 + G \tilde{S}_a \tilde{A}_a} - \frac{G \tilde{A}_a}{1 + G \tilde{S}_a \tilde{A}_a} \sum_{\substack{n=1 \\ n \neq a}}^N \tilde{S}_n W_n. \quad (5.17)$$

Equation (5.17) implies some important remarks that should be taken into account while developing the active vibroacoustic control system. The term $\frac{1}{1 + G \tilde{S}_a \tilde{A}_a}$, included in the first part of the right-hand side of the equation, represents the well-known relation describing the resultant gain of the single input - single output, closed-loop feedback controller. If we were able to create a single-mode in-phase sensor/actuator pair, the system would remain unconditionally stable and the amplitude of the selected mode reaches zero as the feedback gain reaches infinity. Method of creating modal sensors/actuators has been described by Lee and Moon [78]. However, the practical implementation of such transducers is limited to simple one-dimensional beam structures and only to few lowest-order structural modes. Another important disadvantage of single-mode sensors/actuators is the fact that we would need one separate pair of transducers for every mode we would like to control, which would lead to a very complex, multi-layered structure.

Another remark that can be concluded from Equation (5.17), is that one of the conditions of the stability of the considered active control system is meeting

the following condition: $G\tilde{S}_a\tilde{A}_a \neq -1$ for every mode number a , in the whole considered frequency range. The sensor should also be sensitive to the structural modes excited by the corresponding actuator. To provide the described features collocated sensor/actuator pairs can be used. The relevant issues concerning the practical implementation of such solution, are briefly described in Section 4.1 of the present study.

In order to determine the optimal control strategy, i.e., optimal gain value that will ensure minimization of the cost function, using the procedure described in the previous section, the relation between the feedback gain and the resulting modal amplitudes of vibrations has to be determined first. For this purpose, Equation (5.16) is rewritten in the following form:

$$W_a \left(1 + G\tilde{S}_a\tilde{A}_a \right) + G\tilde{A}_a \sum_{\substack{n=1 \\ n \neq a}}^N \tilde{S}_n W_n = \mathfrak{F}_a. \quad (5.18)$$

Equation (5.18) can be written for every single considered structural mode a , where $1 \leq a \leq N$. A set of such equations, providing a complete description of the considered system, can be written in the following matrix form:

$$(\underline{\underline{I}} + \underline{\underline{M}}) \mathbf{W} = \mathbf{F}, \quad (5.19)$$

where $\underline{\underline{I}}$ is a $N \times N$ identity matrix, \mathbf{W} is the vector of modal amplitudes of vibrations, given in the following form:

$$\mathbf{W} = \begin{bmatrix} W_1 \\ W_2 \\ \vdots \\ W_N \end{bmatrix}, \quad (5.20)$$

\mathbf{F} is the vector of modal amplitudes \mathfrak{F}_n , induced by the external excitation force:

$$\mathbf{F} = \begin{bmatrix} \mathfrak{F}_1 \\ \mathfrak{F}_2 \\ \vdots \\ \mathfrak{F}_N \end{bmatrix}, \quad (5.21)$$

and $\underline{\underline{M}}$ is a $N \times N$ control system matrix of feedback coefficients:

$$\underline{\underline{M}} = \begin{bmatrix} G\tilde{A}_1\tilde{S}_1 & G\tilde{A}_1\tilde{S}_2 & \cdots & G\tilde{A}_1\tilde{S}_N \\ G\tilde{A}_2\tilde{S}_1 & G\tilde{A}_2\tilde{S}_2 & \cdots & G\tilde{A}_2\tilde{S}_N \\ \vdots & \vdots & \ddots & \vdots \\ G\tilde{A}_N\tilde{S}_1 & G\tilde{A}_N\tilde{S}_2 & \cdots & G\tilde{A}_N\tilde{S}_N \end{bmatrix}. \quad (5.22)$$

The response of the plate (namely, the modal amplitudes \mathbf{W}) to all the excitation sources (namely, external disturbance and the actuators) is sought. The relevant formula can be obtained by rewriting Equation (5.19) in the following, modified form:

$$\mathbf{W} = (\underline{\underline{I}} + \underline{\underline{M}})^{-1} \mathbf{F}. \quad (5.23)$$

The computations of the inverse matrix $(\underline{\underline{I}} + \underline{\underline{M}})^{-1}$ can be significantly improved by noticing the fact that the matrix $\underline{\underline{M}}$ can be expressed as a product of two vectors and a scalar:

$$\underline{\underline{M}} = G \mathbf{a} \mathbf{s}^T, \quad (5.24)$$

where \mathbf{a} is the vector of modal selectivity values of the actuator expressed in the following form:

$$\mathbf{a} = \mathbf{a}(\omega) = \begin{bmatrix} \tilde{A}_1 \\ \tilde{A}_2 \\ \vdots \\ \tilde{A}_N \end{bmatrix} = \begin{bmatrix} \tilde{A}_1(\omega) \\ \tilde{A}_2(\omega) \\ \vdots \\ \tilde{A}_N(\omega) \end{bmatrix} \quad (5.25)$$

and \mathbf{s} is the vector of modal sensitivity values of the piezoelectric sensor expressed as follows:

$$\mathbf{s} = \begin{bmatrix} \tilde{S}_1 \\ \tilde{S}_2 \\ \vdots \\ \tilde{S}_N \end{bmatrix}. \quad (5.26)$$

In the considered case, due to the form of matrix $\underline{\underline{M}}$ (5.24), the inverse matrix $(\underline{\underline{I}} + \underline{\underline{M}})^{-1}$ can be computed using Sherman-Morrison formula [102], namely:

$$(\underline{\underline{I}} + \underline{\underline{M}})^{-1} = \underline{\underline{I}}^{-1} - \frac{\underline{\underline{I}}^{-1} G \mathbf{a} \mathbf{s}^T \underline{\underline{I}}^{-1}}{1 + G \mathbf{a}^T \underline{\underline{I}}^{-1} \mathbf{s}} = \underline{\underline{I}}^{-1} - \frac{G \mathbf{a} \mathbf{s}^T}{1 + G \mathbf{a}^T \mathbf{s}}. \quad (5.27)$$

Thus, substituting (5.27) into (5.23), the sought relation between the modal amplitudes of vibrations and the feedback gain value is eventually obtained:

$$\mathbf{W} = \left(\underline{\underline{I}}^{-1} - \frac{G \mathbf{a} \mathbf{s}^T}{1 + G \mathbf{a}^T \mathbf{s}} \right) \mathbf{F}. \quad (5.28)$$

Using the obtained relation (5.28), the real and imaginary components of the acoustic pressure, given with Equations (5.6) and (5.7), respectively, can be

computed with the following formula:

$$p_x(G) = \sum_{n=1}^N P_n W_n = \mathbf{P}^T \mathbf{W} = \mathbf{P}^T \mathbf{F} - \frac{\mathbf{P}^T G \mathbf{a} \mathbf{s}^T \mathbf{F}}{1 + G \mathbf{a}^T \mathbf{s}}, \quad (5.29)$$

where $p_x(G)$ is a function of feedback gain value which may refer to either the real or imaginary part of the acoustic pressure (5.6) or (5.7), P_n denote the relevant (either real or imaginary) modal radiation coefficients of the mode number n , and \mathbf{P} is a vector of those coefficients:

$$\mathbf{P} = \begin{bmatrix} P_1 \\ P_2 \\ \vdots \\ P_N \end{bmatrix}. \quad (5.30)$$

Equation (5.29) is the basis for fast and computationally cheap algorithm of determining the sought value of the acoustic pressure, as a function of the feedback gain. Thus, it allows to perform an efficient optimization procedure. However, it is still beneficial at this point to determine the gain values that would minimize the partial cost functions f_{re} and f_{im} , given with Equations (5.9) and (5.10), as those values can be used to estimate the potentially lowest achievable value of the assumed cost function. The relevant procedure is described in detail in the previous section.

It is assumed that the maximum available gain value G^{max} is chosen in such a way, that the system is unconditionally stable, i.e., the following condition is satisfied:

$$\forall_{G \in (0; G^{max})} \quad G \mathbf{a}^T \mathbf{s} \neq -1 \quad (5.31)$$

for the relevant vectors \mathbf{a} and \mathbf{s} . Under the considered conditions, the function $p_x(G)$, given with Equation (5.29) is a monotonic function of the variable G . The optimal gain value G^{opt} , for which the function $p_x^2(G)$, corresponding to either the real or imaginary, partial cost function (5.9) or (5.10), achieves its minimum within the considered, available gain range is sought. Three cases are possible for the considered problem:

1. If $p_x(0) \cdot p_x(G^{max}) \leq 0$, then exists such value G^{opt} , for which $p_x(G^{opt}) = 0$. This optimal feedback gain can be computed using the following relation:

$$G^{opt} = \frac{\mathbf{P}^T \mathbf{F}}{\mathbf{P}^T \mathbf{a} \mathbf{s}^T \mathbf{F} - \mathbf{P}^T \mathbf{F}}. \quad (5.32)$$

2. If any of following occurs:

(a) $p_x(0) \cdot p_x(G^{max}) > 0$ and $p_x(0) > p_x(G^{max}) > 0$, or

(b) $p_x(0) \cdot p_x(G^{max}) > 0$ and $p_x(0) < p_x(G^{max}) < 0$,

then, $G^{opt} = G^{max}$.

3. The last possible case occurs when one of the following conditions is satisfied:

(a) $p_x(0) \cdot p_x(G^{max}) > 0$ and $p_x(0) < p_x(G^{max})$ and $p_x(G^{max}) > 0$, or

(b) $p_x(0) \cdot p_x(G^{max}) > 0$ and $p_x(0) > p_x(G^{max})$ and $p_x(G^{max}) < 0$.

In this case $G^{opt} = 0$.

5.3 Multiple independent feedback loops

The goal of the present section is to develop the investigations described in Section 5.2 into a more general case of an active control system with multiple independent feedback loops. It is assumed that in the considered case the system contain M sensor-actuator pairs. The gains of the feedback amplifiers are described with the vector \mathbf{G} given with (5.1). Despite the number of control loops, all of the other assumptions concerning the system, controlled structure and the external excitation, presented in the previous sections of this chapter are valid. The steady-state vibrations of the plate can be in this case described with a following, modified form of equation (5.23):

$$\mathbf{W} = \left(\underline{\underline{I}} + \underline{\underline{\tilde{M}}} \right)^{-1} \mathbf{F}, \quad (5.33)$$

where $\underline{\underline{\tilde{M}}}$ is a $N \times N$ control system matrix of feedback coefficients, given with:

$$\underline{\underline{\tilde{M}}} = \sum_{k=1}^M \begin{bmatrix} G_k \tilde{A}_{k1} \tilde{S}_{k1} & G_k \tilde{A}_{k1} \tilde{S}_{k2} & \cdots & G_k \tilde{A}_{k1} \tilde{S}_{kN} \\ G_k \tilde{A}_{k2} \tilde{S}_{k1} & G_k \tilde{A}_{k2} \tilde{S}_{k2} & \cdots & G_k \tilde{A}_{k2} \tilde{S}_{kN} \\ \vdots & \vdots & \ddots & \vdots \\ G_k \tilde{A}_{kN} \tilde{S}_{k1} & G_k \tilde{A}_{kN} \tilde{S}_{k2} & \cdots & G_k \tilde{A}_{kN} \tilde{S}_{kN} \end{bmatrix}, \quad (5.34)$$

where \tilde{A}_{ka} is the selectivity function of actuator k to structural mode a (see Equations (4.12) and (4.13)), while \tilde{S}_{ka} denotes the sensitivity of sensor k to the same mode a (see Equation (4.8)). For the sake of brevity and for the computational purposes it is convenient to write matrix $\underline{\underline{\tilde{M}}}$ in the following form:

$$\underline{\underline{\tilde{M}}} = \sum_{k=1}^M \underline{\underline{\tilde{M}}}_k, \quad (5.35)$$

where $\underline{\underline{\tilde{M}}}_k$ is a partial control matrix, connected with a feedback loop number k and defined as:

$$\underline{\underline{\tilde{M}}}_k = \begin{bmatrix} G_k \tilde{A}_{k1} \tilde{S}_{k1} & G_k \tilde{A}_{k1} \tilde{S}_{k2} & \cdots & G_k \tilde{A}_{k1} \tilde{S}_{kN} \\ G_k \tilde{A}_{k2} \tilde{S}_{k1} & G_k \tilde{A}_{k2} \tilde{S}_{k2} & \cdots & G_k \tilde{A}_{k2} \tilde{S}_{kN} \\ \vdots & \vdots & \ddots & \vdots \\ G_k \tilde{A}_{kN} \tilde{S}_{k1} & G_k \tilde{A}_{kN} \tilde{S}_{k2} & \cdots & G_k \tilde{A}_{kN} \tilde{S}_{kN} \end{bmatrix}. \quad (5.36)$$

Analogously as in the case of single feedback loop system (see Equation (5.24)), the partial matrices $\underline{\underline{\tilde{M}}}_k$ are the first order matrices, which can be expressed as:

$$\underline{\underline{\tilde{M}}}_k = G_k \mathbf{a}_k \mathbf{s}_k^T, \quad (5.37)$$

where:

$$\mathbf{a}_k = \begin{bmatrix} \tilde{A}_{k1} \\ \tilde{A}_{k2} \\ \vdots \\ \tilde{A}_{kN} \end{bmatrix} \quad (5.38)$$

and

$$\mathbf{s} = \begin{bmatrix} \tilde{S}_{k1} \\ \tilde{S}_{k2} \\ \vdots \\ \tilde{S}_{kN} \end{bmatrix}. \quad (5.39)$$

The following notation is also introduced:

$$\underline{\underline{\tilde{M}}}_{(k)} = \underline{\underline{\tilde{M}}} - \underline{\underline{\tilde{M}}}_k = \sum_{\substack{l=1 \\ l \neq k}}^M \underline{\underline{\tilde{M}}}_l. \quad (5.40)$$

Equation (5.33) can be rewritten in the following form:

$$\mathbf{W} = \left(\underline{\underline{I}} + \underline{\underline{\tilde{M}}}_{(k)} + \underline{\underline{\tilde{M}}}_k \right)^{-1} \mathbf{F}. \quad (5.41)$$

Taking into account relation (5.37) and – referring to the procedures described in the previous section of the present chapter – the following relation can be

written using Sherman-Morrison formula:

$$\left(\underline{\underline{I}} + \underline{\underline{\tilde{M}}}_{(k)} + \underline{\underline{\tilde{M}}}_k\right)^{-1} = \left(\underline{\underline{I}} + \underline{\underline{\tilde{M}}}_{(k)}\right)^{-1} - \frac{\left(\underline{\underline{I}} + \underline{\underline{\tilde{M}}}_{(k)}\right)^{-1} G_k \mathbf{a}_k \mathbf{s}_k^T \left(\underline{\underline{I}} + \underline{\underline{\tilde{M}}}_{(k)}\right)^{-1}}{1 + G_k \mathbf{a}_k^T \left(\underline{\underline{I}} + \underline{\underline{\tilde{M}}}_{(k)}\right)^{-1} \mathbf{s}_k}. \quad (5.42)$$

The relation (5.42) can be used to develop an effective, iterative algorithm for computation of the inverse matrix $\left(\underline{\underline{I}} + \underline{\underline{\tilde{M}}}\right)^{-1}$ for any applicable set of feedback gain values G_1, G_2, \dots, G_M . Such an algorithm would be very beneficial from the point of view of the control optimization procedure described in Section 5.1. It is assumed that in the beginning all of the feedback gains are set to 0. Then, the gain of the first feedback loop is set to the desired value G_1 and the relevant inverse matrix $\left(\underline{\underline{I}} + \underline{\underline{\tilde{M}}}_1\right)^{-1}$ is computed, based on Equation (5.27). Afterwards, the gain of the second feedback loop is set to the desired value G_2 and the inverse matrix $\left(\underline{\underline{I}} + \underline{\underline{\tilde{M}}}_1 + \underline{\underline{\tilde{M}}}_2\right)^{-1}$ is computed using Equation (5.42) and the result of the previous step. The procedure is repeated until the complete system control matrix $\underline{\underline{\tilde{M}}}$ is determined. The algorithm can be described with the following, subsequent equations:

$$\left(\underline{\underline{I}} + \underline{\underline{\tilde{M}}}_1\right)^{-1} = \underline{\underline{I}} - \frac{G_1 \mathbf{a}_1 \mathbf{s}_1^T}{1 + G_1 \mathbf{a}_1^T \mathbf{s}_1}, \quad (5.43)$$

$$\left(\underline{\underline{I}} + \underline{\underline{\tilde{M}}}_1 + \underline{\underline{\tilde{M}}}_2\right)^{-1} = \left(\underline{\underline{I}} + \underline{\underline{\tilde{M}}}_1\right)^{-1} - \frac{\left(\underline{\underline{I}} + \underline{\underline{\tilde{M}}}_1\right)^{-1} G_2 \mathbf{a}_2 \mathbf{s}_2^T \left(\underline{\underline{I}} + \underline{\underline{\tilde{M}}}_1\right)^{-1}}{1 + G_2 \mathbf{a}_2^T \left(\underline{\underline{I}} + \underline{\underline{\tilde{M}}}_1\right)^{-1} \mathbf{s}_2}, \quad (5.44)$$

⋮

$$\left(\underline{\underline{I}} + \underline{\underline{\tilde{M}}}\right)^{-1} = \left(\underline{\underline{I}} + \underline{\underline{\tilde{M}}}_{(M)}\right)^{-1} - \frac{\left(\underline{\underline{I}} + \underline{\underline{\tilde{M}}}_{(M)}\right)^{-1} G_M \mathbf{a}_M \mathbf{s}_M^T \left(\underline{\underline{I}} + \underline{\underline{\tilde{M}}}_{(M)}\right)^{-1}}{1 + G_M \mathbf{a}_M^T \left(\underline{\underline{I}} + \underline{\underline{\tilde{M}}}_{(M)}\right)^{-1} \mathbf{s}_M}. \quad (5.45)$$

The algorithm described with Equations (5.43) to (5.45) also allows to automatically omit those terms for which the desired feedback gain value is equal to 0, and thus further improve computational time and cost. The calculation

order may be obviously chosen freely and it does not have to follow the assumed numeration of the feedback loops, i.e., $1, 2, \dots, M$, as in the presented example.

Despite the described algorithm, in order to perform a fast and effective control optimization procedure, the potentially optimal feedback vectors \mathbf{G}_{re}^{opt} and \mathbf{G}_{im}^{opt} (defined in Section 5.1) are sought. The relevant partial cost functions that should be minimized are described with following equation:

$$[p_x(\mathbf{G})]^2 = (\mathbf{P} \mathbf{W})^2, \quad (5.46)$$

where $p_x(G)$ is the function of feedback gain vector, which may refer to either the real or imaginary part of the acoustic pressure (see Equations (5.6) and (5.7)). Substituting Equation (5.42) into (5.41) and (5.46), the following relation is finally obtained:

$$p_x(\mathbf{G}) = \mathbf{P}^T \left[\frac{\left(\underline{\underline{I}} + \underline{\underline{\tilde{M}}}_{(k)} \right)^{-1} - \frac{\left(\underline{\underline{I}} + \underline{\underline{\tilde{M}}}_{(k)} \right)^{-1} G_k \mathbf{a}_k \mathbf{s}_k^T \left(\underline{\underline{I}} + \underline{\underline{\tilde{M}}}_{(k)} \right)^{-1}}{1 + G_k \mathbf{a}_k^T \left(\underline{\underline{I}} + \underline{\underline{\tilde{M}}}_{(k)} \right)^{-1} \mathbf{s}_k}}{\left(\underline{\underline{I}} + \underline{\underline{\tilde{M}}}_{(k)} \right)^{-1}} \right] \mathbf{F}, \quad (5.47)$$

for every single k , where $k \in \{1, 2, \dots, M\}$. Thus, if all of the feedback gains, except the one number k , are fixed and considered as constants, then, upholding the assumptions regarding the available gain ranges presented in the previous section, as it can be shown based on the properties of Equation (5.47), under such conditions function $p_x(\mathbf{G})$ is a monotonic function of every single gain parameter G_k . This observation implies a very important conclusion, namely: if any of the elements G_k of a vector \mathbf{G} is neither equal to 0 nor to its maximum available value G_k^{max} , then the value of function $p_x(\mathbf{G})$ can be both increased and decreased by changing the value of the parameter G_k .

For the sake of brevity, the following definitions are introduced:

The control polytope denotes the set of all vectors \mathbf{G} whose elements G_k satisfy the condition $0 \leq G_k \leq G_k^{max}$ – i.e., the whole available control space.

The vertices of the control polytope denote the set of all of the vectors \mathbf{G} belonging to the control polytope whose elements G_k are either equal to 0 or to their maximum permitted values G_k^{max} . This definition can be also formulated using the following notation:

$$\forall_{k \in \{1, 2, \dots, M\}} G_k = 0 \vee G_k = G_k^{max}. \quad (5.48)$$

The edges of the control polytope denote the set of all of the vectors \mathbf{G} belonging to the control polytope whose all elements G_k except exactly one are either equal to 0 or to their maximum permitted values G_k^{max} . The one – and the only one – element of the vector is neither equal to 0 nor to its maximum value. This definition can be also formulated using the following notation:

$$\exists!_{1 \leq l \leq M} \forall_{k \in \{1, 2, \dots, M\}} \begin{cases} 0 < G_k < G_k^{max}, & k = l, \\ G_k = 0 \vee G_k = G_k^{max} & k \neq l. \end{cases} \quad (5.49)$$

The neighboring vertices of the control polytope are defined as such pairs of vectors G^{v1} and G^{v2} belonging to the set of vertices of the control polytope whose all elements except one are equal. The differing element defines the common edge between the neighboring vertices.

Using the introduced nomenclature and referring to the previously described observations regarding the properties of Equation (5.47), the following conclusions concerning the process of determining optimal feedback gain values \mathbf{G}_{re}^{opt} and \mathbf{G}_{im}^{opt} can be drawn:

1. If the value of the function $p_x(\mathbf{G})$ is not equal to 0 for any vector \mathbf{G} belonging to the considered control polytope, then the sought optimal feedback gain vector (either \mathbf{G}_{re}^{opt} or \mathbf{G}_{im}^{opt}) can be found within the vertices of the control polytope
2. If a vector \mathbf{G} , belonging to the control polytope, for which $p_x(\mathbf{G}) = 0$ exists, then the sought value of the global minimum of the considered component of the cost function (either f_{re} or f_{im}) is also equal to 0. This also implies that there exists such gain vector \mathbf{G}^0 , belonging to either vertices or edges of the control polytope, for which the condition $p_x(\mathbf{G}^0) = 0$ is also satisfied. If the vector \mathbf{G}^0 belongs to the edges of the control polytope, then at least one pair of neighboring vertices G^{v1} and G^{v2} for which the following condition is satisfied exists: $p_x(G^{v1}) \cdot p_x(G^{v2}) < 0$. The optimal gain vector \mathbf{G}^0 can be found within the set of vectors creating the common edge between the vertices G^{v1} and G^{v2} , by considering all other gains as constants and solving the single feedback loop problem.

The presented conclusions allow to select only a small subset of the control polytope, with a finite number of elements, among which the optimal feedback gain values \mathbf{G}_{re}^{opt} and \mathbf{G}_{im}^{opt} should be sought. This namely refers to the edges of the control polytope. Thus, if the number of feedback loops is equal M , then the maximum number of points for which computations should be performed is equal

2^M , for each of the components of the cost function. The defined procedures enable performing a fast and effective optimal control algorithm according to the guidelines described in Section 5.1, in the considered, general case of the system with multiple independent feedback loops.

5.4 Identification of the external disturbance

In the considerations described in the previous sections of the present chapter, vector \mathbf{F} , characterizing the parameters of the external excitation force (in terms of the response of the considered structure) was treated as known. However, due to the undertaken assumptions, the control system does not possess such knowledge and it has to have the ability to adapt to changing (steady-state) excitation conditions. No external sensors, such as, for instance, microphones, are included in the system, so, all the information regarding the current state of the structure has to be based on the electric signal induced on the piezoelectric sensors. The adaptation process should in general have the following form:

1. The parameters of the external disturbance are determined based on the signals from piezoelectric sensors and on the knowledge on the modal characteristics of the controlled structure.
2. Optimal feedback gain values are computed using the procedures described in Sections 5.1–5.3 and set in the relevant amplifiers.
3. The system continues monitoring the electric signals from the sensors, checking for deviations from the predicted values, corresponding to the assumed vibrational pattern.
4. If the change in excitation conditions is detected, the algorithm is performed again, starting from the first step.

According to the assumed form of description of the control system, the voltage amplitudes of signals induced on the piezoelectric sensors due to vibrations of the plate can be written in the following, vector form:

$$\mathbf{U} = \begin{bmatrix} \tilde{U}_1 \\ \tilde{U}_2 \\ \vdots \\ \tilde{U}_M \end{bmatrix}. \quad (5.50)$$

The voltage amplitude of the the electric signal induced on a sensor number m is equal:

$$\tilde{U}_m = \sum_{n=1}^N \tilde{S}_{mn} W_n, \quad (5.51)$$

where \tilde{S}_{mn} is the sensitivity function of sensor m to structural mode n . The amplitude W_n of the n^{th} mode is equal:

$$W_n = \mathfrak{F}_n + \sum_{m=1}^M \tilde{A}_{mn} V_m, \quad (5.52)$$

where V_m denotes the amplitude of the voltage signal driving the m^{th} actuator, given with the following relation:

$$V_m = -G_m \tilde{U}_m. \quad (5.53)$$

Substituting Equations (5.51), (5.52) and (5.53) into (5.50), the following relation is obtained:

$$\mathbf{U} = \begin{bmatrix} \sum_{n=1}^N \tilde{S}_{1n} F_n - \sum_{n=1}^N \left(\tilde{S}_{1n} \sum_{m=1}^M G_m \tilde{U}_m \tilde{A}_{mn} \right) \\ \sum_{n=1}^N \tilde{S}_{2n} F_n - \sum_{n=1}^N \left(\tilde{S}_{2n} \sum_{m=1}^M G_m \tilde{U}_m \tilde{A}_{mn} \right) \\ \vdots \\ \sum_{n=1}^N \tilde{S}_{Mn} F_n - \sum_{n=1}^N \left(\tilde{S}_{Mn} \sum_{m=1}^M G_m \tilde{U}_m \tilde{A}_{mn} \right) \end{bmatrix}. \quad (5.54)$$

Thus:

$$\mathbf{U} = \begin{bmatrix} \tilde{U}_1 + \sum_{n=1}^N \left(\tilde{S}_{1n} \sum_{m=1}^M G_m \tilde{U}_m \tilde{A}_{mn} \right) \\ \tilde{U}_2 + \sum_{n=1}^N \left(\tilde{S}_{2n} \sum_{m=1}^M G_m \tilde{U}_m \tilde{A}_{mn} \right) \\ \vdots \\ \tilde{U}_M + \sum_{n=1}^N \left(\tilde{S}_{Mn} \sum_{m=1}^M G_m \tilde{U}_m \tilde{A}_{mn} \right) \end{bmatrix} = \begin{bmatrix} \sum_{n=1}^N \tilde{S}_{1n} \mathfrak{F}_n \\ \sum_{n=1}^N \tilde{S}_{2n} \mathfrak{F}_n \\ \vdots \\ \sum_{n=1}^N \tilde{S}_{Mn} \mathfrak{F}_n \end{bmatrix}. \quad (5.55)$$

All coefficients in Equation (5.55) are known, except for the sought parameters of the external excitation \mathfrak{F}_n . In order to determine them, Equation (5.55) is first written in the following form:

$$\underline{\underline{\mathfrak{C}}} \mathbf{F} = \tilde{\mathbf{u}}, \quad (5.56)$$

where $\underline{\underline{\mathfrak{S}}}$ is the system sensitivity matrix, defined as:

$$\underline{\underline{\mathfrak{S}}} = \begin{bmatrix} \tilde{S}_{11} & \tilde{S}_{12} & \cdots & \tilde{S}_{1N} \\ \tilde{S}_{21} & \tilde{S}_{22} & \cdots & \tilde{S}_{2N} \\ \vdots & \vdots & \ddots & \vdots \\ \tilde{S}_{M1} & \tilde{S}_{M2} & \cdots & \tilde{S}_{MN} \end{bmatrix} \quad (5.57)$$

and the vector $\tilde{\mathbf{u}}$ is given with the following relation:

$$\tilde{\mathbf{u}} = \begin{bmatrix} \tilde{U}_1 + \sum_{n=1}^N \left(\tilde{S}_{1n} \sum_{m=1}^M G_m \tilde{U}_m \tilde{A}_{mn} \right) \\ \tilde{U}_2 + \sum_{n=1}^N \left(\tilde{S}_{2n} \sum_{m=1}^M G_m \tilde{U}_m \tilde{A}_{mn} \right) \\ \vdots \\ \tilde{U}_1 + \sum_{n=1}^N \left(\tilde{S}_{Mn} \sum_{m=1}^M G_m \tilde{U}_m \tilde{A}_{mn} \right) \end{bmatrix}. \quad (5.58)$$

All of the elements of both matrix $\underline{\underline{\mathfrak{S}}}$ and vector $\tilde{\mathbf{u}}$ can be computed based on the known parameters of the system and the controlled structure, as well as on the excitation frequency (this concerns the selectivity functions of the actuators which are frequency-dependent). Due to the assumed, harmonic form of the considered signals, the frequency of vibrations can be easily determined, based on the signal from piezoelectric sensors. The method of solving Equation (5.56) for the unknown parameters of the external excitation depends on the relation between the number of considered structural modes of vibrations N and the number of control feedback loops M . Three cases are possible:

1. If $M < N$ then the equation system expressed in the matrix form (5.56) is underdetermined, with an infinite number of solutions for the sought vector \mathbf{F} . The selection of a specific, estimated solution \mathbf{F}^* is based on additional condition - in the present considerations it is assumed, that the L2-norm is minimized and the estimated solution is computed using the following equation:

$$\mathbf{F}^* = \underline{\underline{\mathfrak{S}}}^T (\underline{\underline{\mathfrak{S}}} \underline{\underline{\mathfrak{S}}}^T)^{-1} \tilde{\mathbf{u}}. \quad (5.59)$$

2. If $M = N$ then the equation system expressed in the matrix form (5.56) has one unique solution (assuming that the system sensitivity matrix has full rank - the modal characteristics of the sensors are linearly independent), which can be computed as:

$$\mathbf{F}^* = (\underline{\underline{\mathfrak{S}}})^{-1} \tilde{\mathbf{u}}. \quad (5.60)$$

3. If $M > N$ then the equation system expressed in the matrix form (5.56) is overdetermined and the least-squares method is used in order to estimate the sought vector of the parameters of external excitation:

$$\mathbf{F}^* = (\underline{\underline{\mathfrak{C}}}^T \underline{\underline{\mathfrak{C}}})^{-1} \underline{\underline{\mathfrak{C}}}^T \tilde{\mathbf{u}}. \quad (5.61)$$

The described algorithm can be used to perform the adaptation process, i.e., to provide a necessary knowledge on the parameters of external excitation required for the control optimization procedure. The algorithm takes into account all the assumed available knowledge concerning both the controlled structure (eigenfrequencies and the corresponding mode shape functions), as well as the elements of the control system (modal sensitivity and selectivity functions of the piezoelectric sensors and actuators). However, it is also possible that some additional information, regarding probable, predicted characteristics of the external excitation source are also available. For instance, if the propagation paths of the disturbances in the environment to which the considered structure belongs are to some extent predictable, then some modal components can be regarded as more and other as less probable to occur. The presented approach does not allow to include such knowledge, although, in some cases it could be very beneficial to do so.

In order to enable including the described, additional information, the presented adaptation algorithm has to be modified and developed. It is assumed that the predictions regarding the characteristics of external disturbance are introduced as ratios of selected modal components, in the following form:

$$\frac{F_k^*}{\beta_k} = \frac{F_l^*}{\beta_l}, \quad (5.62)$$

where F_k^* and F_l^* are the elements of the estimated vector of the modal parameters of the external excitation \mathbf{F}^* , corresponding to structural modes of vibrations number k and l , respectively. The β_k and β_l are the corresponding modal weight coefficients. Equation (5.62) defines the desired ratio of two selected modal components of vector \mathbf{F}^* .

It is assumed that one of the modal coefficients, namely, for instance, the one denoted with index k is considered as the reference parameter. The desired, predicted ratios of all other considered coefficients with indexes l , where $1 \leq l \leq N$ and $l \neq k$ are written in the following form, equivalent with (5.62):

$$F_l^* - \frac{\beta_l}{\beta_k} F_k^* = 0. \quad (5.63)$$

All defined relations in the form (5.63) can be arranged as a set of equations and written in the following matrix form:

$$\begin{bmatrix} 1 & 0 & 0 & \dots & -\frac{\beta_1}{\beta_k} & \dots & 0 \\ 0 & 1 & 0 & \dots & -\frac{\beta_2}{\beta_k} & \dots & 0 \\ \vdots & \dots & \ddots & & & & \vdots \\ 0 & 0 & 0 & \dots & -\frac{\beta_1}{\beta_{k-1}} & \dots & 0 \\ 0 & 0 & 0 & \dots & -\frac{\beta_2}{\beta_{k+1}} & \dots & 0 \\ \vdots & \dots & \ddots & & & & \vdots \\ 0 & \dots & \dots & & -\frac{\beta_N}{\beta_k} & \dots & 1 \end{bmatrix} \mathbf{F}^* = \begin{bmatrix} 0 \\ 0 \\ \vdots \\ 0 \end{bmatrix}. \tag{5.64}$$

The left hand side matrix has dimensions $(N - 1) \times N$. The equation (5.64) represents the predicted, desired form of the vector \mathbf{F} . The second equation system, that obviously has to be included in the adaptation algorithm, is given with (5.56) and represents the modal parameters of the external excitation, determined from the measurements. Both relations (5.56) and (5.64) should contribute to the final result, in order to obtain a solution that is consistent with the measurements on the one hand and as close as possible to the predictions, on the other hand. Tikhonov regularization [103] is used to balance those contributions and to determine the optimal solution. The combination of (5.56) and (5.64) leads to the following matrix equation:

$$\underbrace{\begin{bmatrix} \gamma \begin{bmatrix} 1 & 0 & 0 & \dots & \frac{w_1}{w_k} & \dots & 0 \\ 0 & 1 & 0 & \dots & \frac{w_2}{w_k} & \dots & 0 \\ \vdots & \dots & \ddots & & & & \vdots \\ 0 & \dots & \dots & & \frac{w_N}{w_k} & \dots & 1 \end{bmatrix} \\ \underline{\underline{\mathfrak{S}}} \end{bmatrix}}_{\underline{\underline{\mathfrak{S}}}} \mathbf{F}^* = \begin{bmatrix} 0 \\ \vdots \\ 0 \\ \tilde{\mathbf{u}} \end{bmatrix}, \tag{5.65}$$

where γ is the regularization parameter. Equation (5.65) is solved for various values of the regularization parameters, in order to find such a value γ_{opt} and the corresponding, estimated solution \mathbf{F}^*_{opt} for which the following condition is satisfied:

$$\forall_{\gamma \in (0; \infty)} (\underline{\underline{\mathfrak{S}}} \mathbf{F}^*_{opt})^2 + (\gamma_{opt} \underline{\underline{\Gamma}} \mathbf{F}^*_{opt})^2 \leq (\underline{\underline{\mathfrak{S}}} \mathbf{F}^*)^2 + (\gamma \underline{\underline{\Gamma}} \mathbf{F}^*)^2, \tag{5.66}$$

where γ denotes any chosen value of the regularization parameter and \mathbf{F}^* is the corresponding solution to Equation (5.65). The $\underline{\underline{\Gamma}}$ denotes the left hand

side matrix from Equation (5.64). In other words, the total error between the optimal solution \mathbf{F}_{opt}^* and both predictions and measurements is minimized. The presented, modified, and developed version of the adaptation algorithm should be especially useful in the case of highly underdetermined systems (i.e., in the cases when the number of the considered vibrational modes N is much greater than the number of the feedback control loops introduced in the system M).

5.5 Implementation of the active control system

Practical implementation and experimental validation of the active vibroacoustic approach described in the present study require both dedicated hardware and software. The relevant means have been developed, implemented, and tested. A large number of prototypes of various electronic subsystems were constructed and evaluated within the framework of the conducted research. The initial concepts were significantly improved by taking into account the conclusions drawn at the successive design stages. A general schematic diagram of the final version of the developed active control system is presented in Figure 5.1. Only a single control channel (single feedback loop) is presented in order to illustrate the assumed principles of operation - the target system should consists of an appropriate, desired number of such units.

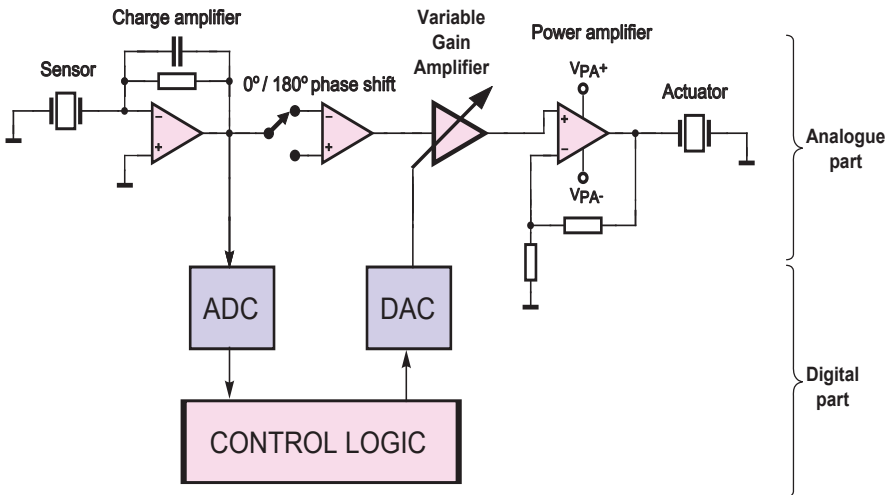


Figure 5.1. General schematic diagram of the developed active vibroacoustic control system (single feedback loop).

The most important, original feature of the developed system is separation of the independent, fully analogue feedback loop connecting piezoelectric sensor and actuator. Such a solution, besides circuit simplification, allows to avoid all the potential complications related with signal conversion (time delays, jitter, noise) and to ensure a high reliability. The considered control system is very sensitive to even small, unintended phase shifts between input and output, as they strongly affect the control performance and may lead to loss of stability. Data acquisition and analysis are performed independently, by a separate digital subsystem. The presented approach allows to significantly reduce the requirements imposed on the control logic.

The piezoelectric sensor is connected directly to a charge amplifier circuit, which ensures impedance matching and amplification. The output of the charge amplifier is connected to an optionally activated $0/180^\circ$ phase inverter. Such a solution enables coupling piezoelectric sensors and actuators with the same or opposite polarizations, and increases the versatility of the developed device. The signal from piezoelectric sensor, after conditioning, is also fed to the input of an analog-to-digital converter, and further to the control logic unit, where it is processed to extract the information necessary to determine a current state of the controlled structure and the relevant optimal control strategy. In parallel, the same signal is also fed to the input of a variable gain amplifier (VGA) whose gain value is governed by the logic unit. This block of the system enables realization of the selected control strategy. The output signal is fed to the piezoelectric actuator via a power amplifier, which is powered from a separate, symmetrical power supply, with a higher voltage. Such a solution enables extending the range of the output driving signal and improving its quality.

A circuit diagram of a single channel of the final version of the analog part of the controller is presented in Figure 5.2. Construction of the signal conditioning circuit is described in detail in Section 4.4. A high number of the selectable feedback components of the charge amplifier (10 resistors and 10 capacitors which can be freely combined in parallel connections using sets of switches) ensures wide possibilities in adjusting both gain and lower cutoff frequency. The phase inverter is constructed based on TL072 low noise operational amplifier working as inverting amplifier with a unity gain.

The SSM2018 voltage controlled amplifier (VCA) is used to adjust the gain of the feedback loop and perform the optimal control strategy. The gain of this amplifier is described with the following exponential relation:

$$g^{SSM} = e^{(-4 \cdot V_C^{SSM})}, \quad (5.67)$$

where V_C^{SSM} is the constant, control voltage applied to the amplifier. The avail-

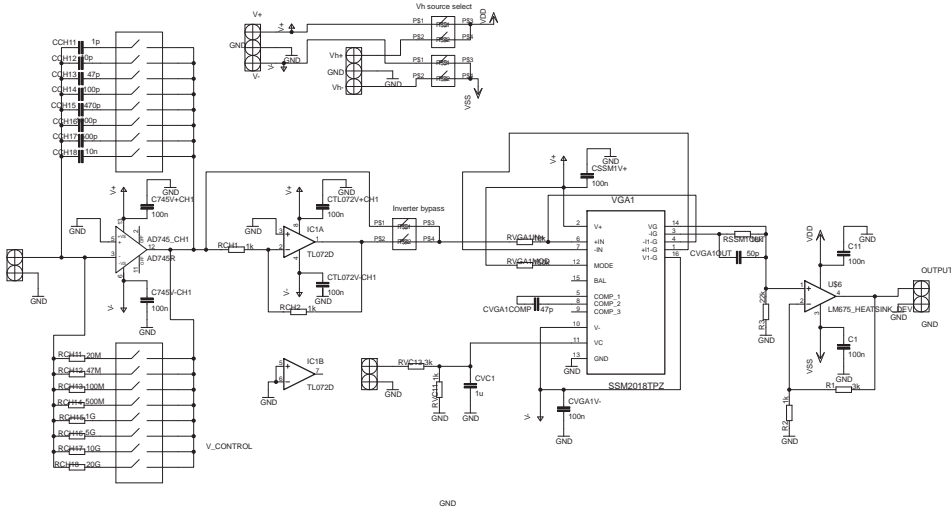


Figure 5.2. Circuit diagram of the final version of the feedback controller used for experimental investigations - analogue part, one single channel (out of four in total).

able gain range is 140 dB (from -100 dB up to 40 dB). The output of the voltage controlled amplifier is connected to the input of LM675 power amplifier which can operate at supply voltages up to 60 V and deliver output currents reaching up to 3 A.

The developed analog part of the active control system was successfully constructed and tested. A picture of the final device, implementing four feedback loops, is presented in Figure 5.3. The electronic components were mounted on a double-sided printed circuit board. The power amplifiers were attached to heat sinks in order to prevent their overheating in case of any system failure.

The digital part of the control system was implemented using National Instruments cRIO platform, model 9075. The communication with the described analog subsystem was performed via additional ADC and DAC modules. The necessary control software was developed under the LabView environment. The software allows to view in the real-time signals from eight channels (four sensors and four actuators) and to adjust gains of four independent feedback loops. The

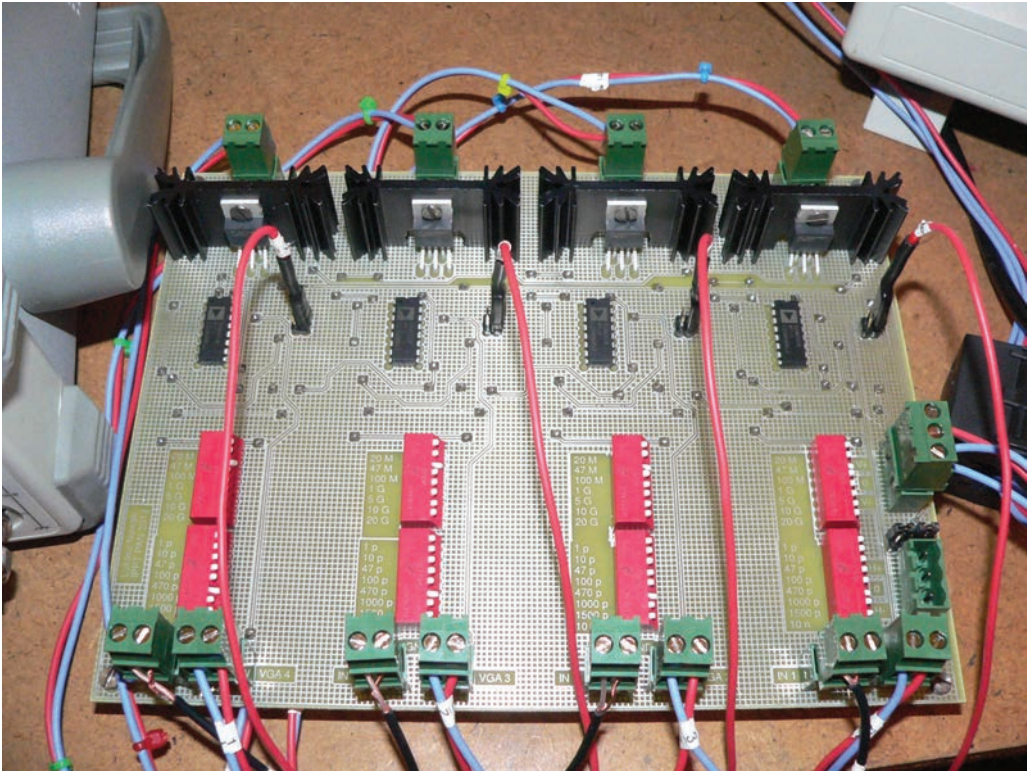


Figure 5.3. Final version of four-channel feedback controller used for experimental investigations - analogue part.

communication with the control logic unit is performed via Ethernet, using a laptop with dedicated software implementing the user interface. The software control panel of the described system is presented in Figure 5.4.

5.6 Experimental investigations

The experimental investigations concerning capabilities and limitations of the developed active vibroacoustic control approach were carried out using a rectangle-shaped aluminium plate, which was 300 mm long, 200 mm wide, and 1 mm thick. The plate was clamped by a 6 cm long middle section of its shorter edge, with all other edges free. The considered structure is presented in Figure 5.5. The plate was also used for other experimental investigations described in the previous chapters of the present study, thus the obtained results and

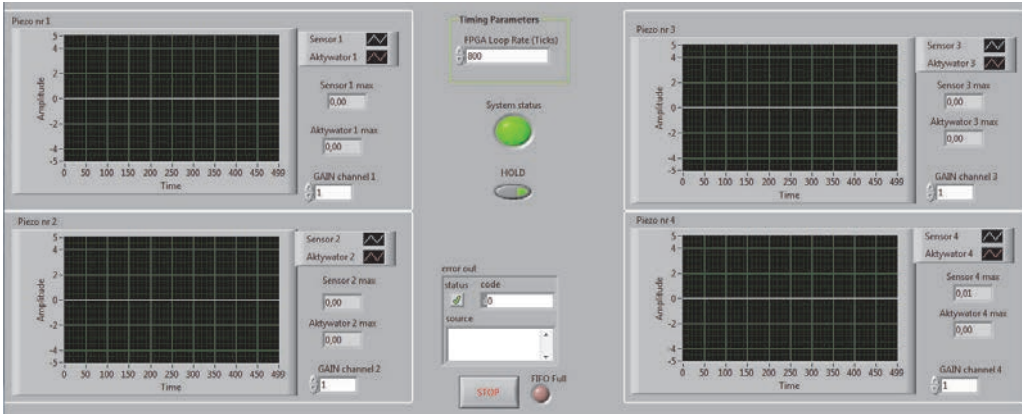


Figure 5.4. Software control panel of the developed active control system.

drawn conclusions concerning the vibrational characteristics (Chapter 2), acoustic radiation (Chapter 3), and sensing and exciting vibrations using piezoelectric transducers (Chapter 4) are valid in terms of the present considerations.

Five pairs of piezoelectric transducers made of Pz29 piezoceramic material (Ferroperm) were attached symmetrically on both sides of the considered structure. The transducers were 3 cm wide, 2 cm long and 0,3 mm thick. The transducers were glued to the plate using the technology described in Section 4.5, with the plate as a common ground electrode. In order to describe the positions of the transducers on the plate and also to define the relative coordinates of points in the ambient space at which the acoustic measurements were taken, a global cartesian coordinate system, with XY axes parallel to the shorter and longer edges of the plate, respectively, is introduced. Assuming the spatial configuration of the plate during the experiments as presented in Figure 5.5, with the longer edge perpendicular to the ground plane, the origin of the coordinate system is situated in the lower left corner of the plate. Positions of the piezoelectric transducers on the surfaces of the plate can be thus described as it is presented in Table 5.1.

Pairs of the transducers with numbers 1 to 4 were used as sensors and actuators (i.e., one of the transducers in each pair served as sensor, while the other, attached symmetrically, as actuator). Thus, up to four independent feedback loops were available in the assumed configuration of the control system. The pair number 5 was used to generate vibrations of the structure, simulating external excitation source – both transducers were connected to the harmonic signal generator, with adjustable amplitude and frequency. Accordingly

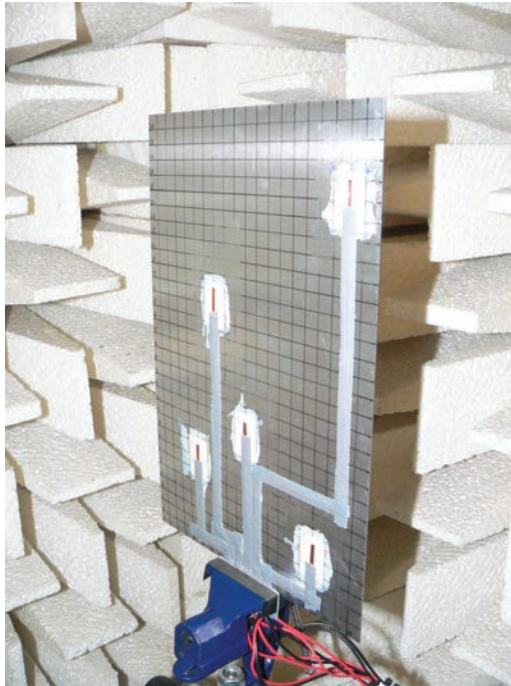


Figure 5.5. Plate structure used for the experimental investigations.

Number of pair of piezoelectric transducers	XY coordinates (in centimeters, middle point of the transducer)
1	(5 ; 7)
2	(7 ; 18)
3	(10 ; 10)
4	(18 ; 25)
5	(16 ; 4)

Table 5.1. Locations of pairs of piezoelectric transducers used for the experimental investigations on the surfaces of the plate structure.

to the considerations presented in Chapter 4, the transducers arranged in the described configurations create collocated sensor-actuator pairs. Such a configuration should theoretically ensure an absolute stability of the control system, at least in the case of a single feedback loop operation, as the products of the corresponding modal sensitivity and selectivity values in the denominator in Equation (5.17) are always positive.

The experiments were carried out in an anechoic chamber. The plate was clamped with a vice attached to a tripod. The acoustic measurements were performed using Brüel&Kjær half inch, precise electret microphone, connected to a Nexus preamplifier by the same manufacturer. The amplitude of the acoustic pressure was determined using Tektronix TDS2004C oscilloscope. The wires attached to the microphone and piezoelectric transducers were routed outside the acoustic chamber, to another room, where all the necessary control and measurement equipment was situated. The stands for both plate and microphone were covered with acoustic foam panels, in order to minimize the reflections. The laboratory stand used for the experimental investigations on the active vibroacoustic control is presented in Figure 5.6.

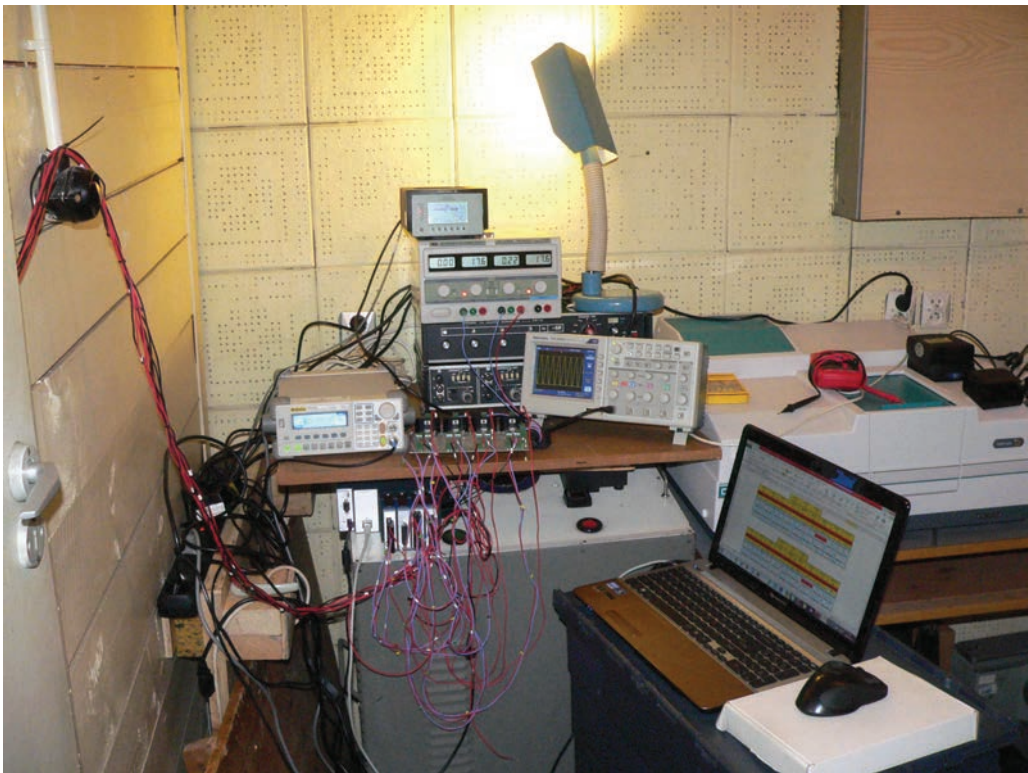


Figure 5.6. Laboratory stand used for the experimental investigations on the active vibroacoustic control.

The piezoelectric transducers used to generate vibrations of the plate were fed with harmonic signals from a programmable generator, with voltage amplitudes reaching up to ± 30 V. The levels of excitations were limited by occurring

nonlinear effects. Very sharp resonant characteristics of vibrations of the plate were observed, with very high amplitudes at frequencies corresponding to the determined eigenfrequencies of the structure (see Table 2.1) and very low levels of vibrations for off-resonant excitations. The acoustic measurements revealed that significant noise levels generated by the plate are observed only for resonant vibrations. For this reason only the excitation frequencies equal to some selected eigenfrequencies of the structure were used in the experiments. According to considerations presented in Sections 2.1 and 4.7 of the present study, in such cases only one mode of vibrations, corresponding to the selected eigenfrequency, can be considered, as the amplitudes of other forms of vibrations are relatively low enough to be neglected. This conclusion was also verified by the measurements performed using a laser vibrometer. Thus, the control strategy, resulting from the theoretical approach presented in Sections 5.1-5.4 can be significantly simplified. The adaptivity process can be based only on the frequency analysis of the signals from the piezoelectric sensors, as the state of the structure in the considered case is uniquely determined by the resonant frequency and the amplitude of vibrations. The optimal control strategy in such case should theoretically consist of setting the gains of all the feedback loops of the system to their maximum available values.

The measurements were performed using a microphone positioned at different points of the ambient space. The coordinates of those points are expressed in terms of the assumed global coordinate system, with the plate located in the plane $z = 0$. The microphone was calibrated before each session of measurements, using a dedicated calibrator from Brüel&Kjær. Thus, the determined amplitudes of the electric signals from the preamplifier were converted into the true values of the acoustic pressure. The experiments were carried out for various configurations of the involved feedback loops in the active control system. The results are presented in plots and tables below. The non-dimensional gain value $G_x \left[\frac{V}{V} \right]$, where x denotes the number of considered feedback loops, define the actual gain of the corresponding voltage controlled amplifier (see schematic diagram in Figure 5.1), set by the digital part of the control system. It does not include either the gain of the charge amplifier or the gain of the output power amplifier – those parameters of the control system were held constant for every measurement.

The presented results concern four different vibrational modes of the plate, namely, the 9th, 11th, 13th, and 14th mode (see Table 2.1 for details). The selected forms of vibrations were chosen due to relatively high observed sound pressure levels and due to the fact that the considered results are representative in terms of the control system performance and stability. In other words, the presented

levels of sound reduction cover the whole range of the observed cases, for all investigated structural modes of the considered structure, including the both highest and lowest reduction levels. The number of introduced results is limited to such a representative set, as the purpose of the present study is not to focus on one, specific structure and system configuration, but to investigate the general idea and the underlying mechanisms basing on a representative example.

Plots in Figures 5.7 and 5.8 present the measured sound pressure level generated by the plate structure vibrating in the 11th structural mode at frequency 320 Hz, at a point of the ambient space with coordinates $x = 2$ cm, $y = 25$ cm, $z = 3$ cm, as a function of the gain of feedback loops no. 1 and 2, respectively. Only one feedback loop of the control system was active during the measurements. As it can be seen, very similar, significant reductions in the sound pressure level – reaching about 3 dB – were achieved in both considered cases. The investigations also revealed problems with stability of the developed active control system which were not predicted by the theoretical considerations. In theory, the utilized collocated pairs of piezoelectric sensors and actuators should ensure a total stability of the system. However, in practice it turned out, that for every frequency of vibrations and every feedback loop exists some critical gain value beyond which the plate falls into some higher order resonances, at eigenfrequencies greater than about 1-2 kHz. Decreasing the gain below this critical value instantly eliminates the problem. Thus, the maximum gain value in all of the presented further plots and tables is not the maximum available gain but it is determined only by the stability issues (unless otherwise noted).

The plot in Figure 5.9 presents the measured sound pressure level generated by the plate structure vibrating in the 11th structural mode at frequency 320 Hz, at a point of the ambient space with coordinates $x = 2$ cm, $y = 25$ cm, $z = 3$ cm, as a function of gains G_1 and G_2 of feedback loops no. 1 and 2, operating together. As it can be seen, by combining the operation of the two independent control loops, further reduction in generated noise can be achieved – the minimum measured sound pressure level in this case is equal 74,72 dB, which is about 3 dB less than the minimum levels obtained for both feedback loops operating alone (about 6 dB drop in total is observed). It is worth noticing, that this result is obtained for lower maximum available gain values than in the cases illustrated in Figures 5.7 and 5.8, as the critical gains determined by the stability issues were significantly lower, as compared to the independent, single-feedback loop operation.

The plots in Figures 5.10 and 5.11 present the measured sound pressure level generated by the plate structure vibrating in the 13th structural mode at frequency 380 Hz, at the same point of the ambient space, with the coordinates

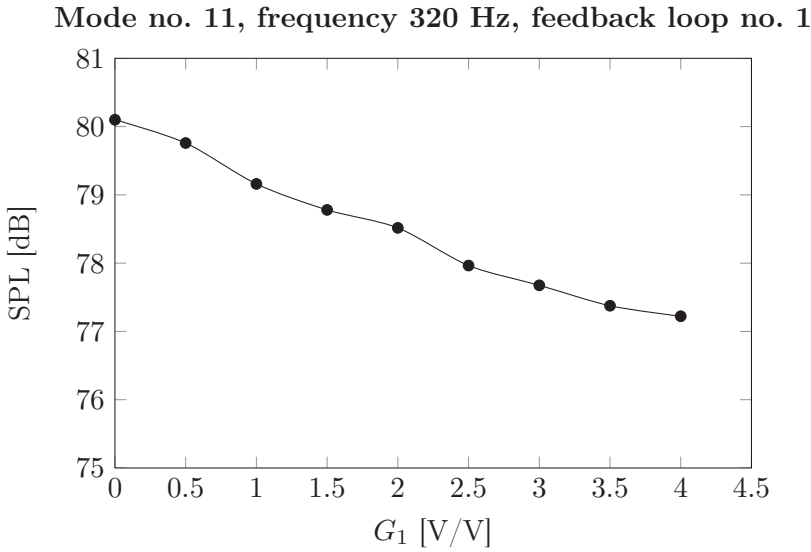


Figure 5.7. Sound pressure level as a function of gain value of feedback loop no. 1 for the plate vibrating in the 11th structural mode, at frequency 320 Hz. Position of the microphone: $x = 2$ cm, $y = 25$ cm, $z = 3$ cm.

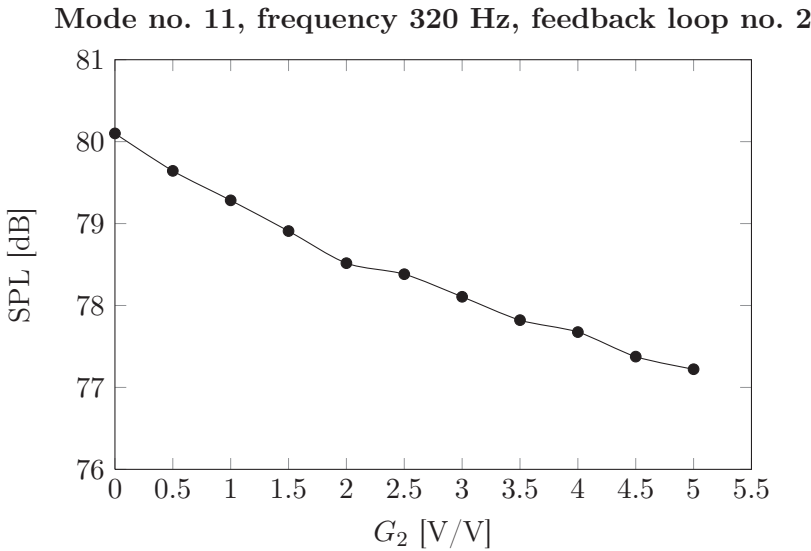


Figure 5.8. Sound pressure level as a function of gain value of feedback loop no. 2 for the plate vibrating in the 11th structural mode, at frequency 320 Hz. Position of the microphone: $x = 2$ cm, $y = 25$ cm, $z = 3$ cm.

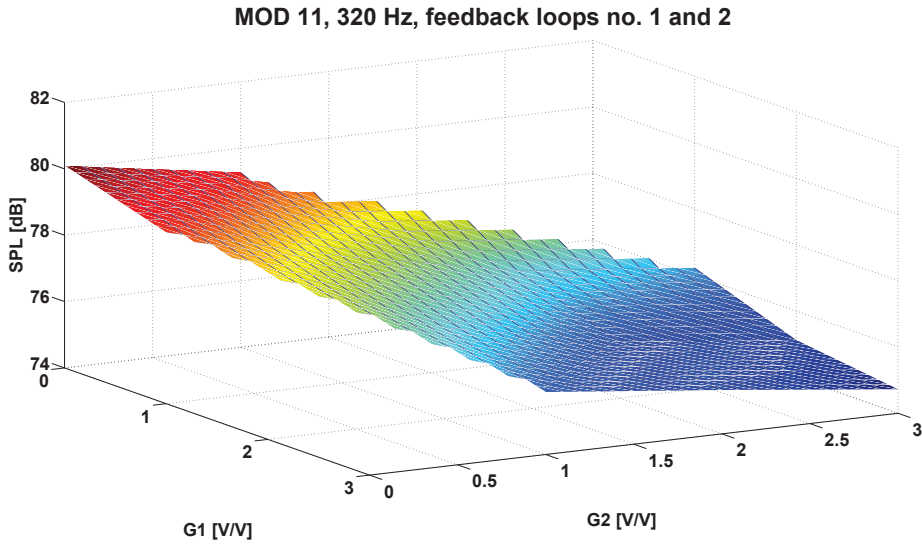


Figure 5.9. Sound pressure level as a function of gain values of feedback loops no. 1 and 2, for the plate vibrating in the 11th structural mode, at frequency 320 Hz. Position of the microphone: $x = 2$ cm, $y = 25$ cm, $z = 3$ cm.

$x = 2$ cm, $y = 25$ cm, $z = 3$ cm, as a function of the gain of feedback loops no. 1 and 2, respectively. About a 3,5 dB drop in the sound pressure level is observed due to the operation of loop no. 1, and almost a 6 db drop for loop no. 2. Thus, the reduction is better than in the previously described case concerning structural mode no. 11, even though the maximum applied gain values were identical in both cases. This observation agrees with the theoretical predictions that the control performance should strongly depend on both parameters of vibrations and modal characteristics of the utilized sensor-actuator pairs.

The plot in Figure 5.12 presents the measured sound pressure level generated by the plate structure vibrating in the 13th structural mode at frequency 380 Hz, at a point of the ambient space with the coordinates $x = 2$ cm, $y = 25$ cm, $z = 3$ cm, as a function of gains G_1 and G_2 of feedback loops no. 1 and 2, operating together. Once again, the observations prove that the joint operation of two independent feedback loops helps to achieve a better control performance than the single-feedback loop operation. In the described case about a 2,5 dB additional reduction is observed for the joint operation and identical maximum gain values.

The plot in Figure 5.13 presents the measured sound pressure level generated by the plate structure vibrating in the 14th structural mode at frequency 411 Hz,

Mode no. 13, frequency 380 Hz, feedback loop no. 1

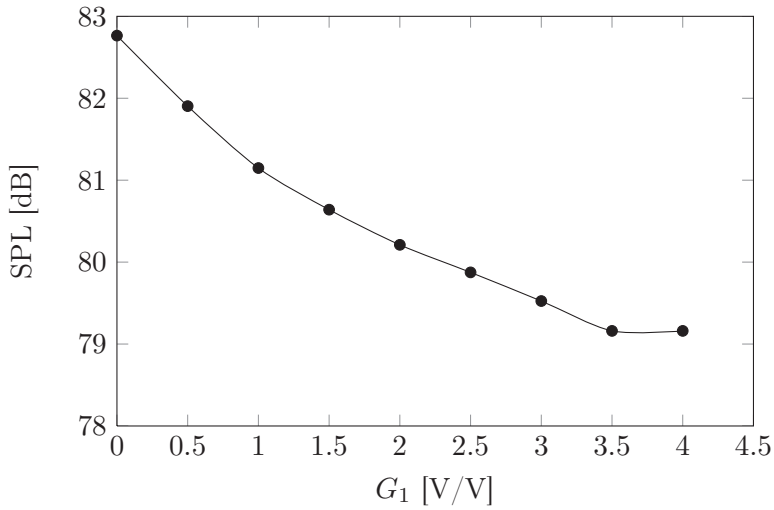


Figure 5.10. Sound pressure level as a function of gain value of feedback loop no. 1 for the plate vibrating in the 13th structural mode, at frequency 380 Hz. Position of the microphone: $x = 2$ cm, $y = 25$ cm, $z = 3$ cm.

Mode no. 13, frequency 380 Hz, feedback loop no. 2

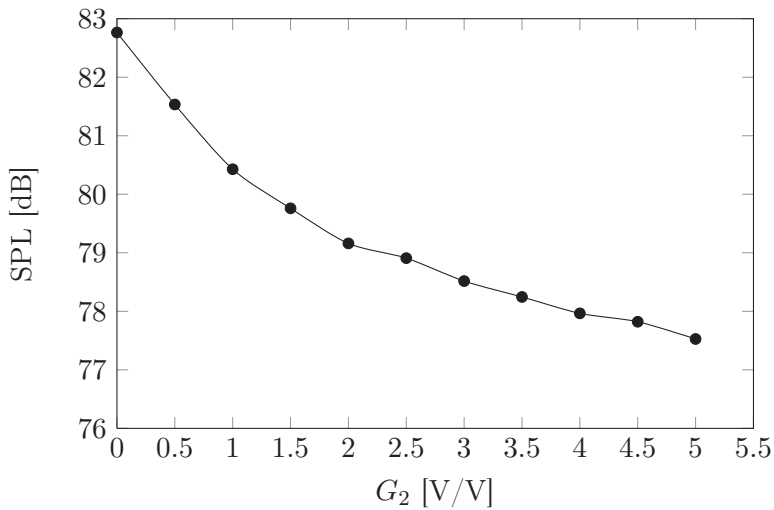


Figure 5.11. Sound pressure level as a function of gain value of feedback loop no. 2 for the plate vibrating in the 13th structural mode, at frequency 380 Hz. Position of the microphone: $x = 2$ cm, $y = 25$ cm, $z = 3$ cm.

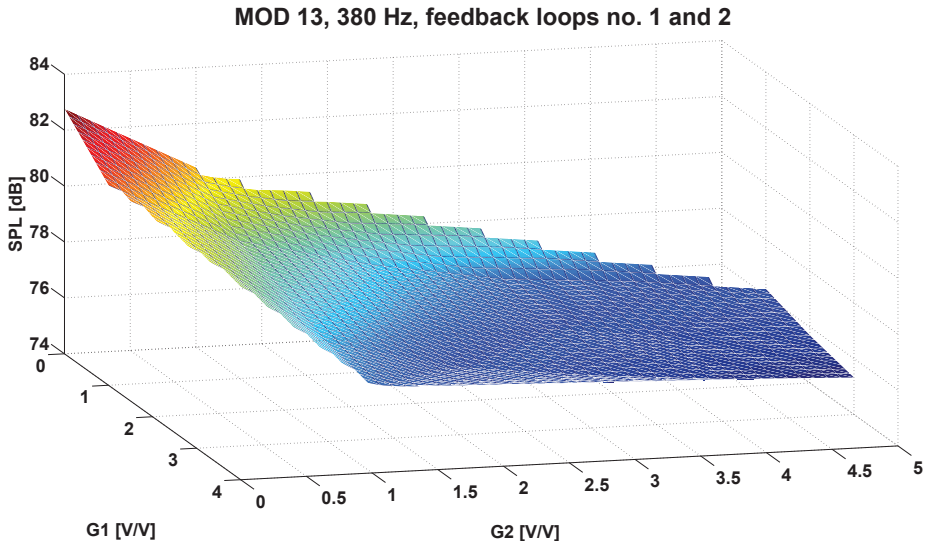


Figure 5.12. Sound pressure level as a function of gain values of feedback loops no. 1 and 2, for the plate vibrating in the 13th structural mode, at frequency 380 Hz. Position of the microphone: $x = 2$ cm, $y = 25$ cm, $z = 3$ cm.

at the point of the ambient space with coordinates $x = 2$ cm, $y = 25$ cm, $z = 3$ cm, as a function of the gain of feedback loop no. 4. In this case, about a 1 dB drop is achieved. This result, as compared to the other results concerning different modes of vibrations and different feedback loops, presented for instance in Figures 5.10 and 5.11, can be regarded as a relatively poor level of noise reduction.

The plot in Figure 5.14 presents analogous results to those presented in the Figure 5.13, however, obtained for two different feedback loops – namely, no. 1 and 2, acting simultaneously. As it can be seen, a significantly greater level of noise reduction is obtained in this case – reaching a maximum of about 4 dB.

Table 5.2 presents measured sound pressure levels for various combinations of cooperation of feedback loops no. 1, 2 and 4, obtained for analogous conditions to which the plots in Figures 5.13 and 5.14 are referred. The results clearly indicate that the most beneficial (in terms of achievable levels of sound reduction) is cooperation of all the considered feedback loops. An interesting observation is that by introducing the feedback loop no. 4 to loops no. 1 and 2, a further 3,5 dB drop in sound pressure level is obtained – despite the fact that the loop number 4 operating alone allowed only for about 1 dB of noise reduction (see plot in Figure 5.13).

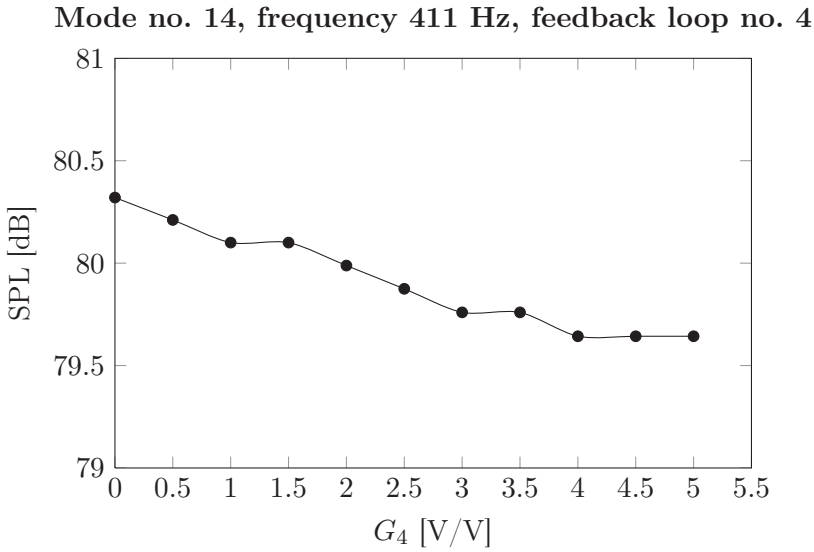


Figure 5.13. Sound pressure level as a function of gain value of feedback loop no. 4 for the plate vibrating in the 14th structural mode, at frequency 411 Hz. Position of the microphone: $x = 2$ cm, $y = 25$ cm, $z = 3$ cm.

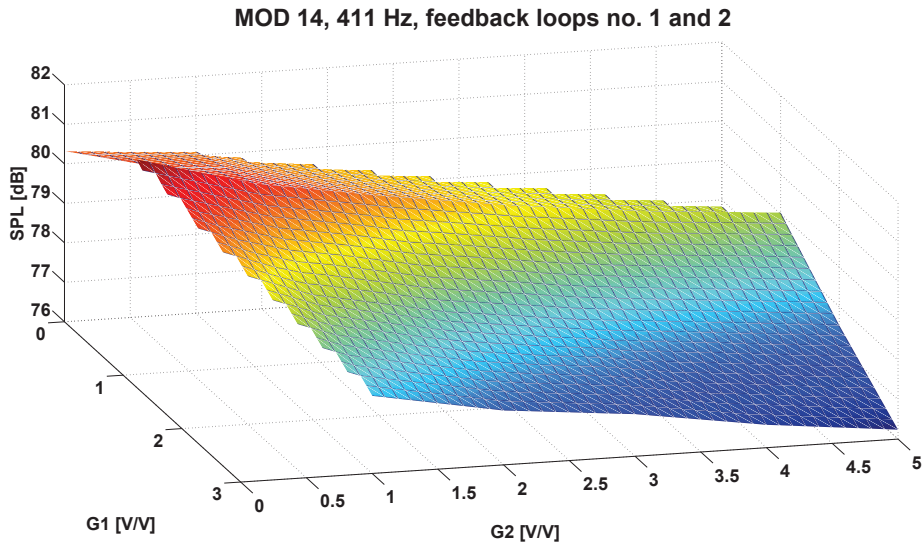


Figure 5.14. Sound pressure level as a function of gain values of feedback loops no. 1 and 2, for plate vibrating in the 14th structural mode, at frequency 411 Hz. Position of the microphone: $x = 2$ cm, $y = 25$ cm, $z = 3$ cm.

G_1	G_2	G_4	SPL [dB]
0	0	0	80.32
3	0	0	78.78
0	5	0	79.64
0	0	3	79.64
3	5	0	76.24
3	0	3	74.93
0	5	3	77.07
3	5	3	72.89

Table 5.2. Sound pressure level as a function of gain values of feedback loops no. 1, 2 and 4 for the plate vibrating in the 14th structural mode, at frequency 411 Hz. Position of the microphone: x = 2 cm, y = 25 cm, z = 3 cm.

The plots in Figures 5.15-5.17 present the sound pressure level generated by the plate structure vibrating in the 9th structural mode at frequency 269 Hz, at a point of the ambient space with coordinates x=10 cm, y=15 cm, z=5 cm, as a function of the gains of the feedback loops no. 2, 3 and 4, respectively. The achieved level of noise reduction is very low in all presented cases – in fact, for feedback loops no. 3 and 4 it may actually be considered as negligible.

Mode no. 9, frequency 269 Hz, feedback loop no. 2

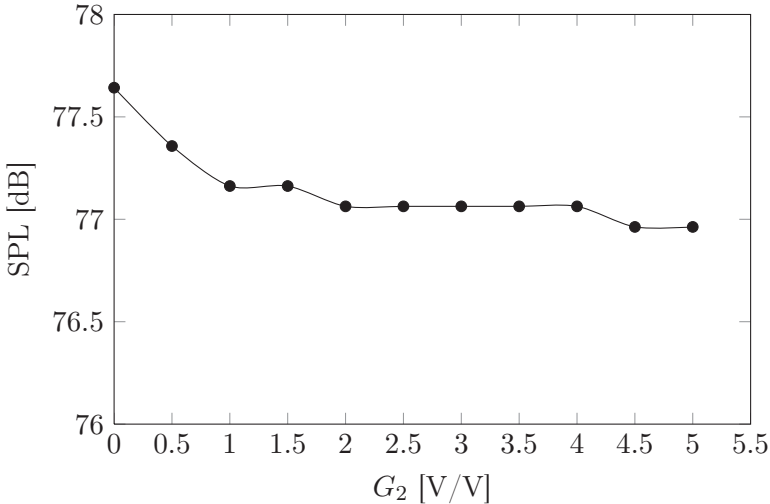


Figure 5.15. Sound pressure level as a function of gain value of feedback loop no. 2 for the plate vibrating in the 9th structural mode, at frequency 269 Hz. Position of the microphone: x = 10 cm, y = 15 cm, z = 5 cm.

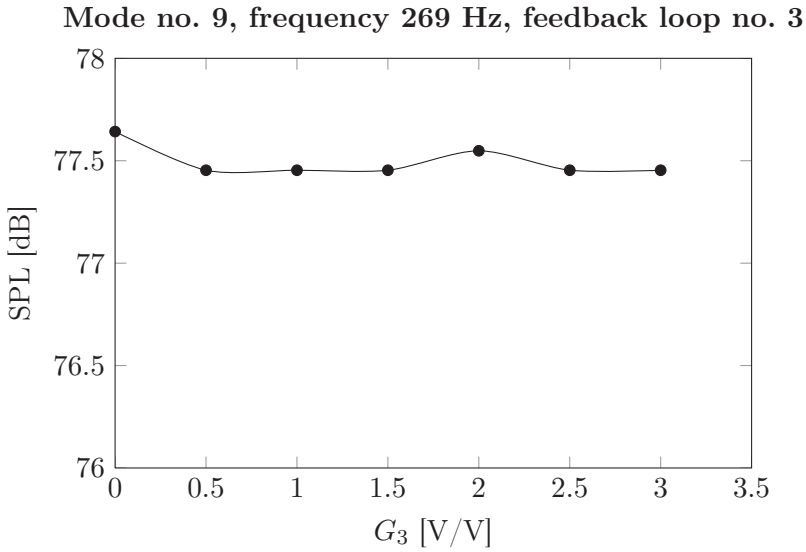


Figure 5.16. Sound pressure level as a function of gain value of feedback loop no. 3 for the plate vibrating in the 9th structural mode, at frequency 269 Hz. Position of the microphone: $x = 10$ cm, $y = 15$ cm, $z = 5$ cm.

The plots in Figures 5.18-5.21 present the sound pressure level generated by the plate structure vibrating in the 13th structural mode at frequency 380 Hz, at a point of the ambient space with the coordinates $x = 10$ cm, $y = 15$ cm, $z = 5$ cm, as a function of the gains of all the considered feedback loops. As it can be seen, the achieved level of noise reduction in the case of feedback loops no. 1 and 2 is higher than in the cases presented in Figures 5.10 and 5.11 concerning different point of the ambient space. The noise reduction achieved with feedback loop no. 3 is almost none. For feedback loop no. 4 only slight drop in the sound pressure level, less than 1 dB is observed.

The results obtained for the joint operation of feedback loops no. 1 and 2, concerning the same operating conditions as in the previously described cases, illustrated in Figures 5.18-5.21, are presented in Figure 5.22. A 10,2 dB maximum noise reduction level is achieved. Once again it can be seen that a simultaneous operation of multiple feedback loops result in significantly higher levels of noise reduction than in the cases of single loops operating alone, with the same maximum gain values.

Table 5.3 presents the measured sound pressure levels generated by the plate structure vibrating in the 13th structural mode at frequency 380 Hz, at a point of the ambient space with the coordinates $x = 10$ cm, $y = 15$ cm, $z = 5$ cm, as a function of various combinations of the gain values of all the feedback loops

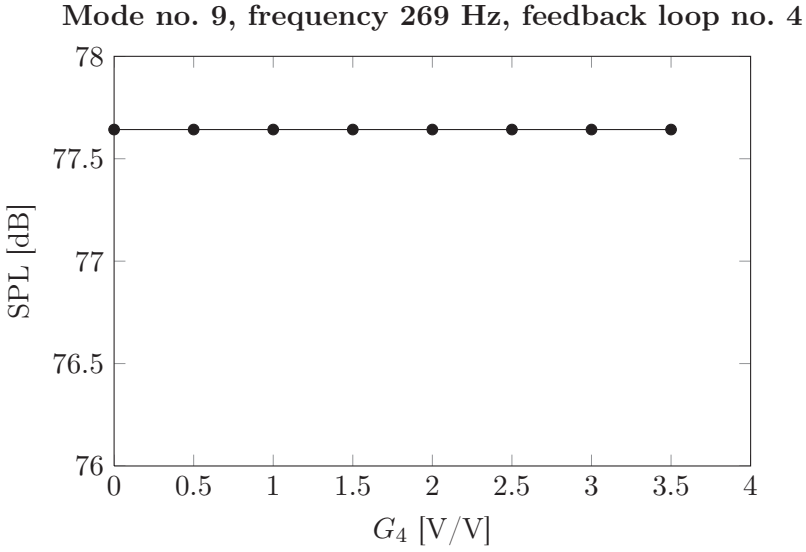


Figure 5.17. Sound pressure level as a function of gain value of feedback loop no. 4 for the plate vibrating in the 9th structural mode, at frequency 269 Hz. Position of the microphone: $x = 10$ cm, $y = 15$ cm, $z = 5$ cm.

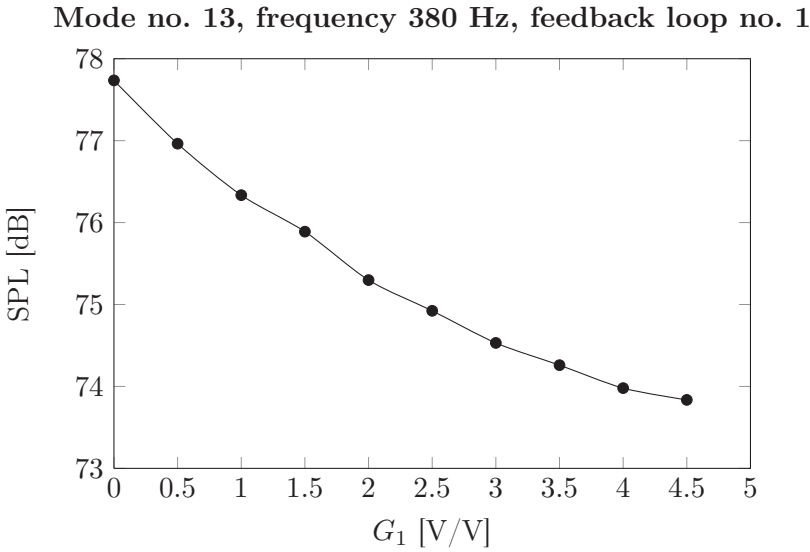


Figure 5.18. Sound pressure level as a function of gain value of feedback loop no. 1 for the plate vibrating in the 13th structural mode, at frequency 380 Hz. Position of the microphone: $x = 10$ cm, $y = 15$ cm, $z = 5$ cm.

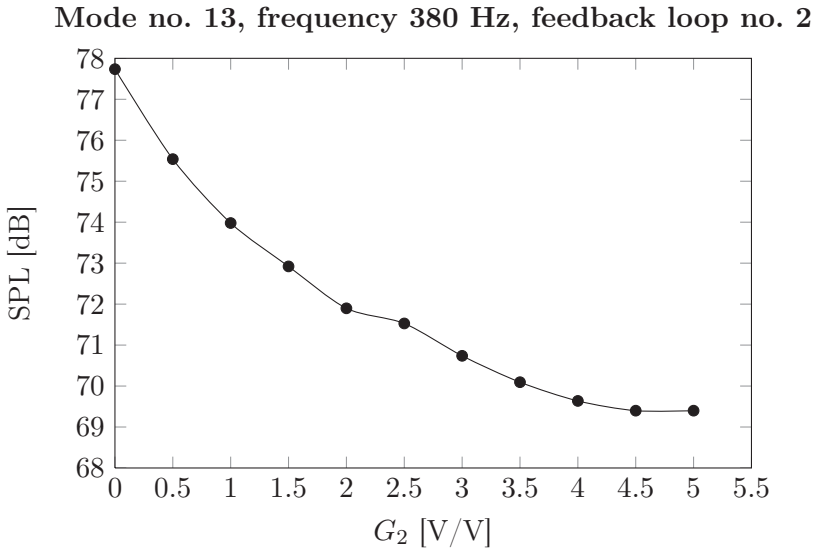


Figure 5.19. Sound pressure level as a function of gain value of feedback loop no. 2 for the plate vibrating in the 13th structural mode, at frequency 380 Hz. Position of the microphone: $x = 10$ cm, $y = 15$ cm, $z = 5$ cm.

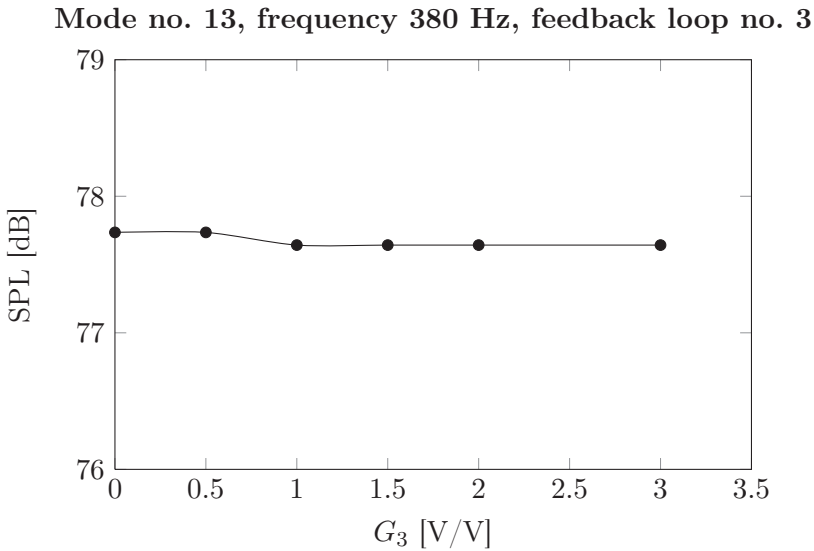


Figure 5.20. Sound pressure level as a function of gain value of feedback loop no. 3 for the plate vibrating in the 13th structural mode, at frequency 380 Hz. Position of the microphone: $x = 10$ cm, $y = 15$ cm, $z = 5$ cm.

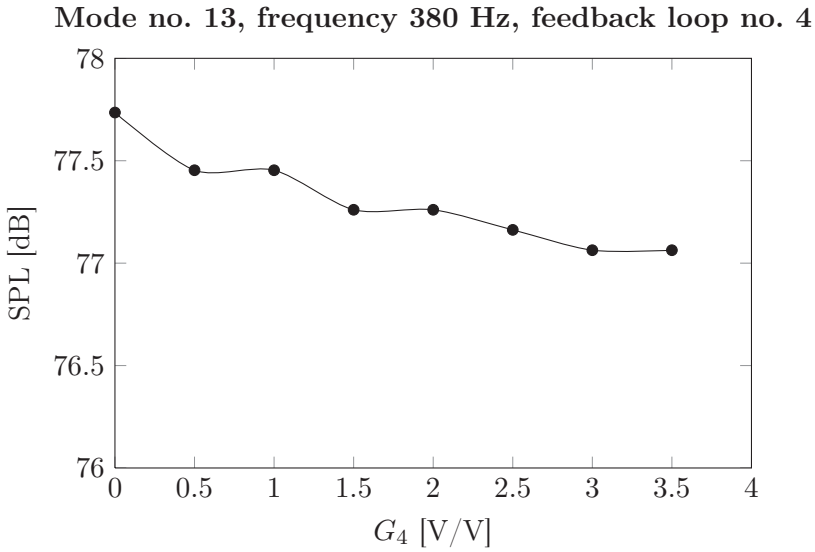


Figure 5.21. Sound pressure level as a function of gain value of feedback loop no. 4 for the plate vibrating in the 13th structural mode, at frequency 380 Hz. Position of the microphone: $x = 10$ cm, $y = 15$ cm, $z = 5$ cm.

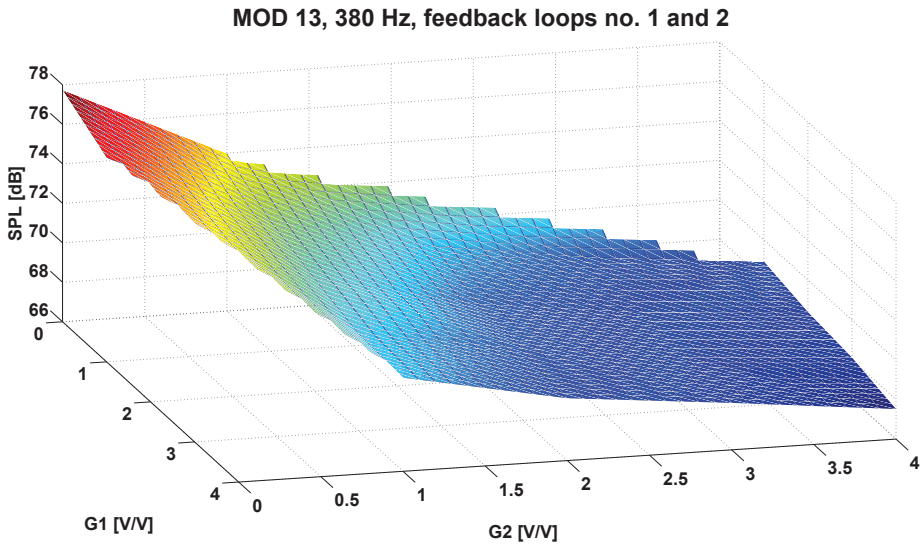


Figure 5.22. Sound pressure level as a function of gain values of feedback loops no. 1 and 2, for the plate vibrating in the 13th structural mode, at frequency 380 Hz. Position of the microphone: $x = 10$ cm, $y = 15$ cm, $z = 5$ cm.

included in the control system. The initial value of the sound pressure level, measured with the control system turned off, is equal 77,74 dB. As it can be seen, in this case introduction of feedback loops no. 3 and 4 has almost no effect on the achieved level of noise reduction.

G_1	G_2	G_3	G_4	SPL [dB]
0	0	0	0	77.74
2	0	0	0	75.3
0	2	0	0	71.9
0	0	2	0	77.64
0	0	0	2	77.26
2	2	0	0	69.87
2	0	2	0	75.42
2	0	0	2	74.92
0	2	2	0	72.08
0	2	0	2	71.53
0	0	2	2	77.36
2	2	2	0	70.09
2	2	0	2	69.87
2	0	2	2	74.92
0	2	2	2	71.71
2	2	2	2	69.87

Table 5.3. Sound pressure level as a function of gain values of feedback loops no. 1, 2, 3 and 4 for the plate vibrating in the 13th structural mode, at frequency 380 Hz. Position of the microphone: x = 10 cm, y = 15 cm, z = 5 cm.

The plots in Figures 5.23-5.25 present the measured sound pressure level generated by the plate structure vibrating in the 11th structural mode at frequency 320 Hz, at a point of the ambient space with the coordinates x = 10 cm, y = 20 cm, z = 20 cm, as a function of the gains of feedback loops no. 1, 2 and 4, respectively. About a 2 dB drop in the sound pressure level is achieved for the maximum available gain of feedback loop no. 1, a 3 dB drop for loop no. 2, and less than 1 dB for loop no. 4. However, by combining the operation of loops no. 1 and 2 in the control system, the maximum achievable noise reduction is increased to 5,56 dB – the relevant results are presented in Figure 5.26.

Table 5.4 presents the measured sound pressure level generated by the plate structure vibrating in the 11th structural mode at frequency 320 Hz, at a point of the ambient space with the coordinates x = 10 cm, y = 20 cm, z = 20 cm, as a function of various combinations of gain values of feedback loops no. 1, 2 and 4.

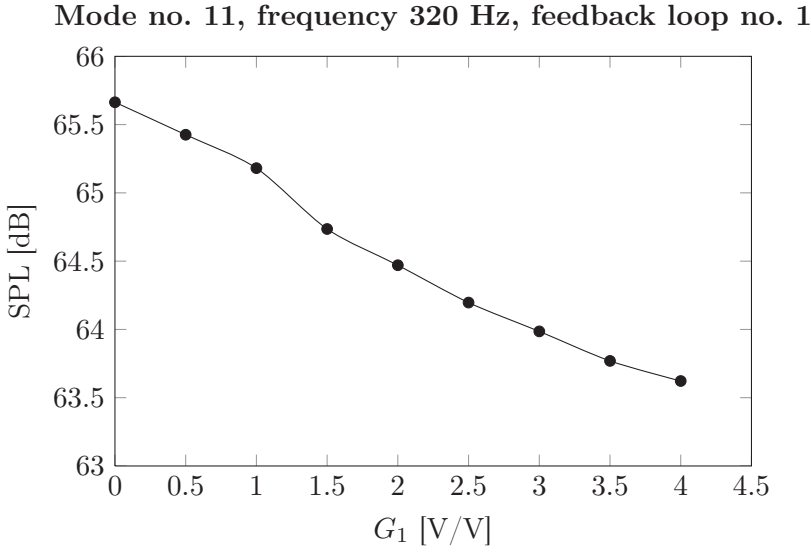


Figure 5.23. Sound pressure level as a function of gain value of feedback loop no. 1 for the plate vibrating in the 11th structural mode, at frequency 320 Hz. Position of the microphone: $x = 10$ cm, $y = 20$ cm, $z = 20$ cm.

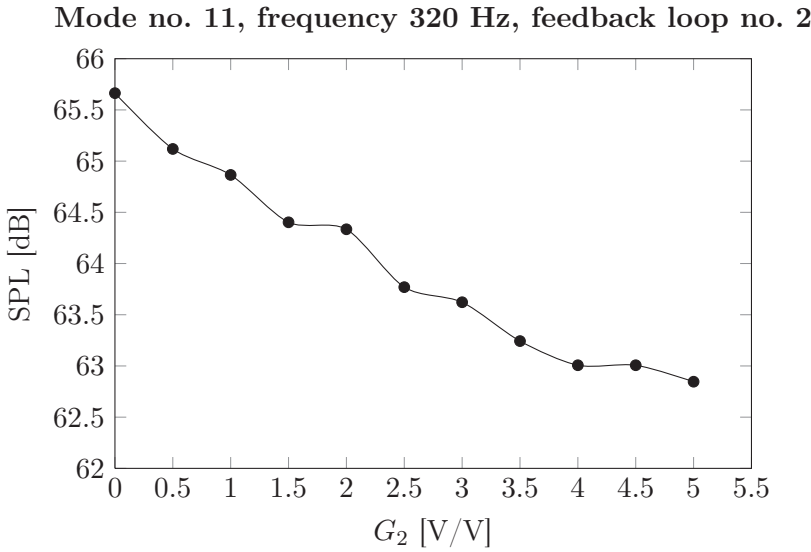


Figure 5.24. Sound pressure level as a function of gain value of feedback loop no. 2 for the plate vibrating in the 11th structural mode, at frequency 320 Hz. Position of the microphone: $x = 10$ cm, $y = 20$ cm, $z = 20$ cm.

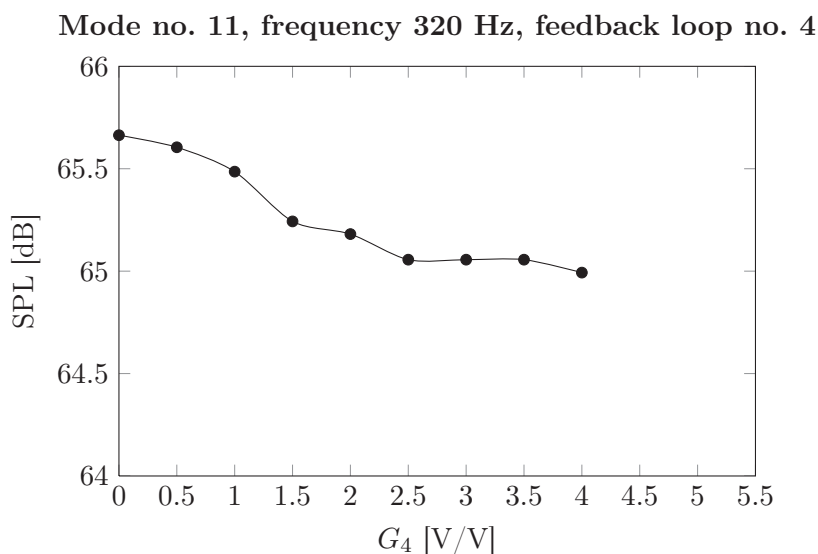


Figure 5.25. Sound pressure level as a function of gain value of feedback loop no. 4 for the plate vibrating in the 11th structural mode, at frequency 320 Hz. Position of the microphone: $x = 10$ cm, $y = 20$ cm, $z = 20$ cm.

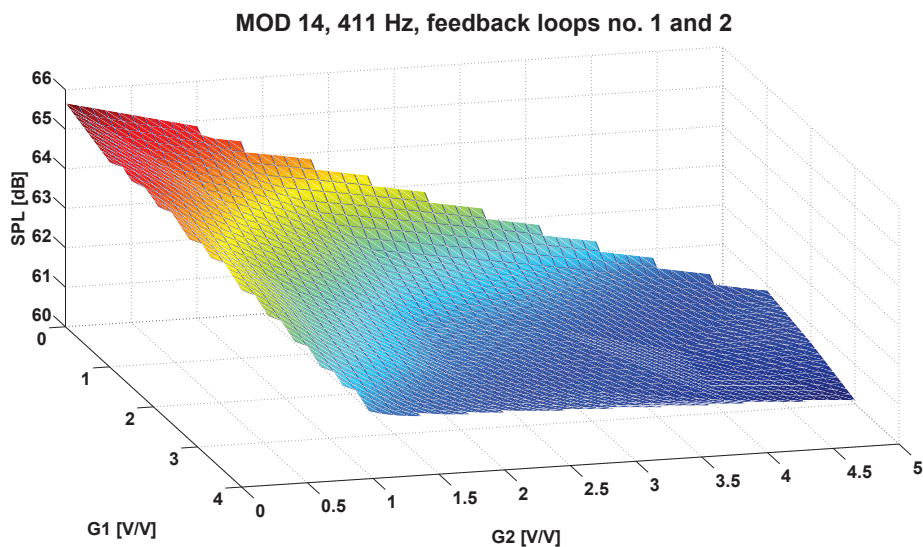


Figure 5.26. Sound pressure level as a function of gain values of feedback loops no. 1 and 2, for the plate vibrating in the 11th structural mode, at frequency 320 Hz. Position of the microphone: $x = 10$ cm, $y = 20$ cm, $z = 20$ cm.

Despite the fact that in this case the maximum gains of all the loops were assumed to be significantly lower than in the previously described cases concerning analogous situation, presented in Figures 5.23-5.26, the maximum achieved level of noise reduction is higher, equal to 6,02 dB. Thus, in this case it was possible to compensate the lower values of applied feedback gains with the higher number of involved control loops.

G_1	G_2	G_4	SPL [dB]
0	0	0	65.66
3	0	0	63.62
0	3	0	63.62
0	0	3	65.12
3	3	0	60.74
3	0	3	62.68
0	3	3	62.17
3	3	3	59.64

Table 5.4. Sound pressure level as a function of gain values of feedback loops no. 1, 2 and 4 for the plate vibrating in the 11th structural mode, at frequency 320 Hz. Position of the microphone: $x = 10$ cm, $y = 20$ cm, $z = 20$ cm.

5.7 Conclusions

Theoretical and experimental investigations on possibilities of an active control of sound radiated by a vibrating thin plate structure have been described in the present chapter. The developed control approach, based on the original concept and design of the active control system has been introduced and evaluated.

The theoretical investigations led to derivation of equations describing the relations between the parameters of the control system and the vibrational characteristics of the considered structure. Based on the considerations presented in Chapter 3 of the present study, under the assumed acoustic boundary conditions, the modal amplitudes of vibrations can be converted directly into the parameters describing the acoustic pressure field in a given point of the ambient space. The derived equations, presented in the previous sections of the present chapter, reveal a complex character of the involved phenomena. Each of the piezoelectric sensors responds to vibrations of the structure in some predefined manner. The induced electric signals are amplified and fed to the relevant actuators which in turn become the secondary sources of vibrations, influencing the

responses of all involved sensors. The resulting steady state conditions are thus described with relatively complicated formulas which include all the introduced relationships.

The signals from the piezoelectric sensors can be also used to determine the modal parameters of vibrations of the plate. However, due to the fact that only a limited number of transducers is available in the control system, the information obtained in such way is in general incomplete. The developed adaptation algorithms, presented in Section 5.4 allow to take advantage of any available additional knowledge about the parameters of the considered structure or the primary excitation force, in order to improve the adaptivity capabilities of the control system.

The experimental investigations carried out in an anechoic chamber revealed that only the resonant vibrations of the considered structure are the source of significant noise emission. For off-resonant frequencies the measured sound pressure levels and amplitudes of signals induced on the piezoelectric sensors were too low to efficiently perform the control process. Low signal to noise ratios caused in such cases instant problems with stability, as the feedback gains had to be set to relatively high values, in order to induce significant amplitudes of vibrations using piezoelectric actuators. The measured amplitudes of the acoustic pressure in the ambient space were close to the noise floor, and the achievable control performance under such conditions was almost absent. The plate revealed very sharp resonant characteristics in the considered, low frequency range and thus, the experiments were focused on resonant vibrations only.

The experimental evaluation of the developed and implemented active vibroacoustic control system revealed that under the assumed conditions relatively high levels of noise reduction, reaching up to about 10 dB, can be achieved. The use of multiple feedback loops in the system ensured in all cases significantly better results than single feedback loop operation. The achievable control performance strongly depends on the relation between vibrational characteristics of the plate and modal parameters of the involved sensor-actuator pairs, as well as on the choice of a reference point in the ambient space, at which the sound pressure level is measured. This complex relation is consistent with the theoretical predictions.

Collocated sensor-actuator pairs were used in the feedback loops. Accordingly to the results of theoretical considerations, such a configuration should ensure a total stability of the control system. However, the experimental investigations showed that in all cases increasing feedback gains beyond some critical values caused loss of stability and uncontrolled vibrations of the plate in the higher frequency modes (with frequencies 1-2 kHz and more). Those crit-

ical gain values depended on the specific numbers of involved feedback loops and current parameters of the primary excitation source. The described problems are most probably caused by the imperfections in the control system which were not taken into account in theoretical considerations. For instance, slight discrepancies in a relative positioning of the sensor and actuator belonging to the same feedback loop, could explain the observed differences in critical gain values for various control loops. Another factor that could contribute to the loss of stability are non-ideal parameters of the electronic components and circuit, the importance of which can increase at higher frequencies.

Concluding remarks

6.1 Summary

The aim of the present study was to develop, implement, and evaluate an active vibroacoustic control system for reduction of noise generated by vibrating thin plate structures with arbitrary boundary conditions. The system, including both hardware and software, has been successfully designed, implemented, and tested, proving a high potential in terms of the described tasks. Many various aspects regarding the considered subject were investigated.

The source of the acoustic radiation are the vibrations of the considered thin plate structure, excited by an external harmonic force. The issues concerning determination of the response of the plate to the external excitation were discussed in Chapter 2. The relevant formulas were derived and the results of the numerical simulations were presented. It was shown that precise modeling of the actual mounting conditions of the plate is important in terms of view of the accuracy of the determined eigenfrequencies and the corresponding mode shape functions. The orthogonality of the eigenfunctions determined numerically using various mesh resolutions was also investigated. An important conclusion drawn from the results of those investigations, was the necessity of using relatively dense meshes of finite elements in order to avoid errors in further computations, as many among the derived relations are based on the assumption of fulfilling the orthogonality criteria by the shape functions.

The issues concerning coupling between the vibrating structure and the acoustic medium were discussed in Chapter 3. It was shown that in the considered case, if the plate is surrounded with air, the influence of the inertial loading introduced by the medium on the vibrational parameters can be neglected. An original algorithm for determination of a free-field acoustic pressure distribution, based on the Indirect Variational Boundary Element Method, was proposed. The algorithm was successfully implemented and tested. The obtained results of simulations were validated by comparison with the results of experi-

mental investigations carried out in an anechoic chamber. The overall agreement between the numerical predictions and measurements was fair, and the results of simulations were most accurate for the far-field region. Taking into account a high computational efficiency of the proposed approach, it may be regarded as effective and useful tool for determining the acoustic pressure field distribution generated by vibrating thin, rectangle-shaped plate structures.

The developed active vibroacoustic control system uses piezoelectric sensors and actuators to sense and excite vibrations of the controlled structure. The issues regarding various aspects of utilization of piezoelectric transducers in such applications were discussed in chapter 4. A new form of a theoretical description, introducing modal sensitivity and selectivity functions was proposed. Using the introduced approach, modal parameters of sensors and actuators attached to various beam and plate structures were determined both numerically and experimentally. It was shown that proper positioning of small, rectangle-shaped piezoelectric transducers on the surfaces of the considered structures can provide either a very high or very low sensitivity to selected forms of vibrations.

Special attention was given to the problem of exciting resonant vibrations of the structure with piezoelectric transducers. Due to the fact that in such cases the amplitudes of vibrations are limited by occurring nonlinear effects which were not included in simple models used for theoretical considerations an important question was raised if the relation between those amplitudes and the amplitude of the electric signal driving actuator is linear. The carried out experimental investigations confirmed this hypothesis, with a very good accuracy.

An original technology for gluing piezoelectric transducers to the surfaces of structures made of electrically conductive material was introduced. The developed method allows to ensure both very good bonding conditions and sure electrical connection, while preventing short-circuiting of the electrodes of the transducer. The technology was implemented in practice and proved highly efficient in numerous experimental investigations. The relevant description can be found in Section 4.5 of the present study.

Based on the developed form of description of modal parameters of piezoelectric sensors and actuators, the equations linking the modal amplitudes of vibrations with the parameters of the control system were derived. Fast and computationally effective algorithms for solving the introduced formulas were developed and described in Sections 5.2 and 5.3. The results of investigations presented in Chapter 3 concerning the phenomenon of structure-borne sound generation allowed to link the amplitudes of vibrations with the acoustic pressure field distribution in the ambient space. Based on the introduced form of cost function, a control optimization algorithm was proposed. In order to ensure

the adaptivity capabilities of the system, an original algorithm for determining the parameters of the external excitation source was developed and described. The presented theoretical considerations are of great importance from the point of view of the experimental part of the present study, as they allow to better understand the observed phenomena.

The design and construction of the hardware components of the developed active control system were presented in Section 5.5 of the present study. An original approach, with a separate fully analogue feedback loop and digital control unit was proposed. The system, as well as the relevant control software including the user interface, were implemented in practice and tested in numerous experimental investigations. High levels of noise reduction, reaching up to about 10 dB were observed for various points of the ambient space, forms of vibrations and configurations of the control system (i.e., numbers of included feedback loops).

The obtained results of theoretical investigations, numerical simulations, and experimental research allow to conclude that the thesis of the present study is confirmed.

6.2 Scope of contribution

The following investigated issues are the original contribution of the present study on the background of the current state of the art presented in Section 1.3:

- A novel active vibroacoustic control system (hardware and software) has been developed and constructed. The system is described in Section 5.5.
- A dedicated control algorithm for determination of the optimal feedback gain values in a decentralized active control system has been developed. The detailed description of the algorithm is presented in Sections 5.1-5.3.
- A novel form of description of the active vibroacoustic control system based on piezotransducers, introducing modal sensitivity and selectivity functions has been developed. The modal parameters of sensors and actuators were determined analytically and numerically and compared to the results of the experimental investigations carried out using various beam and plate structures made from aluminium or composite materials, including the actual materials used in aviation. The introduced approach and the results of investigations are presented in Chapter 4.
- A dedicated adaptation algorithm for determination of the modal parameters of the external force exciting vibrations of the controlled structure has been developed. The algorithm is described in Section 5.4.

- A dedicated algorithm implementing the Indirect Variational Boundary Element Method, intended for determination of acoustic radiation characteristics of a vibrating, rectangle-shaped, thin plate structure with arbitrary boundary conditions has been developed and implemented. The algorithm takes advantage of the features of simple geometry of the considered problem to optimize the computational time and cost. The obtained results of the numerical simulations have been compared to the results of the experiments carried out in an anechoic chamber. The relevant description can be found in Sections 3.4 and 3.5.
- The control performance and stability of the developed active vibroacoustic control system have been evaluated during numerous experimental investigations carried out in an anechoic chamber. The results of experiments are presented in Section 5.6.

6.3 Recommendations for future work

The presented theoretical investigations concerning active control of vibrations of thin plates with arbitrary boundary conditions can be developed into cases of different, more complex structures. If only the undertaken assumptions regarding linearity of the involved phenomena are fulfilled, then such procedure would require only derivation of new, relevant forms of modal sensitivity and selectivity functions of piezoelectric transducers, as well as relations describing response to the external excitation source. Those functions could be directly implemented into equations describing the control system, introduced in Sections 5.2-5.4 of the present study. If such a new structure would reveal significant levels of noise emission for off-resonant excitations, then the potential and capabilities of the proposed approach could be entirely utilized.

The developed algorithm for determination of acoustic radiation characteristics of thin plate structures, based on the Indirect Variational Boundary Element Method, could also be a subject of further investigations. In this case, the recommended further research would include the following issues:

- development of the proposed approach into more complex geometries,
- implementation of the developed solver using different, independent and more computationally-effective environment,
- direct integration with structural dynamics analysis.

An interesting direction of further investigations is utilization of piezoelectric transducers with more complex shapes in the control system – especially defining such shapes of transducers that could ensure specific modal characteristics,

for a given number of forms of vibrations. Based on the introduced theoretical description of the control process, the geometry of such elements could be optimized in terms of some specific operating conditions. Different materials, such as, for instance, thin piezoelectric cables could be used in order to achieve various, complex forms of transducers.

One of the major problems encountered during experimental investigations on active vibroacoustic control, was the loss of stability associated with exceeding certain critical feedback gain values. Due to the fact that the amplification levels are directly connected with achievable control performance, elimination of the described problem, or at least maximization of the stability range is highly desired. This aim can be achieved by either improving the parameters of collocated sensor-actuator pairs, or by modifications of the electronic circuits of the control system. Additional low-pass filters could be implemented, but one should notice that every filter introduces an additional, frequency-dependent phase shift, and that the considered system is very sensitive to phase differences. Thus, this effect should be compensated, possibly with additional, controllable electronic circuit. The solution to the stability problem could bring the presented approach closer to practical implementations in various real-life structures and systems.

Bibliography

1. Paul Lueg. Process of silencing sound oscillations, 1936.
2. Kambiz Vafai. *Handbook of Porous Media*. Crc Press, 2009.
3. Jean Allard and Noureddine Atalla. *Propagation of Sound in Porous Media: Modelling Sound Absorbing Materials*. Wiley, 2009.
4. Frederick Alton Everest, Ken C. Pohlmann, and Tab Books. *The Master Handbook of Acoustics*. McGraw-Hill, New York, 2001.
5. M. Bulent Ozer and Thomas J. Royston. Passively minimizing structural sound radiation using shunted piezoelectric materials. *Journal of the Acoustical Society of America*, 114(4):1934–1946, 2003.
6. Tomasz Szolc and Łukasz Jankowski. Semi-active control of torsional vibrations of drive systems by means of actuators with the magneto-rheological fluid. In *Proc. of 8th International Conference on Vibrations in Rotating Machines-SIRM 2009*, 2009.
7. Tomasz Szolc, Łukasz Jankowski, Andrzej Pochanke, and Agnieszka Magdziak. An application of the magneto-rheological actuators to torsional vibration control of the rotating electro-mechanical systems. In *Proc. of the 8th IFToMM Int. Conference on Rotordynamics*, pages 12–15, 2010.
8. Agnieszka Pregowska, Robert Konowrocki, and Tomasz Szolc. On the semi-active control method for torsional vibrations in electro-mechanical systems by means of rotary actuators with a magneto-rheological fluid. *Journal of Theoretical and Applied Mechanics*, 51(4):979–992, 2013.
9. Sk Faruque Ali, Ananth Ramaswamy, et al. Testing and modeling of mr damper and its application to sdof systems using integral backstepping technique. *Journal of Dynamic Systems, Measurement, and Control*, 131(2):21009, 2009.
10. A. S. Knyazev and B. D. Tartakovskii. Abatement of radiation from flexurally vibrating plates by means of active local vibration dampers. *Soviet Physics-Acoustics*, 13:115–117, 1967.

11. Chris R. Fuller, S. J. Elliot, and P. A. Nelson. *Active Control of Vibration*. Academic Press, London, 1996.
12. Istan L. Ver and Leo L. Beranek. *Noise & vibration control engineering: Principles & applications*. John Wiley & Sons, 2005.
13. Daniel J. Inman. *Engineering Vibration*. Prentice-Hall, 1996.
14. Colin N. Hansen. *Understanding active noise cancellation*. Taylor & Francis, 2002.
15. Harry F. Olson and Everett G. May. Electronic sound absorber. *Journal of the Acoustical Society of America*, 25(6):1130–1136, 1953.
16. Harry F. Olson. Electronic control of noise, vibration, and reverberation. *Journal of the Acoustical Society of America*, 28(5):966–972, 1956.
17. P. A. Nelson and S. J. Elliott. *Active Control of Sound*. Academic Press, 1993.
18. Sen M. Kuo and Dennis R. Morgan. Active noise control: a tutorial review. *Proceedings of the IEEE*, 87(6):943–973, 1999.
19. Glenn E. Warnaka. Active attenuation of noise—the state of the art. *Noise Control Engineering Journal*, 18:100–110, 1982.
20. Chris R. Fuller. Experiments on reduction of aircraft interior noise using active control of fuselage vibration. *Journal of the Acoustical Society of America*, 75:S88, 1985.
21. Chris R. Fuller. Apparatus and method for global noise reduction, 1987.
22. Chris R. Fuller and R. J. Silcox. Acoustics 1991: Active structural acoustic control. *Journal of the Acoustical Society of America*, 91:519, 1992.
23. C. H. Hansen and S. D. Snyder. Effect of geometric and structural/acoustic variables on the active control of sound radiation from a vibrating surface. *Recent Advances in Active Control of Sound and Vibration*, 1:487–505, 1991.
24. E. Unver Thi and M. Zuniga. Comparison of design approaches in sound radiation suppression. *Proceedings of Recent Advances in Active Control of Sound and Vibration*, 1:15–17, 1991.
25. D. R. Thomas, P. A. Nelson, and S. J. Elliott. Experiments on the active control of the transmission of sound through a clamped rectangular plate. *Journal of Sound and Vibration*, 139(2):351–355, 1990.
26. William T. Baumann, William R. Saunders, and Harry H. Robertshaw. Active suppression of acoustic radiation from impulsively excited structures. *Journal of the Acoustical Society of America*, 90(6):3202–3208, 1991.

27. Tomasz G. Zielinski. Multiphysics modeling and experimental validation of the active reduction of structure-borne noise. *Journal of Vibration and Acoustics*, 132(6):Art.No. 061008, 1–14, 2010.
28. Jie Pan, Scott D. Snyder, Colin H. Hansen, and Christopher R. Fuller. Active control of far-field sound radiated by a rectangular panel – a general analysis. *Journal of the Acoustical Society of America*, 91(4):2056–2066, 1992.
29. S. J. Elliott and M. E. Johnson. Radiation modes and the active control of sound power. *Journal of the Acoustical Society of America*, 94(4):2194–2204, 1993.
30. L. Meirovitch and S. Thangjitham. Active control of sound radiation pressure. *Journal of Vibration and Acoustics*, 112:237–244, 1990.
31. Alain Berry, Jean-Louis Guyader, and Jean Nicolas. A general formulation for the sound radiation from rectangular, baffled plates with arbitrary boundary conditions. *Journal of the Acoustical Society of America*, 88:2792, 1990.
32. Lucyna Leniowska. *Aktywne metody redukcji drgań płyt kołowych*. Wydawnictwo Uniwersytetu Rzeszowskiego, 2006.
33. Chris R. Fuller. Active control of sound transmission/radiation from elastic plates by vibration inputs: I. analysis. *Journal of Sound and Vibration*, 136:1–15, 1990.
34. V. L. Metcalf, Chris R. Fuller, R. J. Silcox, and D. E. Brown. Active control of sound transmission/radiation from elastic plates by vibration inputs, ii: experiments. *Journal of Sound and Vibration*, 153(3):387–402, 1992.
35. R. A. Burdisso and Chris R. Fuller. Theory of feedforward controlled system eigenproperties. *Journal of Sound and Vibration*, 153(3):437–451, 1992.
36. Robert L. Clark. Adaptive feedforward modal space control. *Journal of the Acoustical Society of America*, 98:2639, 1995.
37. C. Guigou and Chris R Fuller. Adaptive feedforward and feedback methods for active/passive sound radiation control using smart foam. *Journal of the Acoustical Society of America*, 104:226, 1998.
38. Ricardo A. Burdisso and Chris R. Fuller. Design of feedforward asac systems by eigenfunction assignment. *Journal of the Acoustical Society of America*, 94:1816, 1993.
39. Jerzy Zabczyk. *Mathematical control theory: an introduction*. Springer, 2008.

40. John Comstock Doyle, Bruce A. Francis, and Allen Tannenbaum. *Feedback control theory*. Macmillan Publishing Company New York, 1992.
41. Robert L. Clark. A hybrid autonomous control approach. *Journal of Dynamic Systems, Measurement, and Control*, 117(2):232–240, 1995.
42. W. R. Saunders, H. H. Robertshaw, and R. A. Burdisso. An evaluation of feedback, adaptive feedforward and hybrid controller designs for active structural control of a lightly-damped structure. In *2nd Conference on recent advances in active control of sound and vibration*, Technomic Press, Blacksburg, VA, USA, 1993.
43. Jeffrey S. Vipperman and Robert L. Clark. Hybrid model-insensitive control using a piezoelectric sensor/actuator. *Journal of Intelligent Material Systems and Structures*, 7(6):689–695, 1996.
44. Brian Porter and Roger Crossley. *Modal control: theory and applications*. Taylor & Francis London, 1972.
45. Mark J. Balas. Active control of flexible systems. *Journal of Optimization Theory and Applications*, 25(3):415–436, 1978.
46. Jeffrey S. Vipperman. *Adaptive piezoelectric sensor/actuators for active structural acoustic control*. PhD thesis, Duke University, 1997.
47. S. Yildirim. Vibration control of suspension systems using a proposed neural network. *Journal of Sound and Vibration*, 277(4):1059–1069, 2004.
48. Lucyna Leniowska and Ryszard Leniowski. Active vibration control of a circular plate with clamped boundary condition. *Molecular & Quantum Acoustics. Jour*, 22:145–156, 2001.
49. M. A. Ahmad, M. H. Suid, M. S. Ramli, M. A. Zawawi, and R. M. T. Raja Ismail. Pd fuzzy logic with non-collocated pid approach for vibration control of flexible joint manipulator. In *Signal Processing and Its Applications (CSPA), 2010 6th International Colloquium on*, pages 1–5, 2010.
50. Simon G. Hill, Nobuo Tanaka, and Hiroyuki Iwamoto. Local sensing/control or global error sensing/control in structural acoustics: A comparison of two techniques influence over sound power. *Applied acoustics*, 71:965–978, 2010.
51. Kenneth D. Frampton. Vibro-acoustic control with a distributed sensor network. *Journal of the Acoustical Society of America*, 119(4):2170–2177, 2006.
52. Arthur W. Leissa and Mahamad S. Qatu. *Vibrations of Continuous Systems*. Mc Graw Hill, 2011.

53. Ignacy Malecki. *Theory of Waves and Acoustic Systems*. PWN, 1964. (in Polish).
54. T. G. Zielinski, M. A. Galland, and M. N. Ichchou. Fully coupled finite-element modeling of active sandwich panels with poroelastic core. *Journal of Vibration and Acoustics - Transactions of the ASME*, 134(2):Art.No. 021007, 1–10, 2012.
55. Thomas Christensen. *The Cambridge History of Western Music Theory*. Cambridge University Press, 2002.
56. John William Strutt Rayleigh. *The theory of sound*. Macmillan and co., London, 1877.
57. Miguel C. Junger and David Feit. *Sound, Structures, and Their Interaction*. The MIT Press, 1972.
58. G. Maidanik and E. M. Kerwin. Influence of fluid loading on the radiation from infinite plates below the critical frequency. *Journal of the Acoustical Society of America*, 40(5):1034–1038, 1966.
59. Alan D. Stuart. Acoustic radiation from submerged plates. i. influence of leaky wave poles. *Journal of the Acoustical Society of America*, 59(5):1160–1169, 1976.
60. Alan D. Stuart. Acoustic radiation from submerged plates. ii. radiated power and damping. *Journal of the Acoustical Society of America*, 59(5):1170–1174, 1976.
61. Lucyna Leniowska. Acoustic power of fluid-loaded circular plate located in finite baffle. *Archives of Acoustics*, 22(4):423–435, 1997.
62. H. Nelisse, O. Beslin, and J. Nicolas. A generalized approach for the acoustic radiation from a baffled or unbaffled plate with arbitrary boundary conditions, immersed in a light or heavy fluid. *Journal of Sound and Vibration*, 211:207–225, 1998.
63. Lukasz J. Nowak and Tomasz G. Zielinski. Acoustic radiation of vibrating plate structures submerged in water. *Hydroacoustics*, 15:163–170, 2012.
64. Paweł Jabłoński. *Metoda elementów brzegowych w analizie pola elektromagnetycznego*. Wydawnictwo Politechniki Czestochowskiej, 2003.
65. R. D. Ciskowski and C. A. Brebbia. *Boundary Element Methods in Acoustics*. Computational Mechanics Publications, 1991.
66. Lothar Gaul, Martin Kögl, and Marcus Wagner. *Boundary Element Methods for Engineers and Scientists*. Springer, 2003.

67. Stephen Kirkup. *The Boundary Element Method in Acoustics*. Integrated Sound Software, 2007.
68. Wim Desmet. Boundary element method in acoustics. In *ISAAC 23 - course on numerical and applied acoustics*, 2012.
69. Ahlem Alia, Mhamed Souli, and Fouad Erchiqui. Variational boundary element acoustic modelling over mixed quadrilateral-triangular element meshes. *Communications in numerical methods in engineering*, 22:767–780, 2006.
70. Z. Cheng, J. Fan, B. Wang, and W. Tang. Radiation efficiency of submerged rectangular plates. *Applied Acoustics*, 73:150–157, 2012.
71. M. Amabili. Free vibrations of annular plates coupled with fluids. *Journal of Sound and Vibration*, 191:825–846, 1996.
72. C. C. Liang, Y. S. Tai, and P. L. Li. Natural frequencies of annular plates having contact with fluid. *Journal of Sound and Vibration*, 228:1167–1181, 1999.
73. V. H. Vu, M. Thomas, A. Lakis, and L. Marcouiller. Effect of added mass on submerged vibrated plates. In *Proceedings of the 25th Seminar on machinery vibration*, pages 40.1–40.15. Canadian Machinery Vibration Association, 2007.
74. M. Caresta and N. Keississoglou. Active control of sound radiated by a submarine hull in axisymmetric vibration using inertial actuators. *Journal of Vibration and Acoustics*, 134:011002–1–8, 2012.
75. S. K. Shariati and S. M. Mogadas. Vibration analysis of submerged submarine pressure hull. *Journal of Vibration and Acoustics*, 133:011013–1–6, 2011.
76. Roman Salamon. *Systemy hydrolokacyjne*. Gdańskie Towarzystwo Naukowe, 2006.
77. Weiping Wang and Nouredine Atalla. A numerical algorithm for double surface integrals over quadrilaterals with a $1/r$ singularity. *Communications in Numerical Methods in Engineering*, 11:885–890, 1997.
78. C. K. Lee and F. C. Moon. Modal sensors/actuators. *Journal of Applied Mechanics*, 57:434–441, 1990.
79. C. K. Lee. Theory of laminated piezoelectric plates for the design of distributed sensors/actuators. part i: Governing equations and reciprocal relationships. *Journal of the Acoustical Society of America*, 87(3):1144–1158, 1990.

80. Stephen J. Elliott, Paolo Gardonio, Thomas C. Sors, and Michael J. Brennan. Active vibroacoustic control with multiple local feedback loops. *J. Acoust. Soc. Am.*, 11(2):908–915, 2002.
81. E. H. Anderson and N. W. Hagood. Simultaneous piezoelectric sensing/actuation: Analysis and application to controlled structures. *Journal of Sound and Vibration*, 174(5):617–639, 1994.
82. Jeffrey J. Dosch, Daniel J. Inman, and Ephraim Garcia. A self-sensing piezoelectric actuator for collocated control. *Journal of Intelligent Material Systems and Structures*, 3:166–185, 1992.
83. Jeffrey S. Vipperman and Robert L. Clark. Implementation of an adaptive piezoelectric sensor/actuator. *Journal of the Acoustical Society of America*, 34(10):2102–2109, 1996.
84. Garnett E. Simmers, Jeffrey R. Hodgkins, David D. Mascarenas, Gyuhae Park, and Hoon Sohn. Improved piezoelectric self-sensing actuation. *Journal of Intelligent Material Systems and Structures*, 15(12):941–953, 2004.
85. Sharon L. Padula and Rex K. Kincaid. Optimization strategies for sensor and actuator placement. Technical report, National Aeronautics and Space Administration, 1999.
86. Mary I. Frecker. Recent advances in optimization of smart structures and actuators. *Journal of Intelligent Material Systems and Structures*, 14(4-5):207–216, 2003.
87. Vivek Gupta, Manu Sharma, and Nagesh Thakur. Optimization criteria for optimal placement of piezoelectric sensors and actuators on a smart structure: A technical review. *Journal of Intelligent Material Systems and Structures*, 21(12):1227–1243, 2010.
88. Zhicheng Qiu, Xianmin Zhang, Hongxin Wu, and Honghua Zhang. Optimal placement and active vibration control for piezoelectric smart flexible cantilever plate. *Journal of Sound and Vibration*, 301:521–543, 2007.
89. Osama J. Aldraihem, Tarunraj Singh, and Robert C. Wetherhold. Optimal size and location of piezoelectric actuator/sensors: practical considerations. *Journal of Guidance, Control, and Dynamics*, 23(3):509–515, 2000.
90. Robert L. Clark and Chris R. Fuller. Optimal placement of piezoelectric actuators and polyvinylidene fluoride error sensors in active structural acoustic control approaches. *Journal of the Acoustical Society of America*, 92(3):1521–1533, 1992.

91. A. M. Sadri, J. R. Wright, and R. J. Wynne. Modelling and optimal placement of piezoelectric actuators in isotropic plates using genetic algorithms. *Smart Materials and Structures*, 8(4):490, 1999.
92. S. T. Quek, S. Y. Wang, and K. K. Ang. Vibration control of composite plates via optimal placement of piezoelectric patches. *Journal of intelligent material systems and structures*, 14(4-5):29–245, 2003.
93. S. Julai and M. O. Tokhi. Vibration suppression of flexible plate structures using swarm and genetic optimization techniques. *Journal of Low Frequency Noise, Vibration and Active Control*, 29(4):293–318, 2010.
94. Jae-Hung Han and In Lee. Optimal placement of piezoelectric sensors and actuators for vibration control of a composite plate using genetic algorithms. *Smart Materials and Structures*, 8(2):257, 1999.
95. Joseph D. Sprofera, Randolph H. Cabell, Gary P. Gibbs, and Robert L. Clark. Structural acoustic control of plates with variable boundary conditions: Design methodology. *Journal of the Acoustical Society of America*, 122(1):271–279, 2007.
96. James Karki. Signal conditioning piezoelectric sensors. App. rept. on mixed signal products (sloa033a), Texas Instruments Incorporated, 2000.
97. Shashank Priya. Modeling of electric energy harvesting using piezoelectric windmill. *Applied Physics Letters*, 87(18):184101–184101, 2005.
98. Ramon Pallas-Areny, John G. Webster, and Ramo Areny. *Sensors and signal conditioning*. Wiley, New York, 2001.
99. Y. B. Jeon, R. Sood, J. Jeong, and S. Kim. Mems power generator with transverse mode thin film pzt. *Sensors and Actuators A: Physical*, 122(1):16–22, 2005.
100. Walter G. Jung. *Op Amp applications handbook*. Newnes, 2005.
101. I. Masters and K. Evans. Models for the elastic deformation of honeycombs. *Composite Structures*, 35(4):403–422, 1996.
102. Gene H. Golub and Charles F. Van Loan. *Matrix computations*. JHU Press, 2012.
103. Andreĭ Nikolaevich Tikhonov. *Numerical methods for the solution of ill-posed problems*. Springer, 1995.